# Solar Absorption Cycle for Cooling / Refrigeration

Thesis submitted for the

Degree of Doctor of Philosophy

by

Marwan Juma Ali AL Juma

March 2014

# Abstract

The purpose of this thesis is to critically highlight the development of solar absorption refrigeration technologies through time. The factors that have prompted the urgent need to reconsider this area of engineering will also be analyzed in depth. The relevant research in the area of solar absorption to date will be shown with specific emphasis on its contribution to industrial and domestic cooling systems. The Middle East may be awash with oil in the present circumstances with 48% of the known oil reserves in the world but challenges exist owing to fossil fuel being a finite resource and its exploitation fraught with environmental problems. Therefore developing solar cooling systems appears to be an essential and inevitable requisite for harnessing solar energy in order to make a lasting contribution to the development of the region, as well as the world

Targeting the coefficient of performance (COP) of the solar absorption refrigeration systems was considered to be the fundamental part of this research. By investigating the absorber chamber in an absorption refrigeration system, it was found that enhancing the quality of the spray of the absorber fluid could raise the COP.

Using a Phase Doppler Anemometry (PDA), a detailed analysis of the spray characteristics was achievable; this helped in targeting parameters which will have influence on the spray characteristics. These include the nozzle geometry, for instance, the size of orifice, as well as the internal forces of the liquid such as viscosity and surface tension. Operating parameters were also considered to influence the spray quality. The main operating parameter is to create a partial vacuum to simulate the absorber chamber working condition.

Results revealed that high viscosity of the fluid and the vacuum had negative effects towards spray quality. But when combining these with a surfactant such as 2-ethyl-1-hexanol, the spray quality increases in terms of droplet diameter, which in turn decreases and thereby causes an increase in the surface area to volume ratio, resulting in the enhancement of COP.

# Acknowledgements

I would like to start by thanking my supervisors Professor Anthony J Griffiths and Dr. Richard Marsh for providing me the opportunity, support and guidance throughout this emotional journey.

I would also like to thank Malcolm Seabourne, Steve Mead and Paul Malpas for their help and support. A special mention goes to Malcolm Seabourne for his input in construction and maintenance of the required experimental components, and for his assistance with the facilities needed.

My sincere thanks and gratitude are extended to my parents and family members for their continual support and encouragement to achieve this degree. And a special thanks goes to my father Dr. Juma Ali Al Juma for his moral support and valuable advice.

I would also like to take this opportunity to thank my beloved wife for her ongoing mental and physical support, and my cherished daughter Faye for inspiring my journey.

Marwan Al Juma

## Declaration

This work has not previously been accepted in substance for any degree and is not being concurrently submitted in candidature for any degree.

Signed........................................................... (candidate)
Date...............................................................

## Statement 1

This thesis is being submitted in partial fulfillment of the requirements for the degree of PhD.

Signed........................................................... (candidate)
Date...............................................................

## Statement 2

This thesis is the result of my own independent work/investigation, except where otherwise stated. Other sources are acknowledged by footnotes giving explicit references.

Signed........................................................... (candidate)
Date...............................................................

## Statement 3

I hereby give consent for my thesis, if accepted, to be available for photocopying and for inter-library loan, and for the title and summary to be made available to outside organisations.

Signed........................................................... (candidate)
Date...............................................................

# Nomenclature

## Roman Characters

| Symbol | Definition | Unit |
|---|---|---|
| a | Radius of a Droplet | m |
| $d_{10}$ | Length | m |
| $D_v$ | Diffusion Coefficient of Vapor | $m^2/s$ |
| $h_{fg}$ | Latent Heat of Vaporization | J/kg |
| $i_{corr}$ | Corrosion Current Density | $A/m^2$ |
| k | Thermal Conductivity-Gas Phase | W/mK |
| $m_{LiBr}$ | Molality of Lithium Bromide | mol/kg |
| $\dot{m}$ | Mass Reduction Rate of Droplet | kg/s |
| $Q_e$ | Evaporator Heat Transfer Rate | kJ/s |
| $Q_g$ | Generator Heat Transfer Rate | kJ/s |
| X | Mass fraction of LiBr | % |
| t | Time | s |
| $T_a$ | Absorber Temperature | °C |
| $T_c$ | Condenser Temperature | °C |
| $T_g$ | Generator Temperature | °C |
| $U_{av}$ | Average Velocity | m/s |

## Greek Characters

| Symbol | Definition | Unit |
|---|---|---|
| $\sigma_l$ | Surface Tension of Liquid | kg/s2 |
| $\rho_l$ | Liquid Density | $kg/m^3$ |
| $\nu$ | Liquid Kinematic Viscosity | $m^2/s$ |
| $\mu$ | Liquid Dynamic Viscosity | kg/ms |

## Acronyms

| Symbol | Definition | Unit |
|---|---|---|
| 2EH | 2-ethyle-1-hexanol | - |
| AER | Additive Enhancement Ratio | - |
| ATM | Atmospheric Conditions | - |
| COP | Coefficient of performance | - |
| DDBP | Droplet Diameter Bubble Plot | - |
| LP-Rig | Low Pressure Rig | - |
| PDA | Phase Doppler Anemometry | - |
| SMD | Sauter Mean Diameter | m |
| GCC | Gulf Cooperation Council | - |

## Dimensionless Parameters

| Symbol | Definition |
|---|---|
| Oh | Ohnesorge Number |
| Re | Reynolds Number |
| We | Weber Number |

# Table of Contents

# List of Figures

# List of Equations

# List of Tables

# 1 Introduction

## 1.1 Overview of Energy Consumptions

The world energy consumption is highly dependent on fossil fuels, which is estimated to be responsible for more than 80% of the energy produced. Fossil fuels are still forecasted to be the main source of energy for the coming 25 years as shown in Figure 1-1, regardless of the attempts to find alternative energy resources (Barca 2011).

Cooling systems are increasingly consuming more energy worldwide with the growth of the five major emerging national economies BRICS (Brazil, Russia, India, China, South Africa) and the wealthy oil nations of the Gulf Cooperation Council (GCC) (Pao and Tsai 2010; Alnaser and Alnaser 2011).

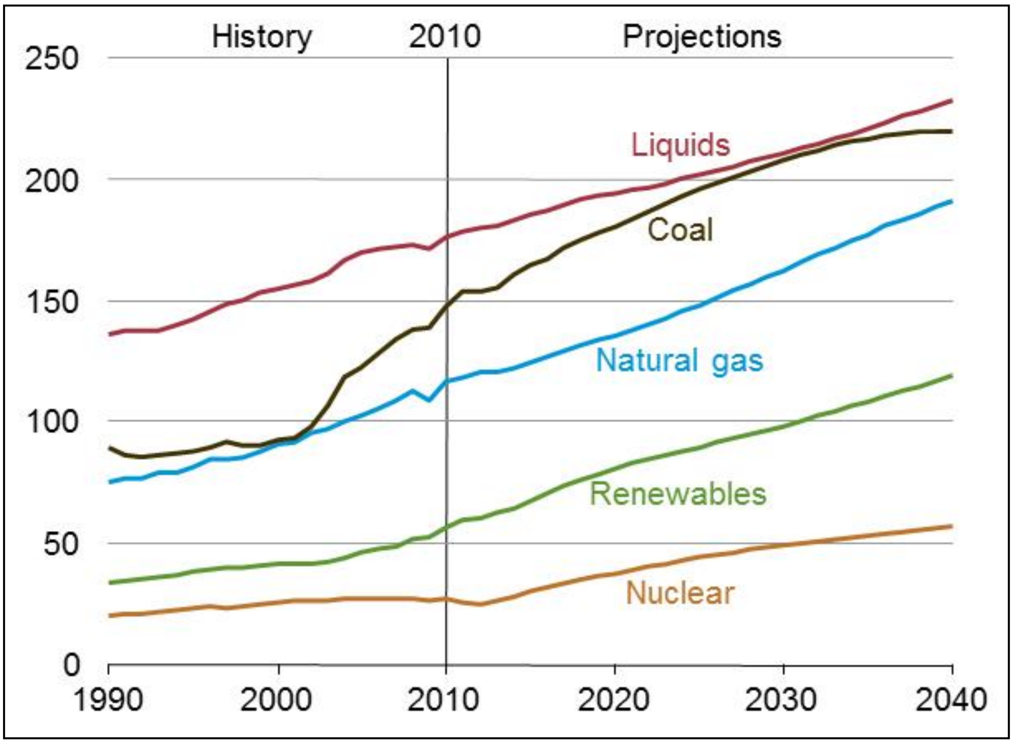

Figure 1-1 Energy consumption by different energy sources worldwide through 1990-2040 (Administration 2013)

## 1.2 Motivation

It is a well-documented fact that the global environment is passing through a huge climate change due to the phenomenon known as greenhouse effect, which is caused by the over utilization of fossil fuel, deforestation, land exploitation and the use of greenhouse gases in refrigeration and air conditioning systems by humans (Akorede et al. 2012). These changes have caused global warming, by which the average temperature of the earth`s atmosphere and oceans have risen for the last few decades. According to Intergovernmental Panel on Climate Change (IPCC 2013), the global temperature is projected to increase by 1.4 °C to 5.8 °C by the year 2100, followed by drastic climatic changes sowing disasters such as drought, floods, hunger, diseases and wars caused by the lack of resources (Chiari and Zecca 2011).

Furthermore, and based on a rise in population around the world, the activities, which causes climate change, mentioned above have exponentially increased in terms of volume and momentum. This matter is brought out by the fact that, many developing countries such as BRICS (Bodas Freitas et al. 2012) or those with small population like the GCC countries are going through their own economic and financial re-structuring activities to catch up with the developed countries of the world (Patlitzianas et al. 2007; Reiche 2010).

As noted above, the conventional refrigeration and air-conditioning are two of the systems, which have been identified to have a large impact on the environment in terms of its contribution to global warming. This is because of three main reasons: First they account for no less than 15% of world energy consumption (Li et al. 2014) due to their widespread use . Secondly, the type of refrigerant gases such as CFC, which are used for the purpose of cooling, will be harmful to the environment in case of leakage and this aggravates the depletion of the ozone layer. Thirdly, the utilization of a large amount of energy by these systems makes them a major contributor to the emission of high amount of carbon dioxide in the air. Till now the biggest contributor is the electrical energy being generated by generators, which utilizes fossil fuel.

This fact assumes an alarming dimension, when the day-to-day rise in human population results in the purchase of cooling systems in huge volumes by the people, not as goods of luxury, but to brace themselves from the boiling temperatures. For these reasons, many organizations around the world such as International Institute of Refrigeration have come to conclude that an immediate action has to be taken to reduce direct emission of greenhouse gases introduced by cooling and refrigerant plants to 50% in the year 2020 and a new system should be designed and employed in the aim of reduction of energy consumption of refrigerant plants by 30-50% during the same period. The institute went on to note on the methods to be used on the reduction of the greenhouse effect by the year 2020, which include the improvement of refrigerant coolant in containing the CFC and the use of refrigerants with the lowest overall impact on global warming (International-Institute-of-refrigeration 2005).

The importance of the reduction of greenhouse gases is also highlighted by United Nations Framework Convention on Climate Change in its Kyoto Protocol where the aim of the protocol is to limit the global greenhouse emission through setting targets for the reduction of the greenhouse gases which participating nations must meet (Dagoumas et al. 2006).

For this reason, the Kyoto Protocol has identified different mechanisms, which are to be used for realizing the Protocol's aims. These include, for example, the trading of emissions by countries, which are not able to reduce their noted emission targets, with other countries and the promotion of sustainable development through sustainable technologies by encouraging participating countries to implement or expand existing environmental impact countermeasures to achieve these reductions.  The enhancement of energy efficiency, reforestation, development of new and renewable forms of energy, development of environmental sound technologies and the phasing out of the market imperfections in all greenhouse gas emitted sectors are the notable countermeasures. (United-Nations 1997; Lau et al. 2012).

Fossil fuels are inherently a finite resource (Shafiee and Topal 2009), which ultimately calls for such strides in engineering as the solar cooling systems models provide. Large domestic areas in the Middle East are one huge market for solar cooling technology when the huge requirement for domestic air-conditioning is taken into consideration. Another key market would be in industrial applications such as airports, factories and sporting stadia. One very novel yet highly practical and innovative application of air-conditioning in the Middle East related to a sporting event would be the forth-coming football

World Cup competition in Qatar 2022. It would be a world first indeed if all stadia were fitted with solar powered air-conditioning to face the searing heat.

Another pragmatic and beneficial application of solar cooling in the Middle East would be in the area of food production. This is in view of the difficulties faced in cultivating crops in very hot and arid climatic conditions in these countries, leading them to be over-dependent on imported food (Davies 2005).

Places such as the Middle East are replete with year-round sunshine making this piece of research extremely relevant in such parts. The upcoming Football World Cup to be hosted by Qatar could be an excellent example of making use of solar cooling technologies in their refined and most efficient state. It is also most challenging and yet feasible to develop smaller units to be used in both residential and small business settings in a cost-efficient way. Factories are also another area of growth in demand for solar powered air conditioning.

In Africa, where large mining activities are carried out, it would be more profitable for solar powered air conditioning to be harnessed in place of electricity powered air conditioning or the use of coal or oil for this purpose. Office buildings are yet another area of growing demand for solar powered air conditioning. In Australia there has been a marked increase in demand for air conditioning products owing in part to change in living standards, global warming and other climate phenomena (Tsagarakis et al. 2012).

Increased demands upon national electricity grids have made it necessary therefore to develop new air conditioning technologies based on reusable energy sources such as solar energy. It has also got to be considered whether any new technologies exist that make air-conditioning and refrigeration environmentally safe. This is where solar powered air-conditioning and refrigeration technologies come in.

### 1.2.1 Motivation of Research by Location

As noted, the global temperature has been on an ascending curve and one primary factor that has contributed to this is the utilization of air-conditioning and refrigeration systems by different countries. The utilization of these systems is highly demanded in hot climate countries, in particular those, which have been rapidly developing, and where new cities are being constructed. This calls for large numbers of air-conditioning and refrigeration systems in order to sustain a comfortable life style.

One of these countries is Oman, where vibrant and rapid industrial expansion has paved way for the construction of major cities and where a solution based on renewable and environmentally friendly technologies is necessarily required well in advance of the residential and commercial phases of these cities.

Figures 1-2 and 1-3 show the amount of solar radiation and how long it is available throughout the Middle East and they prove the necessity of using solar energy as an alternative energy source. The rate of increase in electricity consumption in GCC countries from 2005 to 2009 was 8.87% and the highest was in Oman, 22.6% (Alnaser and Alnaser 2011).

Table 1-1 shows that Oman's two major cities have a relatively high solar radiation rate on average per year, which proves and supports the motivation of this study. These studies also show that there is a great potential in developing solar refrigeration systems, as they are demonstrably essential for the general public as well as the industrial sector.

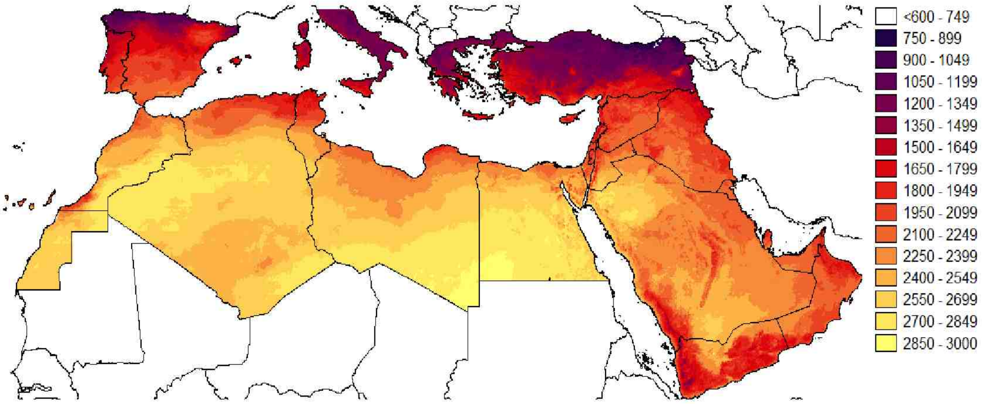

Figure 1-2 The Annual average of the daily-recorded global solar radiation (in kW h/m2) in Arab countries (Hoyer-Klick et al. 2009).

Table 1-1 The monthly and annual recorded mean of the global solar radiation (in kW h/$m^2$/day) in two major cities in Oman (Alnaser et al. 2004)

| Month | Muscat | Salalah |
|---|---|---|
| **January** | 4.0 | 4.6 |
| **February** | 4.7 | 4.9 |
| **March** | 5.5 | 6.6 |
| **April** | 6.3 | 6.8 |
| **May** | 6.9 | 6.1 |
| **June** | 6.7 | 5.2 |
| **July** | 6.1 | 3.3 |
| **August** | 6.0 | 3.0 |
| **September** | 5.8 | 4.6 |
| **October** | 5.2 | 5.4 |
| **November** | 4.4 | 4.8 |
| **December** | 3.8 | 4.4 |
| **Yearly** | 5.4 | 4.8 |

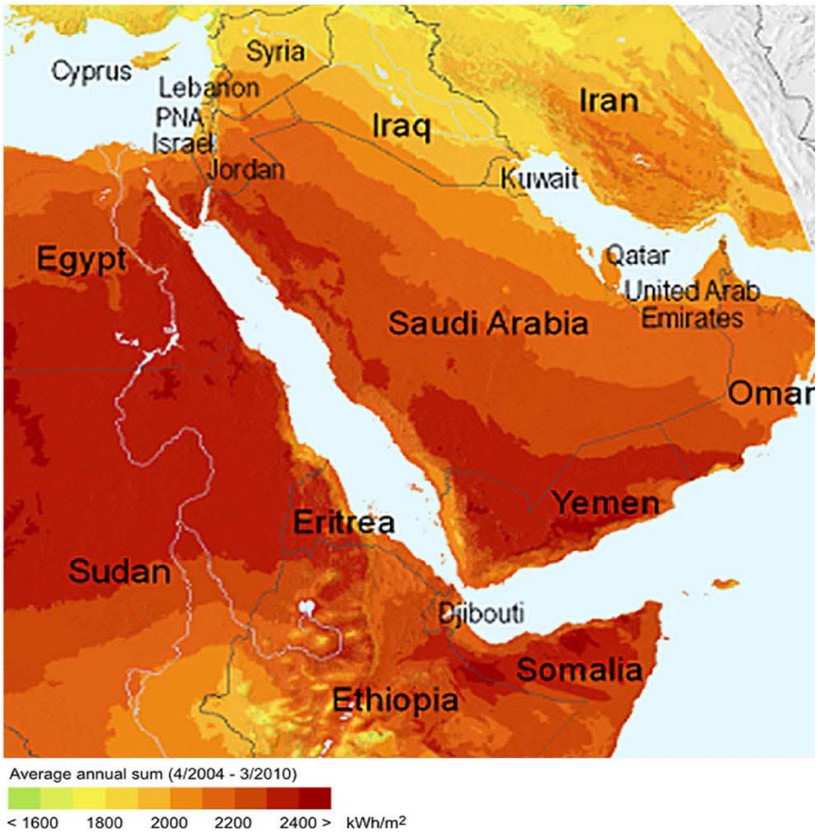

Figure 1-3 The annual sunshine duration average of the Arab countries (Hoyer-Klick et al. 2009).

## 1.3 Absorption Refrigeration Systems

Absorption refrigeration systems utilize heat energy to generate chilled water instead of electrical energy as used by the commonly used vapour compression cycle refrigeration systems.

Similar to the vapour compression cycle refrigeration systems, the absorption refrigeration systems achieve cooling effect by evaporation of a refrigerant followed by the expulsion of heat to the surrounding by condensation of the refrigerant.

The major difference between an absorption refrigeration system and a vapour compression refrigeration system is that a vapour compression refrigeration system uses a compressor to make the pressure difference required to circulate the refrigerant while the absorption refrigeration system uses a generator chamber and an absorber chamber, and hence the name absorption was given to the latter system(Dincer and Kanoglu 2010). As the absorption refrigeration system requires heat as an energy source, solar or waste heat could be utilized.

It has been proved through research and scientific study that solar absorption refrigeration systems are to be more suitable for large building air-conditioning systems. Indeed it is therefore appropriate to claim that solar cooling has been proved to be technically feasible for domestic implementation (Zhai et al. 2008).

### 1.3.1 Working principle

The absorption cooling cycle is achieved by means of an absorbent-refrigerant mix, such as LiBr-$H_2O$. Lithium bromide is hygroscopic, which means it can mix with water in any ratio. The solar heat is used in a generator to vaporize some of the water in the LiBr-$H_2O$ mix. This vapour is led to the condenser unit and then is expanded to a gaseous phase where it draws heat from the surroundings which are to be cooled (Sorensen 2007).

For solar assisted air conditioning systems with common solar collectors, single effect absorption chillers using LiBr-$H_2O$ mix are the most commonly used systems (Henning 2004; Cengel and Boles 2007).

Figure 1-4 shows a single effect absorption refrigeration system with all of its chambers and components. The steps of operation are detailed with each operation labelled by a number corresponding to its place of operation.

The complete refrigeration cycle is operated under a partial vacuum, and is dependent on the water as the refrigerant and lithium bromide as the refrigerant carrier (absorber), because of strong attraction between those two solutions.

The detailed working principle is described as follows:

(1) Solution Pump:

Diluted LiBr solution is collected in the bottom of the absorber, and then using a solution pump the diluted LiBr solution is pumped through heat exchanger to preheat it.

(2) Generator:

After passing through the heat exchanger, the dilute lithium bromide solution enters into the generator chamber. Using the steam or hot water that is heated by the solar energy, heat is transferred to the dilute lithium bromide solution.

Then the lithium bromide solution boils and sends the water refrigerant vapor into the condenser chamber while leaving behind a concentrated lithium bromide solution. This concentrated solution then flows down to the heat exchanger.

(3) Condenser:

Tubes that have cooling water flowing through them returning from the cooling tower condense the refrigerant vapor, hence the name condenser then. As the refrigerant condenses, it is collected at the bottom of the condenser. The liquefied refrigerant then flows from the condenser to the evaporator chamber.

(4) Evaporator:

The liquefied refrigerant is then sprayed over the evaporator tubes that act as heat exchangers. Due to extreme vacuum of 0.8kPa absolute pressure, the refrigerant liquid will boil at 3.9°C, and hence produce chilled water flowing through the evaporator tubes, which are used for refrigeration and cooling (YORK-International 1997).

(5) Absorber:

The concentrated lithium bromide solution that is returning from the generator is sprayed from the top of the absorber. The concentrated lithium bromide solution attracts the refrigerant vapour into the concentrated solution because of its hygroscopic characteristic.

This strong attraction and absorption of the refrigerant creates a great vacuum in the evaporator. It also generates heat, which is removed by the cooling water flowing through the tubes returning from the cooling tower. Then the dilute solution of lithium bromide is collected at the bottom of the absorber, which completes the cycle.

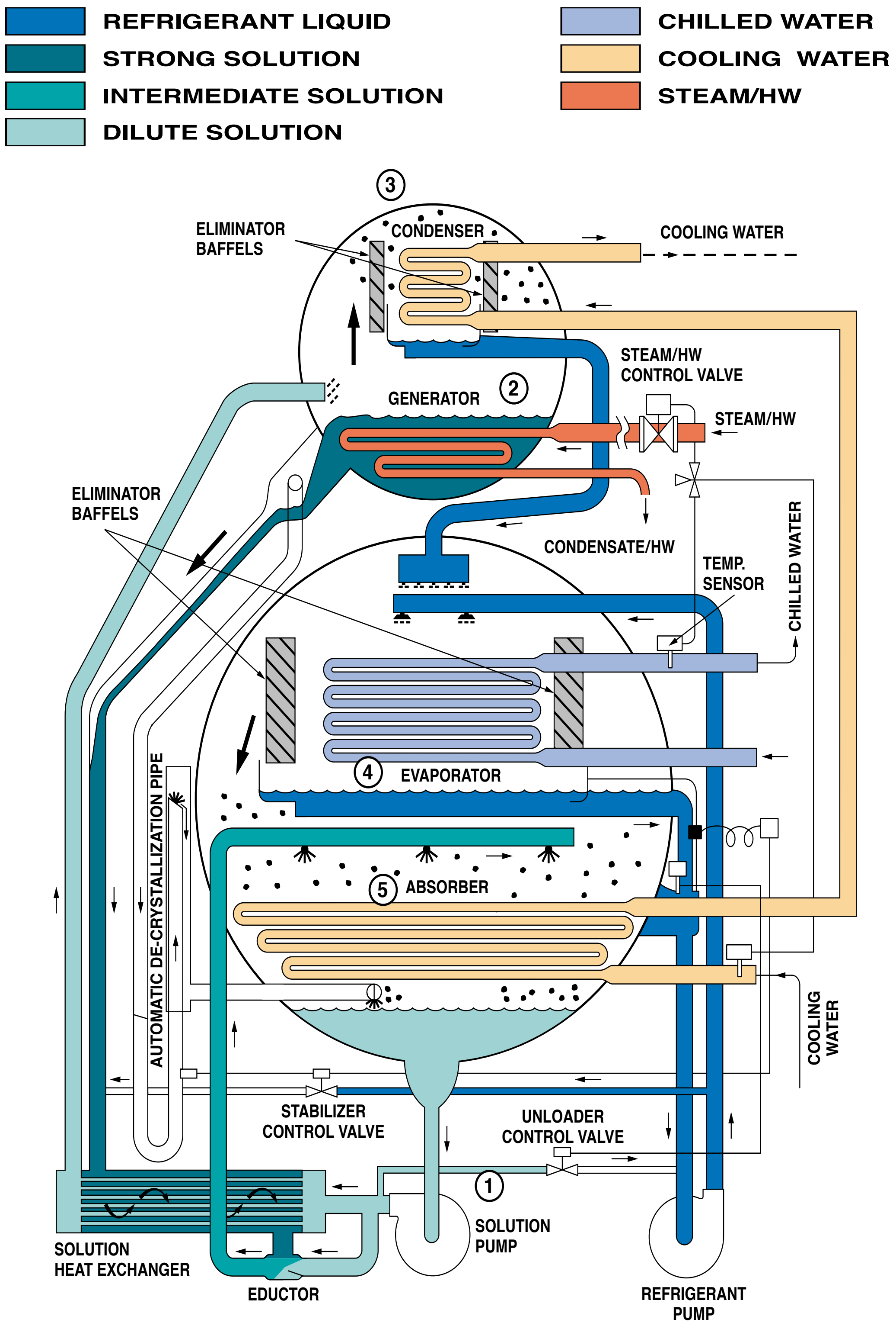

Figure 1-4 Complete chilling cycle of absorption refrigeration system (YORK-International 1997)

## 1.4 Atomization

From the working principle it is clearly understood that there are two chambers that use spray system, which are the evaporator chamber and the absorber chamber. In the absorber chamber a high concentration of lithium bromide solution is sprayed at the top of the absorber, i.e. spraying a viscous solution, which is the major focus of this thesis.

The break-up of large volumes of fluid into small particles is an important process in the absorber chamber as it enhances the absorption rate and the heat transfer rate by increasing the surface area to volume ratio.

The development of fuel atomizers in various industrial applications is beneficial towards finding an appropriate atomizer that can withstand the viscosity of heavy fuels. The principle of this development is similar to what is required by this research study to achieve, and hence the relation towards fuel atomizers (Sojka and Lefebvre 1990).

## 1.5 Aims and Objectives of the Research

The aim of this thesis is to investigate the atomization quality in the absorber chamber of the absorption refrigeration system, in order to enhance the coefficient of performance of the absorption refrigeration system. To achieve these aims, the following objectives need to be addressed:

- Perform a thorough review of the current absorption refrigeration system literature to obtain information on the operating parameters.
- From the finding of literature review, design a test matrix to investigate the influence of the operating parameters on the spray quality.
- Develop a PDA system with an appropriate sampling area within the

spray and to program the sampling times to insure that the characteristics of the spray are recorded.

- Use glycerol to simulate the viscosity of the lithium bromide solution, which is a corrosive fluid that will damage the testing equipment. The corrosiveness rate of lithium bromide is shown in Figure 1-5.
- Test each parameter individually to determine the relative influence of each parameter investigated. These parameters include pressure difference across the nozzle, partial vacuum condition, nozzle geometry, viscosity and the use of surfactants.
- Compare the results obtained from the experiments to the existing industrial applications, and provide recommendations to enhance the COP of the absorption refrigeration systems.

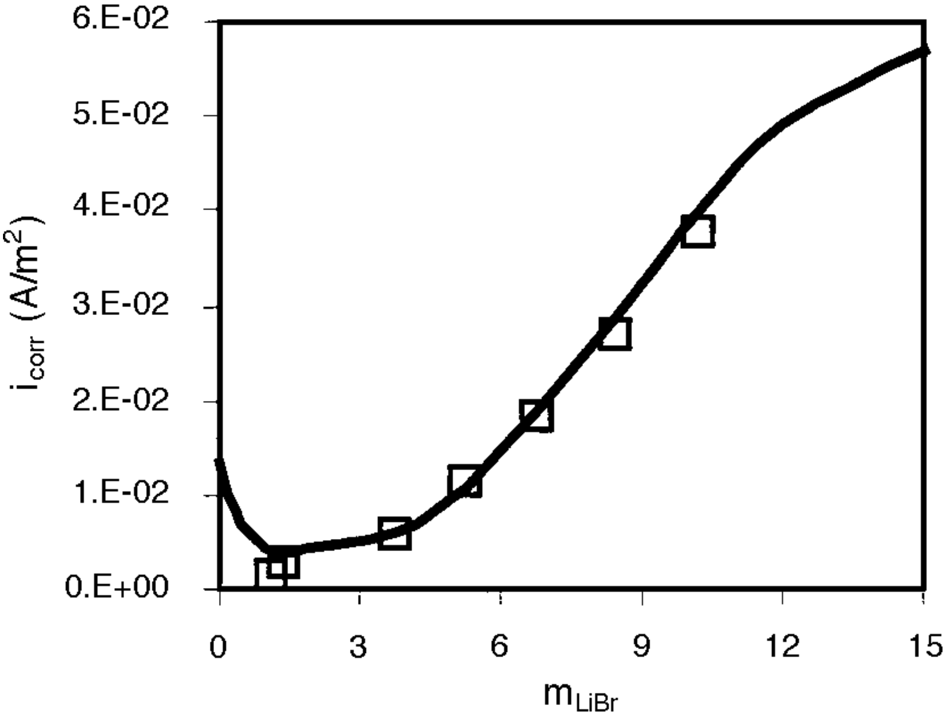

Figure 1-5 Corrosions rate for carbon steel in lithium bromide solution at different concentrations at 25°C (Anderko and Young 2000).

## 1.6 Structure of the Thesis

- Chapter two will discuss and review the literature on solar absorption refrigeration systems, and literature on atomization principles and operating parameters in a partial vacuum.
- Chapter three will reviews the operating variables and parameters of the experimental tests and their effect on spray quality. The limitations will also be pointed out and how they affect this thesis investigation.
- Chapter four describes the development of the equipment and apparatus at Cardiff University School of Engineering, used to study the behavior of sprays under a partial vacuum as well as explaining the working principles of the Phase Doppler Anemometry.
- Chapter five analyses the results of the experiments carried out to examine the effect of a vacuum on solutions undergoing pressure jet atomization at a variety of viscosities and surface tensions. The results will also discuss the effect of the atomizer geometry.
- Chapter six evaluates the results achieved from the experiments carried out and compares them to the absorption refrigeration systems industry. It will also provide some recommendations to enhance the performance of the absorption refrigeration systems.
- Chapter seven summarizes the work done and concludes the thesis outcome from the results obtained in the experimental tests. Finally the chapter provides a list of recommendations for further work that can be done.

# 2 Literature Review

## 2.1 Introduction to Absorption Refrigeration Systems

This chapter appropriately opens up with a discussion of absorption cooling on a historical perspective, absorption cooling systems in general and then go onto absorption refrigeration technology as the purpose of the study is to achieve greater COPs by specifically making adjustments within the absorber unit in the absorption refrigeration system.

Literature on such techniques like spray-technologies, nozzles, additive effect, falling film, other forms of atomization and techniques that have been scientifically considered in attempts to achieve high COPs will be reviewed in a critical analysis (Cheng et al. 2013).

The purpose of carrying out this study is to discover new ways at achieving greater COPs within smaller absorption refrigeration systems, so that such smaller units could be used for domestic and business cooling purposes. Creating smaller and cost-effective units is the main aim of solar cooling technologies that can show a marked increase in COPs.

It is envisaged that waste heat such as steam could be harnessed to achieve faster heat transfer across increased surface-areas, this being made possible by the adoption of improved spray technology instead of falling-film. Existing spray-technology must therefore be critically reviewed in order to come up with more efficient versions. That is the thrust of this research and it is hoped that successful implementation will lead to the creation of smaller absorption refrigeration units better suited for both domestic and commercial air conditioning.

A feasibility study of absorption cooling must be considered in the light of environmental factors. Fossil fuel consumption is a major global concern, which is why any meaningful contribution to cooling and heating technology must factor in environmentally friendly options. It has been noted as late as 2009 that solar thermal cooling systems are still in their infancy regarding practical applications, although the technology was sufficiently developed (Mateus and Oliveira 2009). Even in 2014 solar thermal cooling systems are still in the developmental stages, while they are also being used (Al-Alili et al. 2014).

This study is therefore relevant and of importance in seeking to develop solar thermal cooling technology further in order that domestic and business applications be advanced. If buildings are to take up solar energy cooling technologies, it is crucial that the units available be much smaller and yet more efficient. To this end this author seeks to make considerable changes within the absorber in the absorption refrigeration in order to achieve greater COPs leading to better efficiency.

It has been stated that the building cooling market still has a high potential for growth (Uppal and Muneer 1987; Market-Research 2013). This is the fact upon which author has sought to research through this study of development of more efficient absorption cooling systems by the development of smaller absorption refrigeration units of greater efficiency and easier use in buildings.

The core thrust of this study is to consider improvements on the coefficient of performance (COP) for absorption chiller technology for use in solar cooling systems by using a number of approaches, for example, improved spray-technology and nozzle systems.

## 2.2 Absorption Refrigeration System Background

Absorption technology can be traced back to 1850 when Edmond Carre developed the first absorption machine. This first machine was based on absorption technology facilitated by water and sulphuric acid (Foley et al. 2000).

In 1859 Ferdinand Carre successfully showed how water and ammonia could be harnessed to achieve refrigeration. It was not surprising therefore when in 1860 Ferdinand Carre successfully patented the first American commercial absorption unit (Foley et al. 2000).

In 1926 absorption refrigeration was made commercially available to the American market and up to the late 1960s American companies were leaders in the manufacture of absorption refrigeration worldwide. The technology used then for that purpose was the LiBr-$H_2O$ absorption refrigeration system (Sayigh and Mcveigh 1992).

## 2.3 Development of Solar Absorption Refrigeration

### 2.3.1 Problem statement

Absorption refrigeration systems are typically endowed with greater resource efficiency as opposed to other systems such as those using compressor technology; this is the reason in choosing to develop and improve on available absorption refrigeration technologies.

There is comparatively less loss of measurable fuel resource in absorption refrigeration technology applications, measured at between 5% and 10% of the fuel resource (Henning 2004).

Cost efficiency is enhanced by the fact that in comparison to electricity costs absorption refrigeration technology uses far less billable resource. An extra incentive, strongly considered, is the fact that the solar absorption cooling system being studied and improved upon actually makes ample use of otherwise waste energy in the form of waste thermal energy which includes geothermal energy, solar energy and waste heat from steam plants (Rodgers et al. 2012).

### 2.3.2 Objectives of Literature Study

The main objectives of this research are to study the effect of increasing the surface-area by way of spray nozzle techniques, thereby removing the inefficiencies of vertical falling film techniques. It is also a key objective to raise the COP of the absorption refrigeration system by adopting additives that in no way interfere with crucial heat transfer.

The aim of solar cooling systems is to harness solar thermal energy as a replacement of thermal energy so that fossil fuel is no longer burned. Solar energy could be used in any industrial process leading to a creation of heat rejected to the surroundings as waste, which then can be harnessed through proven absorption refrigeration cycle.

Absorption systems are an advantage as there is no longer need for use of expensive electricity off the grid and also in the perspective of environmental considerations. CFCs are therefore not used in the absorption system investigated; it is hoped therefore that this system be adopted for civilian and industrial uses.

The absorption process involves the absorption of the refrigerant that has vaporised, thereby reducing the pressure, while the temperature of the remnant refrigerant is greatly reduced directly as a consequence of the vaporisation. The refrigerant reaches saturation at some point and it is at this stage that separation must be effected so as to continue with the absorption process, LiBr-$H_2O$ is the refrigerant and absorbent of choice owing to its non-volatility. It is the absorber which has been identified as the most critical part in the absorption cooling system studied here. From Equation 2-1 it is observed that reducing the temperature of the absorber will increase the COP value (Herold et al. 1996). The condenser’s temperature could also enhance the COP of the absorption cooling system, but the absorber`s change in temperature induces a potentially higher thermodynamic gain.

This statement pinpoints the focus on the absorber as the critical part of the study. Theoretically a maximum COP for a single absorption system, a COP of 1.8 could be achieved, but the COP of actual absorption refrigeration systems is usually less than 1 (Ng et al. 1994).

$$COP = \frac{Q_e}{Q_g} = \frac{T_c(T_g - T_a)}{T_g(T_a - T_c)} \qquad \textbf{\textit{Equation 2-1}}$$

It is simpler to consider absorber action within a vapour refrigerant setting using a falling film, shown in Figure 2-1, of solution over cooled horizontal tubes whereby the absorption process exhibits heat that is simultaneously removed from the liquid film, causing an increased absorption rate. The extremely high recirculation rate required in this option to achieve optimal performance however makes this design unsatisfactory for practical considerations. Use of cooled rotating discs is another option, which has the advantage of requiring smaller unit-design, but this author has not chosen this option, as LiBr-$H_2O$ has been considered to be environmentally safer than $H_2O$-$NH_3$ mix (Pearson 2008; Warnakulasuriya and Worek 2008; Bourdoukan et al. 2009).

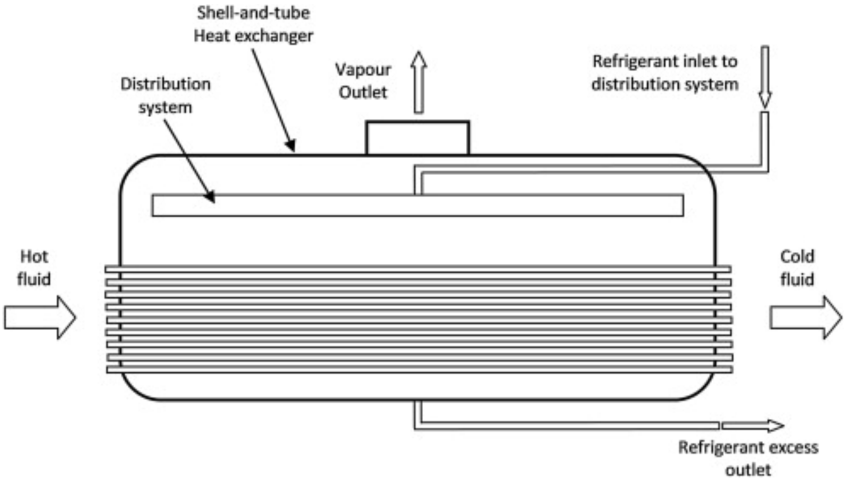

Figure 2-1 Horizontal tube falling film evaporator (Fernández-Seara and Pardiñas 2014)

The extreme heat used in the generator is used to evaporate the refrigerant part of the solution, expelled to the surroundings at the condenser and subsequently used to provide heat to the solution from the absorber. Then that heat is, in turn, expelled to the surrounding areas. To create greater COP, there must be some solution heat exchange to overcome resultant irreversibility. This makes it possible for the absorber size design to be reduced owing to less rejection of heat and less heat input at the generator site (Tatlıer and Erdem-Şenatalar 2004).

Different design options have been considered to compare the most efficient absorption cooling technologies especially the ones exhibiting the greatest COPs. Three methods have been considered, namely the development of better working fluids, improved absorber performance, and the invention of new advance cycles. This study seeks therefore to create greater awareness of environmentally friendly ways of designing absorption refrigeration systems making use of solar energy and smaller absorber units, which can be easily used for domestic and business use.

Solar energy is one source of heat for solar absorption refrigeration systems that provide air conditioning and refrigeration. There has been a plethora of research in the field of solar absorption cooling technology and it comes as no surprise that according to Balaras et al. (2007) there are at least 54 solar absorption air conditioning projects which are currently in operation throughout Europe and of these, at least 33 are based on LiBr-$H_2O$ absorption refrigeration technology, (Ali et al. 2008). Therefore the focal point of this study is on the LiBr-$H_2O$ absorption refrigeration systems.

The manner in which an absorption system operates is based on a vaporising liquid, which extracts heat at a low temperature that ensures the chilling effect. The vapour must then be compressed to increased pressure followed by condensation at a higher temperature, and this is the heat expulsion stage.

Those air-conditioning systems based on solar energy, provide heat energy as a by-product, which in turn powers the entire cooling process. There are at present two types of solar powered cooling systems, namely closed and open systems. Closed systems involve the production of chilled water for example by way of hot water or steam-driven refrigeration processes and it is the chilled water that is used in the provision of air conditioning. The most common application of this closed-system process is absorption refrigeration system, which is the chief concern of this study. Open systems involve processes like desiccant cooling whereby the refrigerant is water, which is always in direct contact with the ambient air.

Typically for air conditioning applications producing chilled water temperature above 5 ºC, LiBr-$H_2O$ liquid solutions are employed to produce refrigeration. Electricity consumption in absorption chiller systems is kept to a minimal internal pump requirement, and current technology that uses bubble pumps in fact does away with electric pumps altogether. Refrigeration in absorption refrigeration systems is brought about by an evaporation of the water at low pressures. Evaporated water is then absorbed within the absorber wherein further dilution of the LiBr-$H_2O$ solution takes place.

Solar cooling technologies clearly have great potential as the Australian study conducted by Al-Zubaydi (2011) has shown, and it is encouraging for this author that the modification of the absorber and the adoption of additives as well as spray techniques are bound to bear great results in the area of commercial domestic and business solar-driven air-conditioning and refrigeration.

The reasons for using this technology in Europe are the need for environmentally benign technologies and the availability of abundant sunshine in European summers. It is therefore a further incentive for the Middle East, which has much more sunlight over a longer period of the year to harness these technologies for air conditioning and refrigeration requirements. The single effect LiBr-$H_2O$ refrigeration system is noted for its low temperature operability wherein solar heated liquids provide heating for both the air circulating in the building and the LiBr-$H_2O$ absorption air conditioner to generate cooling. Solar energy according to studies by Ward and Löf (1975) was shown to provide up to two thirds of the total heating and cooling loads in their pilot project, (Ali et al. 2008). In this study it is expected that 100% solar energy can be used to provide heating and cooling loads.

## 2.4 Absorption Cycle Analysis

A product of refrigeration technology is chilled water, which results from the removal of heat as the water vaporises. The refrigerant liquid is forced into an evaporator where, at reduced pressures and temperatures, it absorbs the heat from the water passing through. After which there follows a vapour compression process where the vapour goes through compression and condensation at high pressures and temperatures, thereby causing a transfer of heat to cooled water. After that there must be a return of the condensed refrigerant to an evaporator, where at low pressures, it goes through the process of heat absorption from the chilled water flow (Sorensen 2007).

The absorption process must show the refrigerant vapour absorbed always at low pressure within the absorber; as this happens heat should be released. In absorption refrigeration cycles, there is high-pressure condensation of the refrigerant vapour and a dissipation of heat to the surroundings, so the refrigerant vapour must be vaporised at low temperature and low pressure resulting in absorption of heat from the chilled water flow.

During the refrigeration cycle there is an observed marked low energy requirement. An absorption refrigeration system is therefore based upon absorption of heat at high temperature and a rejection of heat at low temperature thereby providing the impetus for the heat pump. Two working fluids must be present, namely a refrigerant and a sorbent solution of that refrigerant. In the typical LiBr-$H_2O$ absorption refrigeration that this author has chosen to base this research upon, it is the water which is the refrigerant while the LiBr-$H_2O$ solution is the sorbent. Water is the chosen refrigerant because of its quality of high latent heat, while the non-volatile nature of LiBr makes it a stable and safe sorbent solution. This also determines what the parameters of pressure and temperature are within the absorber and condenser (Herold et al. 1996).

In order to reduce the energy required in the absorption refrigeration system, heat transfer parameters can be modified which is why this author has made it a significant experimental aim to tweak the mechanisms within the absorber. It is hoped that such modifications may also contribute to the solar-driven absorption refrigeration technology used in domestic and light commercial air-conditioning and refrigeration.

The surface area through which heat is transferred within the equipment can be increased although being incorporated within a smaller unit. The concept of increasing intestinal surface area by villi and microvilli is the inspiration for this author who seeks to introduce available spray technology in order to achieve a greater surface area within a smaller space to achieve the greatest COPs, culminating in the most efficient absorption refrigeration cycles. A recirculation process whereby the refrigerant liquid is resent over the heat transfer surface can achieve reduction of temperature differentials and heat transfer areas.

## 2.5 Combined Refrigeration Systems

Combined systems of solar cooling and heating have recently received increasing attention due to the rationality of harnessing all the types of energy available to these systems. Solar absorption cooling technology can only positively benefit from such research involving hybrid systems. An example is the study carried out by Li et al. (2012), whose approach is a solar-powered hybrid system providing both refrigeration and heating. Day-time application would provide 30kg hot water at 47.8 Degrees Celsius showing a mean COP of 0.34 while by night there would be a cooling capacity reaching 0.26 MJ/kg of adsorbent while the cooling capacity would be tagged at 1.3 $MJ/m^2$ of heat-collecting area.

Liu and Wang (2004), studied an alternative double-effect $LiBr-H_2O$ solar absorption system whereby natural gas was utilised. Air-conditioning, space heating and the provision of domestic hot water were all achieved. Feasibility and economy were both highly encouraging in this study according to simulation results.

There is a technique that was reported in the International Journal of Heat and Mass Transfer whereby the feasibility of droplets formed by swirl-jet nozzles in the improvement of absorption was examined (Warnakulasuriya and Worek 2008). The corrosiveness of liquids used in the absorber and the inefficient falling-film heat exchanger rates of vapour absorption are the main reasons that prompted this author to choose the absorber as the piece of equipment most requiring engineering and material changes.

The absorber therefore is reduced in size and consequently contributes to greater efficiency within the absorption refrigeration unit when using the spray technology rather than the falling film technology. The reduction in absorber unit size together with better anti-corrosive additives and greater surface area of heat transfer produce a more energy efficient technology with far much greater COPs, which appears to be the inspiration and motivation behind this study. Clearly achieving a greater total absorption area of the LiBr concentrated solution definitely leads to greater rates of absorption of water vapour by the sorbent (Warnakulasuriya and Worek 2008).

Introduction of the sorbent in the form of tiny droplets has been identified as a technique that clearly has the capacity to increase the surface area of heat transfer. The smaller and finer the droplets, the greater the rate at which the water vapour is absorbed; it is a scientifically proven fact that the spray absorption system produces a far much smaller absorber unit than the case would be with falling film system (Warnakulasuriya and Worek 2008).

Reports by Perez (2007) on the installation of a 12.31 kW cooling (Sayigh and Saada 1982) (3.5 RT, Refrigeration Ton, where 1 RT = 3.517 kW cooling) solar driven absorption refrigeration system in Riyadh, Saudi Arabia provide an insightful and proven application of solar absorption air conditioning technologies of high relevance to this study.

Flat collectors were used and spread over a total surface area of 56 $m^2$, as was a hot water storage tank whose volume was reported at 24 $m^3$. This system produced chilled water at temperatures of 17 C° for a continuous operation of 15 hours, (Ali et al. 2008).

Further studies included that of Al-Karaghouli et al. (1991) in Iraq which reported a system incorporating two absorption refrigeration systems of 211.02 kW cooling (60-RT) each, tube collectors, two thermal storage tanks whose volume was 15 $m^3$ and five cooling towers. A 49% daily average solar collection efficiency was achieved and the refrigeration system exhibited a COP recording of 0.618 with a solar heating fraction of 0.604, (Ali et al. 2008).

Henning et al. (2001); Mavroudaki et al. (2002); Bourdoukan et al. (2009) have studied solar desiccant cooling. Experimental studies have shown potentially encouraging COP values of 0.55 reported in a solar installation. There is a downside when it comes to humid regions, as the desiccant cooling system is influenced by the outside humidity ratio the most (Bourdoukan et al. 2009). In this study desiccant cooling will not be investigated, however the results would be compared against the desiccant cooling system.

A Single-Effect absorption refrigerator using aqueous lithium-bromide when tested experimentally can produce a COP ranging from 0.5 to 0.8, which in itself is a much sought-after value in cooling technologies. This COP is achieved by ensuring that the mass transfer area is as large as possible, hence the cooling coil and the droplets in the absorber should have a large surface area, (Aphornratana and Sriveerakul 2007). In this study the droplet size will be investigated to measure the surface area of the absorption medium to volume ratio. This in turn will enhance the solar absorption refrigeration systems COP.

A study done by Saravanan and Maiya (2003) shows that the COP is not significantly affected by the ambient temperature as the generator is electrically heated. This study was conducted using a LiBr $H_2O$ mix vapour absorption cooler operated by bubble pump, which had a COP of 0.38.

Water and air-cooled single and double-effect LiBr-$H_2O$ absorption refrigeration as studied by Marcos et al. (2011) whose aim is to optimise the

COP reported COP values of 0.74 to 0.85 when the condenser temperature is 25 °C, 30 °C, 35 °C and 40 °C and the mass fraction is 6.7%, 7.5%, 8.3% and 7%, respectively for water cooled single effect refrigeration.

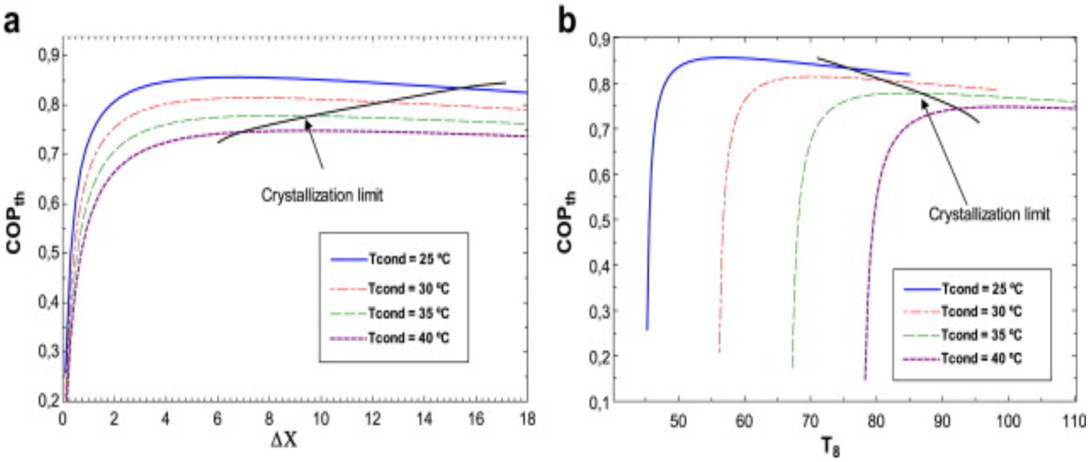

Figure 2-2 COP of a water-cooled single effect absorption refrigeration system (Marcos et al. 2011)

Air-cooled single effect refrigeration showed COP values of 0.65 to 0.72 at given conditions of $T_{COND}$ of 45 °C, 50 °C and 55 °C and the mass fraction is 6.5%, 5% and 3.9%, respectively. Water-cooled double effect refrigeration systems recorded a maximized COP value of up to 1.15 (Marcos et al. 2011).

Figure 2-3 shows a schematic diagram of a single effect absorption refrigeration system studied by Marcos et al. (2011), which also points out the area of research and is highlighted by a doted circle. The figure also points out the absorption chamber and how it fits in the absorption refrigeration system.

A good comparison of different types of solar refrigeration systems was done by Fong et al. (2010) which indicates that the COP of solar absorption refrigeration systems is very low compared to electric compression refrigeration systems. The latter has a COP of 4.658, which is 83% higher than the COP of 0.763 of the absorption refrigeration systems.

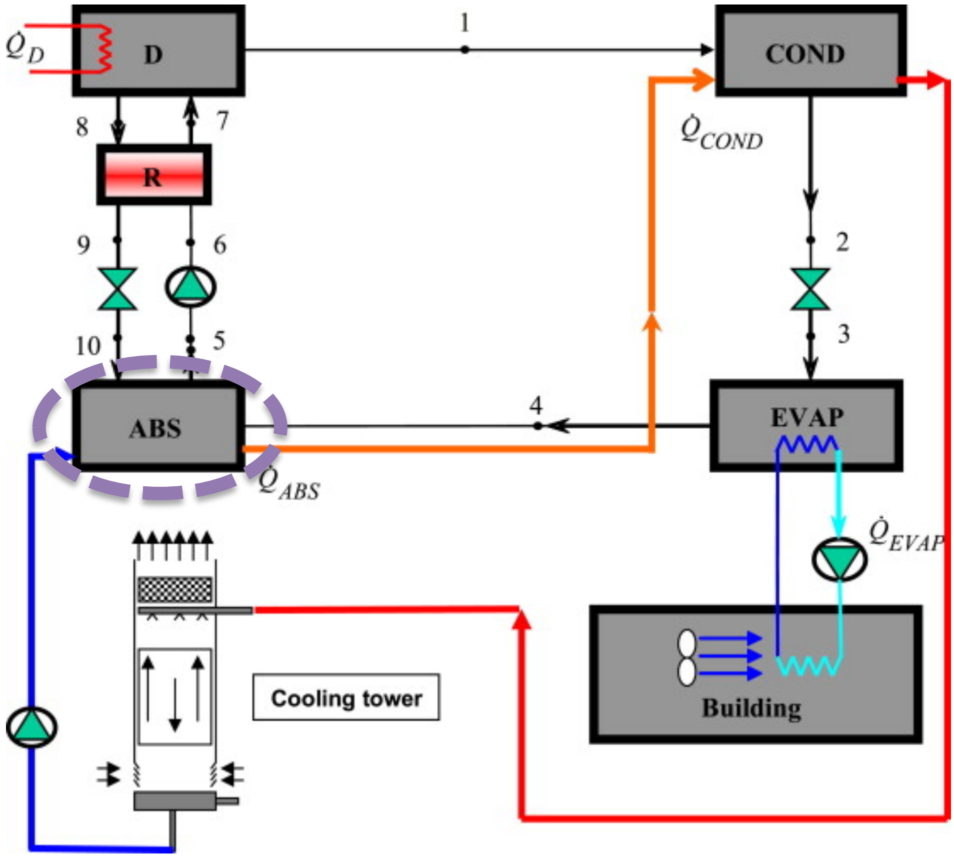

Figure 2-3 Water-cooled single effect absorption refrigeration system (Marcos et al. 2011)

## 2.6 Introduction of viable alternatives

It has been suggested that new generation air-cooled LiBr-$H_2O$ mix absorption refrigeration systems are a viable alternative to cooling tower-based technologies (Kim et al. 1999). Two methods have been developed and tested, namely:

1. Adoption of air-cooling mechanisms that fall within the existing LiBr-$H_2O$ crystallization limits is one method; this is achieved by such mechanical optimization, which would promote air-cooling along the

crystallization line. An example of such mechanical design alterations would be the adoption of high efficiency heat exchangers.

2. A more chemical based approach involving the use of additives would achieve the air-cooling effect at higher crystallization lines. The addition of other chemicals in order to shift the crystallization aspects of the conventional LiBr-$H_2O$ has been widely studied. Laboratory studies have successfully identified chemicals, which markedly shift the crystallization line within air-cooled absorption refrigeration systems.

The additive-effect on the absorption of water vapour into lithium-bromide solutions can be experimentally demonstrated with enough accuracy as shown by experiments observing such eight-carbon alcohol additives like n-octanol, 2-octanol, 3-octanol and 2-ethyl-1-hexanol by the use of a simple stagnant pool absorber. Mass transfer enhancement over the given effective range of additive concentration can thereby be plotted to show a clear increase in water vapour absorption rate with each increased additive concentration up until the 200 ppm range whereafter it stops (Kim et al. 1999).

Although the data provided by (Kim et al. 1999) is so important and perceptive, it lacks some critical detail and would require to have detailed analyses of the absorber chamber and its physical parameters. This study would investigate these parameters, which include, but not limited to, the size of the droplets, the velocity, the surface area of the absorption medium. This literature lacks the understanding of the spray absorber fundamentals in an absorption refrigeration system.

The chemical approach outlined is based therefore on the scientific principle that in order to improve the performance of absorption refrigeration systems there ought to be an improved performance of the absorber in use. Additive-effect has experimentally been shown to greatly improve water-vapour absorption in a very cost-effective manner (Glebov and Setterwall 2002). This literature uses a black box approach towards the working principle of an absorption refrigeration system. It lacks the understanding in how the additives help improve the atomization quality. They focussed their experimentation upon falling film hydrodynamics both based on additive-effect and without it. A mixture of water and glycerol was employed for the experiments with 1-octanol being used as a surface-active agent. A 6m stainless steel tube provided the falling film column. The experiment showed, provided both evaporation and absorption were absent, that the film was stabilised and there also was a reduction in heat and mass transfer as a result of adding surfactant into a falling liquid film (Glebov and Setterwall 2002).

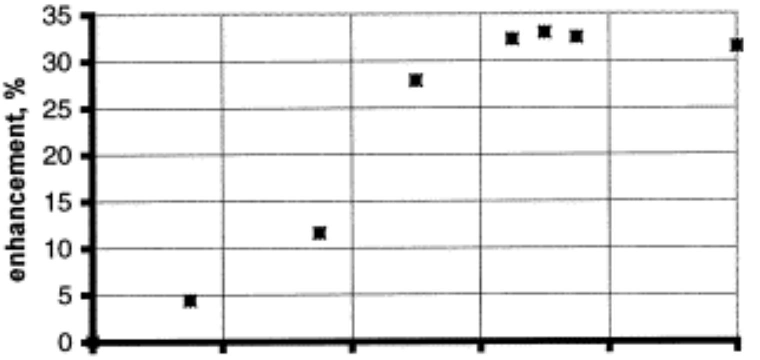

Figure 2-4 2-Methyl-1-pentanol effect on the enhancement ratio of absorption (Glebov and Setterwall 2002)

Glebov and Setterwall (2002) supported Kim et al. (1999) in proving the importance of adding additives to enhance the performance of absorption refrigeration systems as shown in Figure 2-4. Using the Additive Enhancement Ratio, (Glebov and Setterwall 2002) show the increase in performance.

$$\boldsymbol{AER} = \frac{cooling\ effect\ with\ additive - cooling\ effect\ without\ additive}{cooling\ effect\ without\ additive} \qquad \textbf{\textit{Equation 2-2}}$$

Using Equation 2-2 the AER reached up to 20% at the optimum additive concentration. In the other experimental series the additive was added to the refrigerant therefore the AER improved to 32%, which is a substantial improvement, (Glebov and Setterwall 2002).

Solar cooling technologies that are researched are those that primarily harness solar thermal energy, which is in abundance in the Middle East. It is hoped therefore that the suggestions made as a result of this research could be taken up in an economically productive manner.

The solar cooling system advanced in this study use solar heat to propel the cooling process. Although thermal-based cooling machines have been in existence and are shown in the review, the source of heat in these systems has always been either from the national grid or industrial waste based, and hence it is indeed a novel yet very feasible idea to suddenly switch the energy source to solar.

The system that this thesis is based upon is solar collectors, which try to achieve, medium temperature ranges of (100-250°C) that would result in enhanced overall efficiency of the cooling systems with specific relevance to greater heat transfer and greater COPs. Desiccant cooling is a piece of technology that harnesses water in the refrigeration process when it comes in direct contact with air. It is essentially an open cycle where hygroscopic material in the form of solid or liquid acts as the desiccant (Solair 2012).

## 2.7 Solar Powered Absorption Refrigeration Systems

It is envisaged that solar energy produced by way of solar panel technology provides the energy requirements of industrial, domestic and commercial buildings, and the part of the energy dissipated as waste heat is then captured to be used for provision of cooling, heating, dehumidification and hot water. This is where absorption refrigeration and desiccant humidifiers are used to provide the air-conditioning and ventilation in the building surroundings. As example to the waste heat, desalination plants produce 50-110 kWh/m$^3$ of thermal energy and heat loss of 475 kJ /kg steam (UNESCO 2013).

Solar thermal receivers are therefore applied to directly harvest the energy from the sun. This author seeks to research by way of available literature and laboratory experimentation the manner by which both solar and reject energy are harnessed using heat-based absorption refrigeration technologies in order to provide efficient levels of COP. It is the aim of this author therefore to contribute towards the perfection of viable micro scale absorption refrigeration capable of domestic and light commercial use.

It is the aim of the experiments to drive energy into the system by way of solar collectors that then provides heated water for the system. Heat drives the absorption refrigeration system to produce chilled water, which is used for ventilation and air-cooling purposes. It is an observation of the system that there is hardly any use for mechanical energy; savings also of electrical energy are made which is an immense contribution that absorption refrigeration technology driven by solar energy can make both to the environment at large and to the quality of life around the world. Additionally the use of lithium bromide water absorption refrigeration further enhances environmental performance.

Absorption refrigeration systems that make use of solar energy to produce the heat energy, which will bring about refrigeration are what this research has attempted to analyse. Higher coefficient of performance is what this author has sought to achieve by using water as a refrigerant and aqueous lithium bromide as sorbent and by applying workable spray techniques to increase surface area of heat transfer while achieving small unit design. In the evaporator part of the unit this author seeks to use spray nozzles to achieve greater rates of evaporation. Additives such as lithium chromate are used to inhibit corrosion within the equipment.

## 2.8 Atomization in the absorber

The conventional absorber used in commercial absorption refrigeration systems is falling-film heat exchangers, which absorbs the refrigerant (LiBr-$H_2O$) at a certain rate. Therefore if this rate could be increased by introducing the absorption fluid in form of the fine droplets, the absorber could be reduced in size and its performance could be increased, (Warnakulasuriya and Worek 2008). Figure 2-5 shows droplet size of a high viscous solution sprayed at 65 °C with three different nozzles.

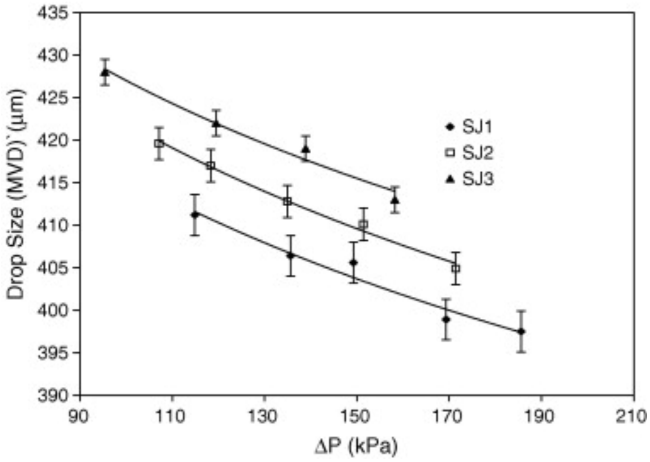

Figure 2-5 Drop size information at 65 °C nozzle temperature for three different nozzles (Warnakulasuriya and Worek 2008).

It is evident that an increase in the absorption surface area of the LiBr fluid would increase as a result in the rate of absorption of the vapour. Therefore to increase the rate of absorption the droplet size should decrease hence an increase in surface area, (Warnakulasuriya and Worek 2008).

The temperature of a droplet in the absorber would be determined by calculating the latent heat loss due to its evaporation and the heat conduction due to the temperature difference between the droplet surface and the surroundings, (Kim et al. 2001).

$$Heat\ gained\ from\ surroundings = 4\pi a^2 k_g \left(\frac{dT}{dr}\right)_a$$ ***Equation 2-3***

$$Heat\ lost\ to\ surroundings = h_{fg}\dot{\mathrm{m}} = 4\pi a^2 D_v h_{fg} \left(\frac{d\rho}{dr}\right)_a$$ ***Equation 2-4***

Figure 2-6 explains equations 2-2 and 2-3, in which the droplet initial temperature at the steady state is not affected by its initial size, taking into consideration that the vacuum chamber is at saturation, however the smaller droplets will decrease in temperature faster (Shin et al. 2000).

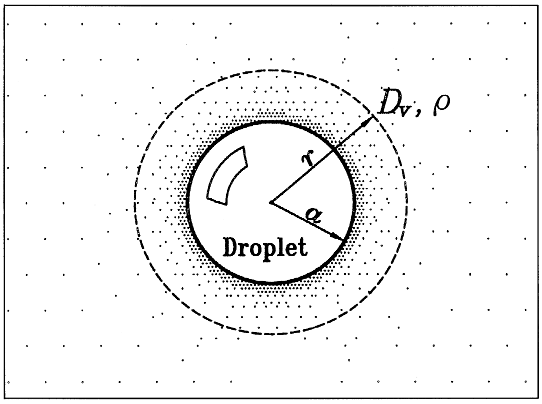

Figure 2-6 Heat loss and gain from surrounding

## 2.9 Atomization Background and Theory

Jet break-up is the mechanism by which liquid jets are injected into a gas medium causing atomization by the aid of aerodynamic forces, which overcome the internal forces of the injected fluid. The jet break-up at low mass flow rates initiates further downstream away from the orifice and at the liquid surface, and at very high mass flow rates, breakup can initiate much closer to the tip of the nozzle.

Operating parameters and fluid properties influence jet atomization quality. Operating parameters include mass flow rate and fluid input pressure, while the fluid properties are viscosity, surface tension and density. The quality is also affected by the geometry of the nozzle such as the orifice diameter.

Numerous studies and investigations on the jet break-up has been done (Lin and Reitz 1998; Eggers 2004), as well as Lord Rayleigh's significant studies on jet break-up were reviewed and analyzed (Pimbley 1976). The atomization of liquid jets have been rigorously studied for various industrial jet break-up atomizers (Li 1995) such as the Y-jet atomizer and hole type atomizer (Song and Lee 1996; Hiroyasu 2000). Recent studies have focused on numerical modeling on jet break-up mechanism (Xu et al. 2005).

### 2.9.1 Primary Atomization

According to Lefebvre (1989) primary atomization is the consequence of internal forces acting on the liquid as it exits the orifice of the atomizer. The operating conditions and the fluid characteristics influence the quality of primary atomization. The literature on primary atomization suggests that it is not fully understood; however it is known that it occurs closer to the nozzle (Lefebvre 1989; Nasr et al. 2002; Shinjo and Umemura 2011).

### 2.9.2 Secondary Atomization

Secondary atomization is defined by Lefebvre (1989) as the atomization set-off by external forces such as the aerodynamic forces. Primary atomization produces relatively large droplets, which will break-up further by secondary atomization. This break-up will only occur if the external forces acting on the liquid droplets is greater than the internal forces (viscosity and surface tension) of the droplet itself (Guildenbecher et al. 2009). The Weber number explains and relates to this phenomenon as Equation 2-5 demonstrates.

$$We = \frac{\rho_l U_{av}^2 d_{10}}{\sigma_l}$$ ***Equation 2-5***

A critical Weber number is when the external forces overcome the internal forces of the droplet and as a consequence break-up occurs (Kay 2006; Zhao et al. 2011). A critical Weber number of 11 and 12 is mostly cited in the literature for relatively low viscosity fluids (Nasr et al. 2002; Kay 2006). Beyond the primary break-up region there is confusion about the breakup-length trends. Haenlein (1932) reported that the jet breakup length increases again with rising droplet velocity at the secondary break-up region. The physical properties of the liquid affect the break-up and can be explained by the “tree regime” mode shown in Figure 2-7.

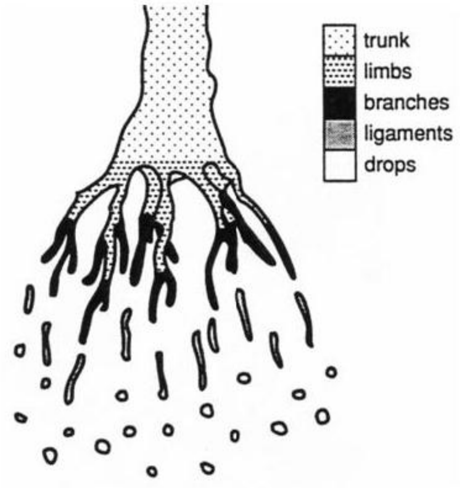

Figure 2-7 Tree regime mode of break-up

### 2.9.3 Atomization in the absorber chamber

Atomization is observed to be in the highest degree with maximum effect when droplets are present; it is such small droplet sizes that achieve highest flow rates and for this reason this author has chosen to critically analyse literature from various researches on pressure-swirl atomizers and Delevan nozzles.

The substitution to droplets from falling film improves the rate of absorption in conventional absorbers by means of increasing the total surface area. Higher flow rates are also observed to be achievable regardless of extremely viscous solutions used (Warnakulasuriya and Worek 2008).

Figure 2-8 shows an absorption refrigeration system implementing the spray jet technology, which replaced the falling film in the absorber. Using this type of technology can increase the total surface area by 200 times according to Warnakulasuriya and Worek (2008).

Studies were carried out which confirmed that the flow rate of the nozzle is directly related with the nozzle pressure and any change in nozzle pressure directly affects the flow rate and the nozzle performance. Drop absorption is directly determined by drop velocity; it has been demonstrated that lower velocity causes better absorption while higher velocities cause markedly lowered absorption rates (Warnakulasuriya and Worek 2008).

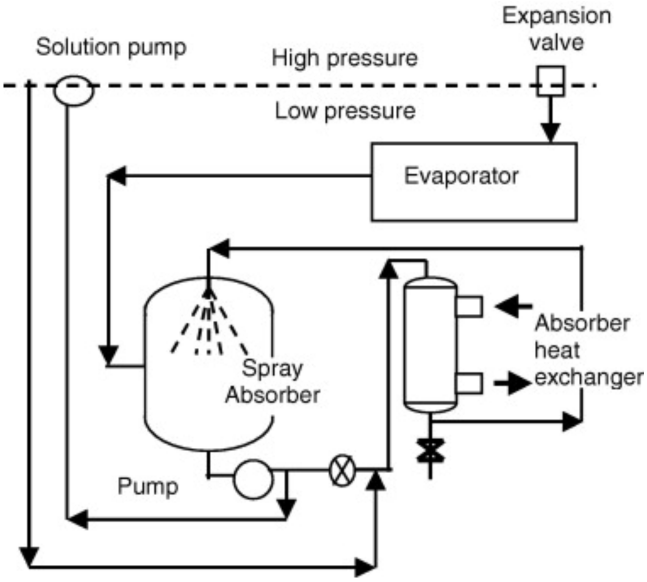

Figure 2-8 Spray absorber with solution sub-cooler.

## 2.10 Parameters influencing spray quality

There are factors that affect atomization, such as the flow inside the atomizer, viscosity and surface tension. The parameters that (Warnakulasuriya and Worek 2008) investigated are drop size, drop velocity, spray angle, number density and drop size distribution. Also the factors that effect drop size were only considered. Therefore to measure the drop size and drop velocity a Phase Doppler Particle Analyser (PDPA) was used (Warnakulasuriya and

Worek 2008). In this study a similar approach will be used to investigate the drop size and velocity using a Phase Doppler Anemometry (PDA).

### 2.10.1 Viscosity

Lefebvre (1989) states that viscosity is an important property of a liquid, which affects the droplet size distributions and the flow rate through the nozzle. He also defines viscosity as a liquid property that has a marked effect on atomization quality on spray angle and which also affects pumping power requirements, and is also highly dependent on liquid temperature.

Viscosity is considered to be a stabilizing force that resists liquid break-up; therefore to have a jet break-up the aerodynamic forces should be greater than viscosity force (Petersen et al. 2001b).

The viscous-shear stress force is the net momentum transport from high velocity to low velocity regions, which is in the direction of flow. It can be calculated using Equation 2-6 (Rogers and Mayhew 1992; Holman 2002).

$$\tau = \mu \frac{du}{dy}$$ ***Equation 2-6***

The dynamic viscosity of the LiBr-$H_2O$ solution mix with a 60% concentration at 60°C is measured to be 0.00348 $kg.m^{-1}.s^{-1}$ (Wimby and Berntsson 1994). The viscosity of glycerol-water solution was also measured and is confirmed by Aliseda et al. (2008). Dynamic viscosity Equation 2-8 can be calculated from the kinetic viscosity, which is calculated using Equation 2-7.

$$\nu = Ct$$ ***Equation 2-7***

$$\mu = \nu\rho$$ ***Equation 2-8***

Viscosity mainly affects the primary atomization, as increasing viscosity of the liquid used enhances the resultant diameter of the jet atomization (Santangelo and Sojka 1995).

### 2.10.2 Density

The motion of molecules within a flow of liquid is random due to the high density; therefore the forces acting between them determine the motion of molecules (Michelson 1990).

### 2.10.3 Surface Tension

Surface tension is a property that resists expansion of a liquid surface area. Surface tension must be overcome by aerodynamic, centrifugal, or pressure forces to achieve atomization (Lefebvre 1989; Dorfner et al. 1995)

Research carried out shows that there is a direct relation between SMD and surface tension. It was found by Simmons and Harding (1981) that $SMD \propto \sigma^a$, where a is 0.19, however 12 findings suggest that $SMD \propto \sigma$. Another study which supports Simmons and Harding (1981) found that $SMD \propto \sigma^a$, where a is 0.25 (Jones 1982; Lefebvre 1983). Therefore it is safe to say that increasing or decreasing the surface tension will affect the SMD in an equivalent manner (Lefebvre and Wang 1987).

### 2.10.4 Additives

The contamination of the surface of any liquid by adding a solvent or surfactant will have an affect on the properties of the surface, thus it will have a significant influence on the break-up of the liquid during atomization (Michelson 1990).

Eight carbon alcohol additives such as 2-ethyle-1-hexanol (2EH), prove to have a great impact on the absorption process in an absorption refrigeration system (Kim et al. 1999), The eight carbon alcohol additives effects is also supported by Yoon et al. (1999). Although the two studies confirm the effect of the additives on the absorption rate, they do not investigate the effect on the droplet diameter and SMD, whereas this study will investigate these effects.

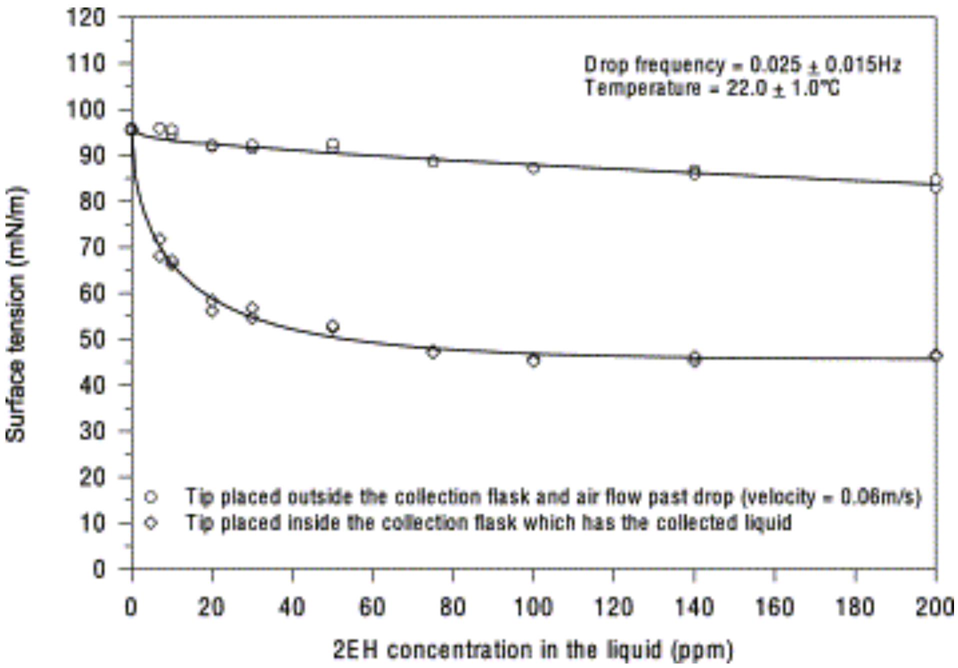

Figure 2-9 Surface tension of 60% LiBr solution versus 2EH concentration in the liquid (Yuan and Herold 2001).

The surface tension of the LiBr-$H_2O$ solution with a 60% by mass 2EH was found to be approximately 45 mN/m from Figure 2-9. The study done by Yuan and Herold (2001) also suggests that adding more than 80ppm of the 2EH will not have any effect on the surface tension as it is reaching an asymptote.

## 2.11 The Vacuum Effect

In absorption refrigeration system, the absorber chamber produces a vacuum that is created by the affinity of lithium bromide towards water. When it comes to a vacuum, the characteristics of any fluid are affected directly and indirectly such as the evaporation temperature. Water evaporates at 100°C at 101.4

kPa which is at atmospheric pressure, but under a partial vacuum of 3 kPa water evaporates at 24°C (Cengel and Boles 2007).
The vacuum will also have an affect on the Weber number of the liquids used, as well as the Reynolds number, where the aerodynamic forces are relatively lower which in turn cannot overcome the internal forces of the given fluid (Lefebvre 1989).

The study done by Kim et al. (2001) only considers spraying water into a vacuum, with their results being used to compare the results obtained in the initial experiments that use water as a nominal condition.

## 2.12 Summary

Absorption refrigeration systems are less efficient compared to compressor refrigeration system, with the COPs averaging 0.5 and 3.5 respectively. On the other hand, the absorption refrigeration systems can utilize waste energy such as solar energy as the driving load.

There are a number of parameters that influence the atomization quality, and they can be divided into three groups. First are the operating conditions, and the second one is the liquid properties such as viscosity and surface tension. The third parameter is the nozzle geometry. The effect of the vacuum on the atomization process is investigated by this research to help improve the absorption refrigeration systems, by increasing the COP.

The available literature studies the absorption refrigeration system and the enhancement of COP by using spray technology, which replaces the falling film technology. It also studies the effect of the internal characteristics of the lithium bromide solution and the effect of adding additives as surfactants to it, in the expectation of increasing COP. This thesis study combines the two approaches and closes the gap in studying the effect of surfactants on atomization.

# 3 Experiment Conditions

This chapter introduces the experimental conditions and experimental limitations as well as the examination of the effect of a number of parameters on the atomization quality of a liquid spray. These parameters were tested under atmospheric pressure and vacuum (partial-vacuum) conditions to meet the aim of this thesis. The parameters that are examined in this chapter are based on the deductions following careful analysis of the literature discussed in Chapter 2.

This chapter will start by identifying the experimental limitations, boundaries and validity of the tests. In addition it will focus on the nominal conditions that are the base line for the rest of the experiments. Then the chapter will continue to outline the conditions and key variables designed to investigate the effects of the chosen parameter on the quality of atomization within the limitations and boundaries given.

## 3.1 Experiment Boundaries and Limitations

There are numerous boundaries and limitations that affect the experiment runs, which can be considered to be physical pertaining to the hardware used. A main limitation is time required for the experiment to run which is considered an intangible factor. Time is considered to be a limiting factor because of the nature of the experiments carried out. The LP-Rig under a partial vacuum will start to get filled up by the solution, which will therefore affect the PDA readings.

### 3.1.1 Experiment Tests

Thousands of experiment runs and repeats could have been executed to study the effect of the parameter on the quality of atomization of the liquid spray. To perform these experiments proved to be impractical, therefore a test matrix was established to facilitate an ideal minimum number of experiments.

The build up to the matrix was influenced by a number of factors, such as the realistic experiment time available and the number of nozzles to be used. As explained earlier, the experiment consisted of a number of PDA tests and each test had two runs. Therefore the preliminary tests were repeated five times to show consistency and once this is achieved, the remaining tests were executed once. However some of the tests were repeated for a second time to prove consistency, and these were selected on an individual test-by-test basis.

### 3.1.2 Data Collection Validity

The PDA was setup to collect data in the following manner: 10,000 samples at each traverse point or timeout after 5 seconds, and then moved to the next traverse point. Due to these arguments the data rate was considered to be relatively low if it were at around the 100Hz mark. As time was considered to be a limitation of the LP-Rig the software was set to time out after 5 seconds for each measurable point.

The validity of the drops was then taken into consideration to show if the traverse points are on the spray plane. This was determined by the data rate recorded for each point and can be shown in the results. These steps were mandatory in order to validate the findings in the results chapter.

## 3.2 Nominal Conditions

The initial experimental conditions were set up to be a control for the rest of the experiment parameters, or also could be defined as the reference for the subsequent experiments. Hence, these conditions were used as a comparative gauge for subsequent test runs under different parameters. The conditions were also made to imitate the conditions in the absorber section in an absorption chiller, as described in Chapter 2.

The experiments consist of two PDA runs, which were attempted in sequence. The first run was attempted under atmospheric conditions and the second was attempted at a partial-vacuum. These two runs were considered to be one test.

The test matrix for the nominal condition experiment in Table 3-1 summarizes the experimental conditions described above. Water was considered to be used as the benchmark liquid as it has got a neutral viscosity and most of the parameters are compared to water. On the other hand some literature uses water to test spray characteristics in a vacuum.

Table 3-1 Test matrix for nominal condition experiment

| Fluid | Nozzle | Pressure | |
|---|---|---|---|
| Water ($H_2O$) | Delevan WM054 | ATM (1.01 bar) | Partial-Vacuum (0.03 bar) |
| | Delevan WM104 | | |
| | Delevan WM1154 | | |

## 3.3 Viscosity Influence

Viscosity was defined to be a major parameter that will influence the spray characteristics and the quality of atomization as explained in Section 2.9.1 Viscosity will affect the droplet size within the liquid spray and affects the flow rate through the nozzle (Lefebvre 1989).

Fluid viscosity will oppose the aerodynamic forces acting on the spray fluid such as the inertia forces, which will resist the fluid atomization. Therefore to overcome this resistance the aerodynamic forces should be relatively larger than the resistance implemented by the viscous force (Petersen et al. 2001a). Therefore, under vacuum conditions the expected SMD outcome is relatively larger.

The Ohnesorge number (Oh), which is a dimensionless number that relates the viscous forces defined by Reynolds number to the inertial and surface tension forces defined by the Weber number, was used to demonstrate the effect of viscosity on the quality of atomization. Ohnesorge number:

$$oh = \frac{\sqrt{We}}{Re}$$ ***Equation 3-1***

$$oh = \frac{\mu_l}{\sqrt{\rho_l \sigma_l d_{10}}}$$ ***Equation 3-2***

A higher Ohnesorge number suggests a larger influence of viscosity and it is an apt tool to relate the effect of viscosity on the dispersion of liquids in gases (Ohnesorge 1936; Lefebvre 1989).

The experiments were carried out using water and water-glycerin solution as the test fluids. This was done to reduce damage to the equipment used. Li-Br concentrate solutions were considered to be hazardous to the testing equipment such as the nozzles, water pump, vacuum pump and the surrounding environment. Nevertheless after each test run the LP-Rig was flushed and cleaned by water, and the vacuum pump was kept running for a further 30 minutes to evaporate the water trapped in the pump from the experiments.

### 3.3.1 Variable Viscosity Mixture Preparation and Measurement Technique

Water and glycerol solution were mixed to create subsequent fluids of variable viscosity. These fluids were created according to volume ratios. The first fluid had a 20% glycerol to water by volume and the second had a 50% glycerol to water by volume.

A calibrated Cannon-Fenske Viscometer Tube was used to measure the kinematic viscosity. The measurements were undertaken three times and an average was taken to insure consistency with the reading. The three tests had an average ± 5% error.

The dynamic viscosity had to be calculated using Equations 3-3 and 3-4.

$$v_l = Ct$$ ***Equation 3-3***

Where C is the Cannon-Fenske Viscometer Tube constant and t is time in seconds.

$$\mu_l = v_l \rho_l$$ ***Equation 3-4***

### 3.3.2 Viscosity Test Matrix

The test matrix for viscosity is summarised in Table 3-2. It shows the number of runs that have been tested.

Table 3-2. Test matrix for testing the viscosity parameter

| Fluid | Nozzle | Pressure | |
|---|---|---|---|
| 20% Glycerol-water by volume | Delevan WM054 | ATM (1.01 bar) | Partial-Vacuum (0.03 bar) |
| | Delevan WM104 | | |
| | Delevan WM1154 | | |
| 50% Glycerol-water by volume | Delevan WM054 | ATM (1.01 bar) | Partial-Vacuum (0.03 bar) |
| | Delevan WM104 | | |
| | Delevan WM1154 | | |

## 3.4 Additive Stimulus

As suggested by literature adding surfactants to the solution mix will alter the internal characteristics of the solution, and this mainly affects the surface tension force. This will change the Weber number of the solution and can be shown then to enhance the atomization. The surfactant of choice was 2-ethyle-1-hexanol (Yuan and Herold 2001) which is a deforming and wetting agent.

Table 3-3 Test matrix for testing the surfactant parameter

| Fluid | Nozzle | Pressure | |
|---|---|---|---|
| 20% Glycerol-water by volume + 50% by mass 2EH | Delevan WM054 | ATM (1.01 bar) | Partial-Vacuum (0.03 bar) |
| | Delevan WM104 | | |
| | Delevan WM1154 | | |
| 50% Glycerol-water by volume + 50% by mass 2EH | Delevan WM054 | ATM (1.01 bar) | Partial-Vacuum (0.03 bar) |
| | Delevan WM104 | | |
| | Delevan WM1154 | | |

The test matrix for surfactant test is summarised in Table 3-3. It shows the number of runs that have been tested, and the varied solution-mix used.

## 3.5 Temperature Effect on Atomization

An important parameter to investigate is the liquid temperatures input and how it may affect the atomization quality in terms of SMD and spray distribution. A simple but effective test experiment is displayed in Table 3-4.

Table 3-4 Test matrix for testing the heat input factor

| Fluid | Nozzle | Pressure | Temperature |
|---|---|---|---|
| Water ($H_2O$) | Delevan WM104 | Partial-Vacuum (0.03 bar) | 17°C to 40°C |

## 3.6 Pressure Difference Effect

The pressure difference effect can be characterised as the driving input pressure as the partial vacuum presser cannot be altered to maintain the absorption refrigeration cycle.

No test matrix was produced to test this parameter as it can be driven from the previous sections and compared to the nominal condition.

## 3.7 Evaporation Effect on Atomization

From the data provided by the literature, the water molecules are expected to flash atomize when sprayed in a partial vacuum of 0.03bar, where water molecules evaporate at 24°C. Therefore an experimental procedure was conducted to test this phenomenon and how it would affect the atomization quality.

The experiment was to conduct a droplet evaporation rate over a 30-minute period at vacuum condition, observing every 5 minutes, to get sufficient data while also being practical with the time available. A hydrophobic tape was used to create droplets of various sizes on the surface of a glass plane. Then it was placed inside the LP-Rig Figure 4-1 and the test rig was then vacuumed to the required pressure. Photographic comparisons then determined the effect of the evaporation rate on the atomization quality.

# 4 Methodology

## 4.1 Introduction

This chapter describes the development of the equipment, apparatus and procedures used to study the behavior of sprays under a partial vacuum. The sub-systems will be detailed and the principles of the Phase Doppler Anemometry (PDA) will be explained. At the end of the chapter the data collection process and the post-processing techniques are outlined.

## 4.2 Constant Volume Low-Pressure Rig

A Constant Volume Low-Pressure Rig as shown in Figure 4-1 was used as a controlled environment for the experiment, which enables control of the different variables that affect the characteristics of the sprays. This rig was designed and manufactured at Cardiff University for a different purpose during a previous PhD research. It was used as a High-Temperature High-Pressure Rig for fuel injection studies on gasoline SI engines (Comer 1999).

The LP-Rig is cylindrical in shape and has a hollow center of a known volume, with four windows allowing access to different types of optics such as laser sheets and PDA. Three of the windows are 130 × 220mm allowing maximum observation area, while the fourth is 75 × 220mm. The smaller window is configured to house different instrumentations to measure pressure and temperature within the low-pressure rig (Kay 2006). The Rig with the integrated components is displayed in Figure 4-19.

The windows are designed in a manner that two of the 130 x 220mm windows and the 75 x 220mm window are perpendicular to each other, and the remaining 130 x 220mm window is at an angle of 70°, which is recommended for the use of PDA as demonstrated in Section 4.3. The windows are made of silica quartz and to minimize reflections from the quartz windows, they are polished and maintained at a high transparency.

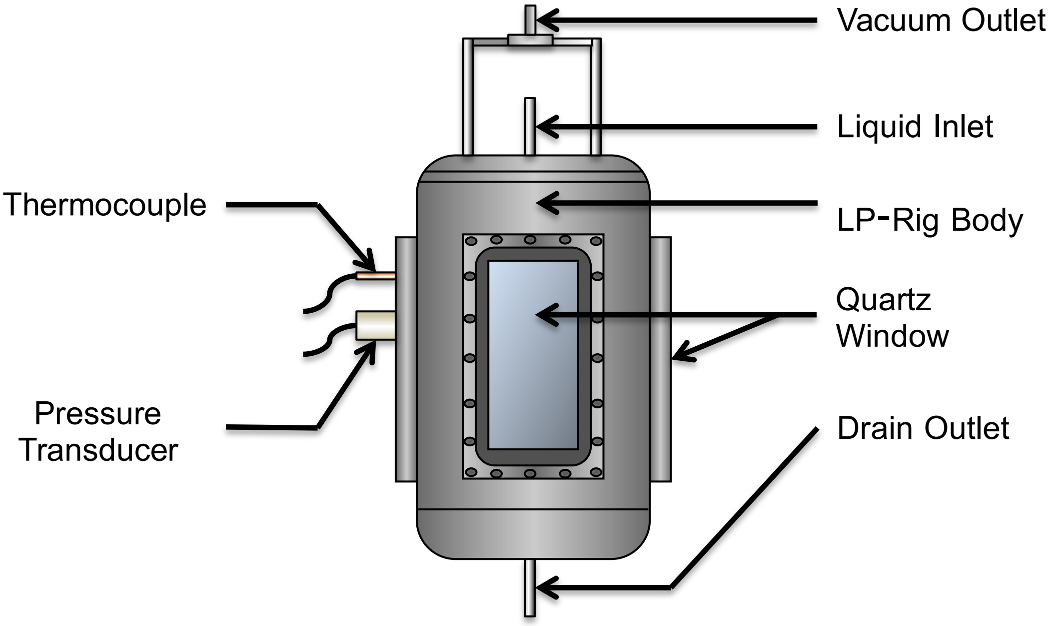

Figure 4-1 Schematic of Low Pressure-Rig

The silica quartz allows a wide range of wavelengths to be transmitted through it. During PDA analysis the transmission is greater than 90% for wavelengths` range of 200 – 2200nm (Kay 2006), where the wavelengths in use are 514.5nm and 488 nm for the green and blue beams respectively (Dantec-Dynamics 2006) which are within the range stated by Kay (2006). The refractive index of the quartz is shown in Figure 4-2 (Hecht 2002).

The Rig has air vents on the circumference of the top lid that are not visible from the observation windows. These vents are connected to a vacuum pump to generate a partial vacuum of 0.03 bar. The positioning of the vents achieves and maintains a constant low pressure throughout the experiment. Nozzles are also mounted in the top lid of the Rig, which can be easily changed from the inside. Figure 4-3 shows the nozzle position and the air vents within the Rig.

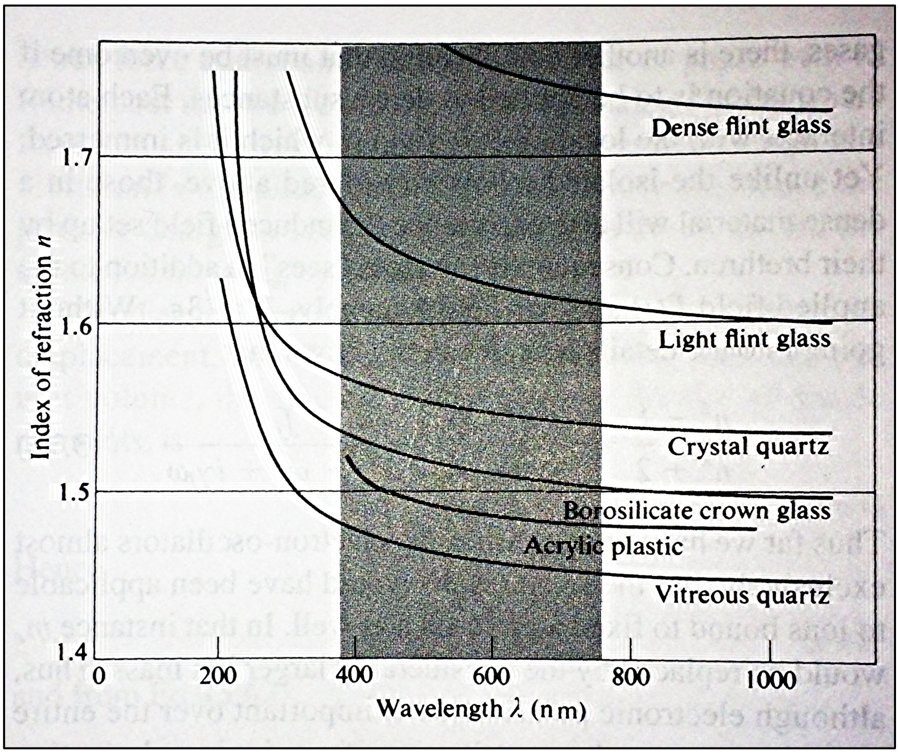

Figure 4-2 The wavelength dependency of the index of refraction for quartz (Hecht 2002).

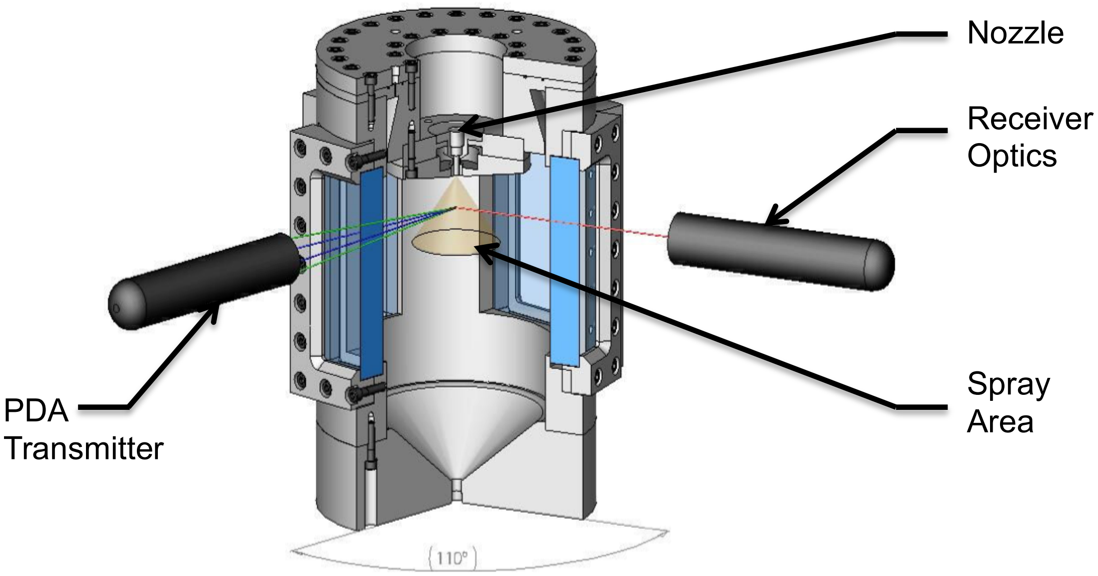

Figure 4-3 Intersection of the LP-Rig with the PDA system (Kay 2006)

### 4.2.1 Liquid Injection Nozzles

Delevan nozzles were used in the experimental procedures as the main atomizers. Delavan Spray Technologies, which is a division of the Goodrich Corporation, supplied the nozzles. The firm is known as one of the world leaders in the manufacture of high quality spray nozzles (Delavan.co.uk 2012).

Three main nozzles are used in the experiments that are interchangeable with each other. Two of the nozzles are Delevan nozzles and the third is a swirl nozzle; details and specifications are in Table 4-1.

Table 4-1 Nozzle Specifications

| Parameter | Delevan WA054 | Delevan WA104 | Delavan WA1154 | Delavan WM3006 | Swirl Nozzle RBQ1160 |
|---|---|---|---|---|---|
| *Cone Angle* | *40°* | *40°* | *40°* | *60°* | *60°* |
| *Orifice Diameter* | 0.8 mm | 1 mm | *1.8 mm* | *2 mm* | *2 mm* |
| *Max. Input Pressure* | *3.7 bar* | *3.7 bar* | *3.7 bar* | *3.7 bar* | *3.7 bar* |
| *Flow Rate (8 bar)* | 2.48 l/h | 5.04 l/h | *55.8 l/h* | *150.4 l/h* | *146.4 l/h* |

According to Warnakulasuriya and Worek (2008) the chosen nozzles are within the range of their chosen experimental nozzle characteristic, therefore it is possible to compare the findings of this thesis with the available literature. In this case the nozzles represent diversity in cone angle and type of nozzle, which will aid in determining the effects of the cone angle on the spray characteristics. Also this will show how different types of nozzles perform under a variety of operating conditions as described in Chapter 3.

### 4.2.2 Vacuum and Water Pumps

To generate a vacuum an Edwards 5 E2M5 dual stage rotary vane mechanical vacuum pump was used as shown in Figure 4-4, which has a pumping speed displacement of 3.75 CFM at 60Hz and an ultimate pressure of $1\times10^{-3}$ mbar.

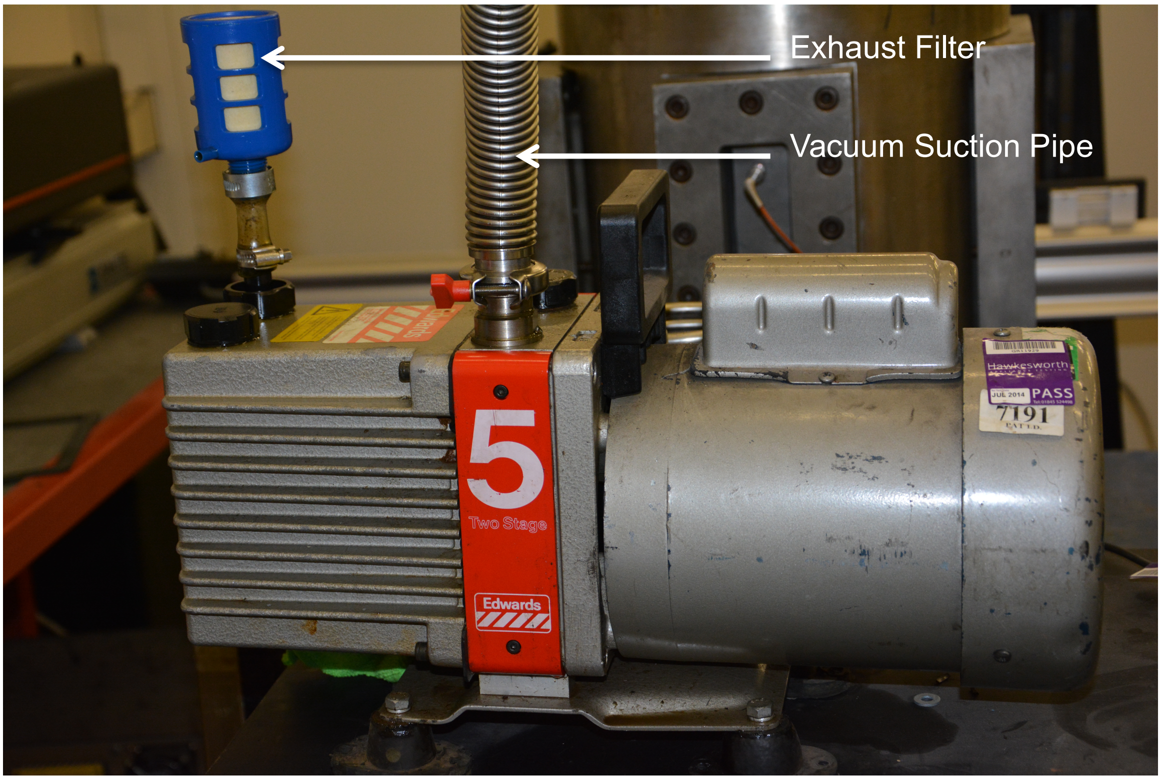

Figure 4-4 Edwards 5 E2M5 Vacuum Pump

At the preliminary stage of the experiment, the vacuum pump will emit the air from within the LP-Rig. Then once the experiment starts the pump will start to pump a small volume of steam. Although this is not an ideal working condition for the pump to work, it is still capable of handling this situation without any major damage or reduction in pump performance.

To maintain a healthy working pump, it has to be running for half an hour before the commencement of any experiment to warm-up, and another 30 minutes after the completion of the experiments to evaporate any water collected in the pump. This procedure helps maintain the efficiency of the pump for the duration of the experiment runs.

For the water supply to the injectors with a given pressure a Clarke Pump CEB102 was used as shown in Figure 4-5, which is capable of producing a flow rate of 35 L/min and maximum head of 35m. This pump also provided the required liquid input pressure to the system.

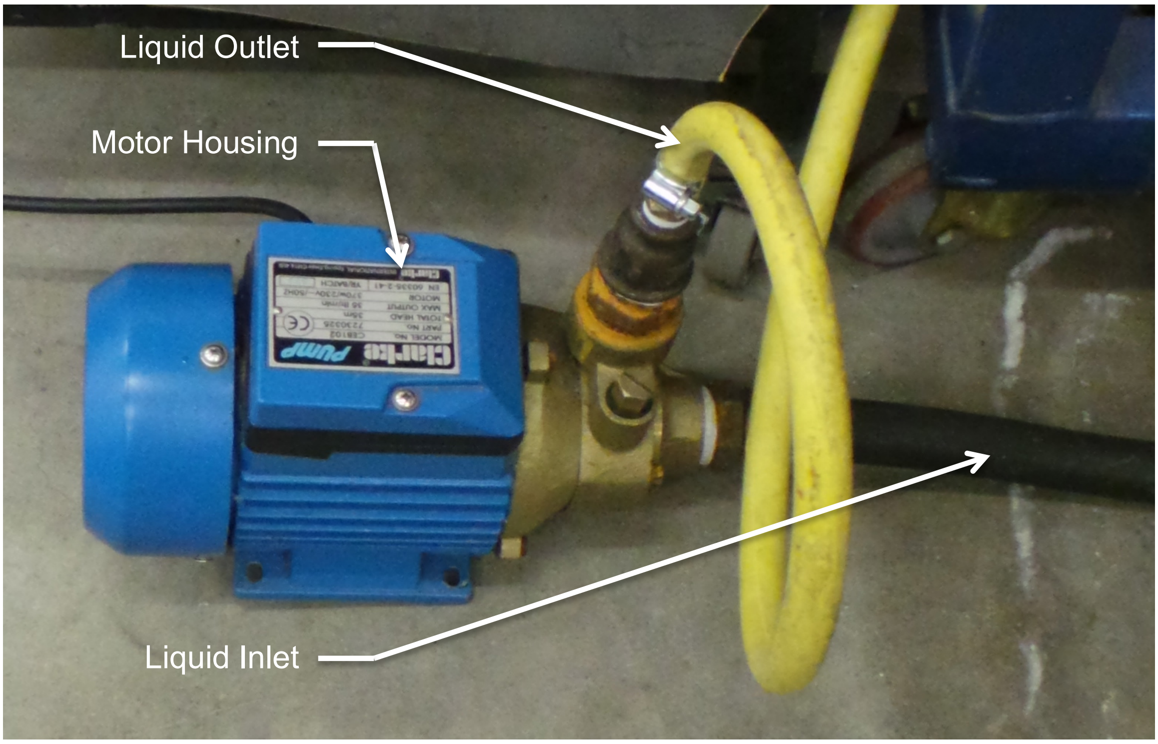

Figure 4-5 Clarke Pump CEB102 Water Pump

## 4.3 Instrumentation

Several types of instruments are used to control and monitor the experimental conditions. An overview and explanation of each of the instruments used in the experiment are outlined in this section.

### 4.3.1 Mass Flow Meter

A mini CORI-FLOW$^{TM}$ M15 mass flow meter/controller by Bronkhorst as shown in Figure 4-6 was used to measure the flow rates (kg/h) of the injected liquid into the system. This mass flow rate meter is capable of measuring flow rates between 0,2 and 300 kg/h with accuracy better than ±0.2%. It also has the capability of measuring density and temperature as a secondary output (Bronkhorst-cori-tech.com).

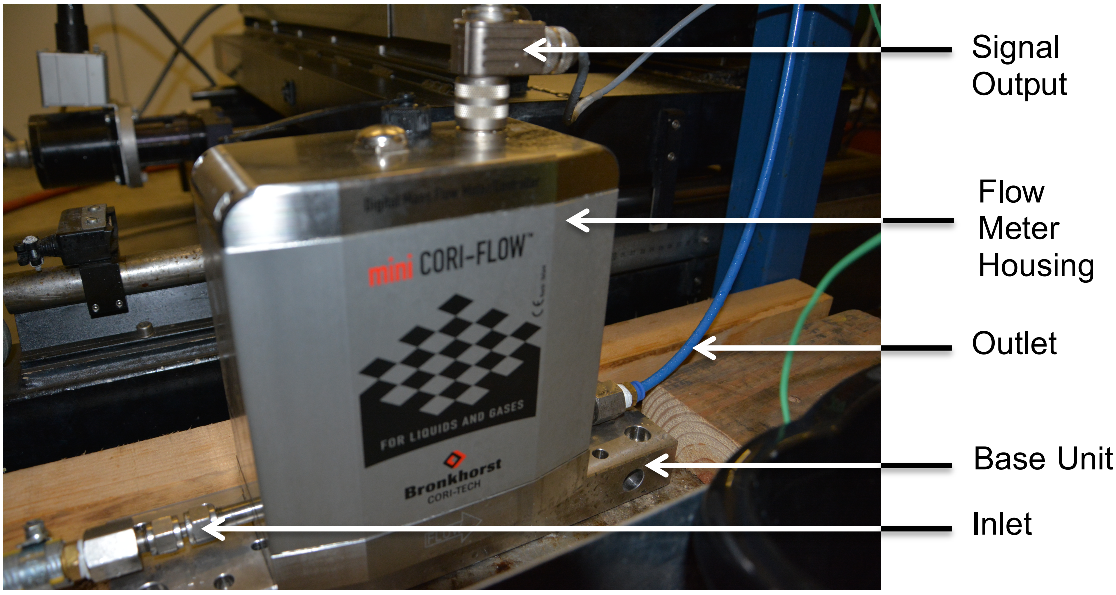

Figure 4-6. mini CORI-FLOW$^{TM}$ M15

The mini CORI-FLOW M15 uses a single looped tube that forms part of an oscillating system. When fluids flows through the looped tube the Coriolis forces cause a phase shift that is detected and outputted as a graphical display output using the software provided by the manufacturer FlowPlot V3.30 as shown in Figure 4-7.

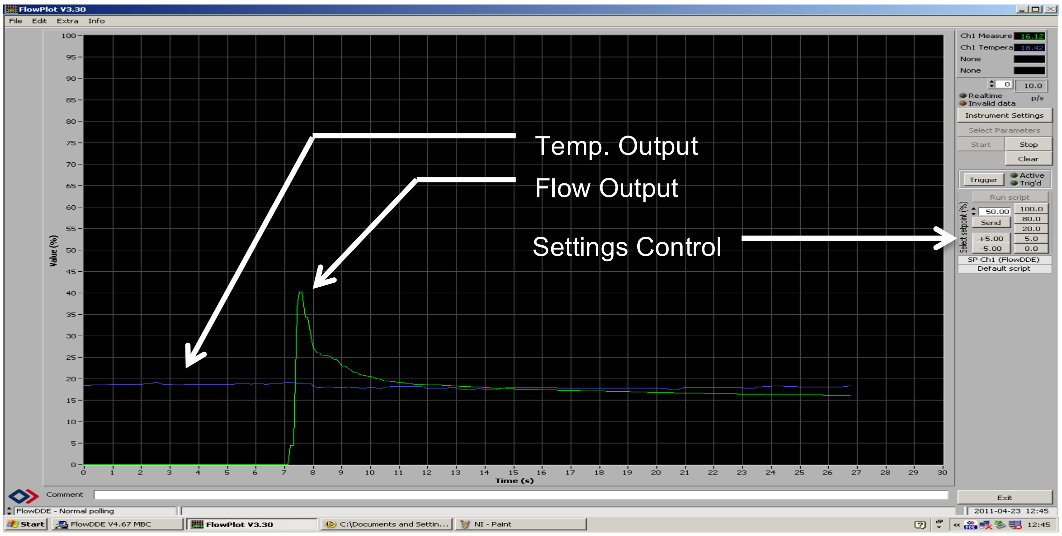

Ch1 Measure 16.12
Ch1 Tempera 18.42
0 10.0 p/s
50.00
FlowDDE - Normal polling
2011-04-23 12:45

Figure 4-7 FlowPlot Software Interphase

### 4.3.2 Pressure Transducers

Two pressure transducers supplied by Roxspur Measurement & Control Ltd are used to measure pressure data. The first pressure transducer PA-AIHVAC-010A is used to measure the input pressure of the liquid entering the LP-Rig, which is mounted on the top of the rig outside the vacuum area as illustrated in Figure 4-8.

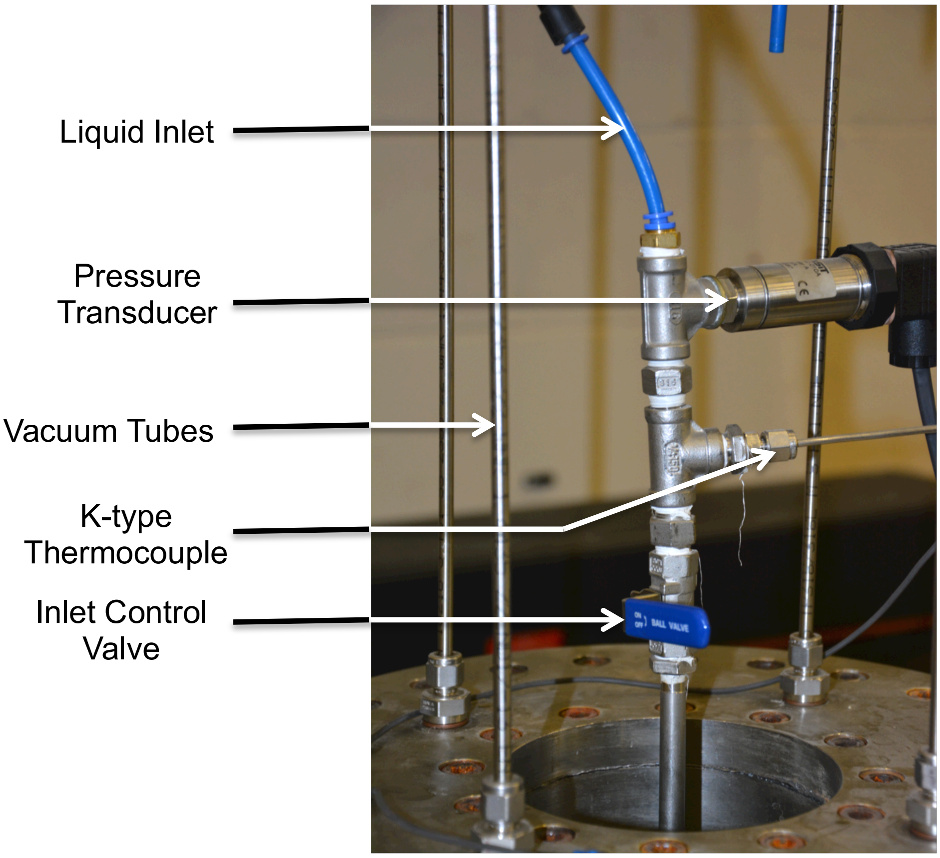

Figure 4-8 Mounting position of liquid inlet pressure transducer and thermocouple

A second pressure transducer PA-AIHVAC-002A is used to measure the internal pressure of the LP-Rig. This transducer is connected via a tapping within the vacuum area as illustrated in Figure 4-9. The manufacturer precalibrated the pressure transducers. The pressure transducers output range is outlined in Table 4-2.

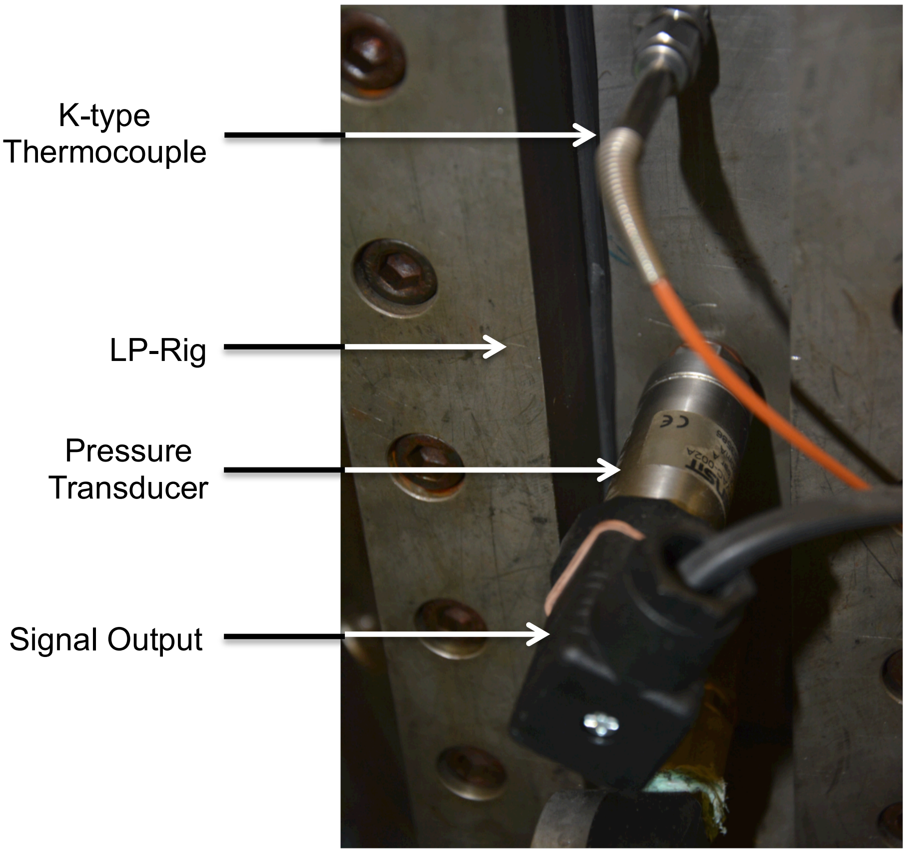

Figure 4-9 Mounting position of LP-Rig pressure transducer and thermocouple

The pressure transducers are powered using a variable power supply. The power supply was set to supply the pressure transducer with 10 V which is the maximum supply allowed for the pressure transducer to work.

Table 4-2 Pressure transducers output range

| Pressure Transducer Pressure Range | |
|---|---|
| *PA-AIHVAC-010A* | *0 – 10 bar absolute* |
| *PA-AIHVAC-002A* | *0 – 2 bar absolute* |

### 4.3.3 Thermocouples

Four K-type thermocouples supplied and calibrated by Roxspur Measurement & Control Ltd are selected for this experiment. The sensitivity of the K-type is 41 μV/°C and can measure from −200 °C to 1350 °C (Benedict 1981). The four thermocouples are strategically integrated into the experimental rig and are integrated as follows:

- The first thermocouple as shown in Figure 4-8 measures the input temperature of the liquid and is mounted on the liquid inlet tube.
- The second thermocouple as shown in Figure 4-9 measures the LP-Rig vacuum temperature and is mounted on the LP-Rig structure.
- The third thermocouple measures the output temperature of the liquid and is mounted on the liquid outlet tube.
- The fourth thermocouple measures the atmospheric temperature.

### 4.2.4 Data Acquisition (DAQ)

National Instruments (NI) compactDAQ Figure 4-10 is used to process the signals from the pressure transducers and the K-type thermocouples such as voltage and current. The NI compactDAQ system uses interchangeable I/O analog modules for different applications, which is also displayed in Figure 4-10.

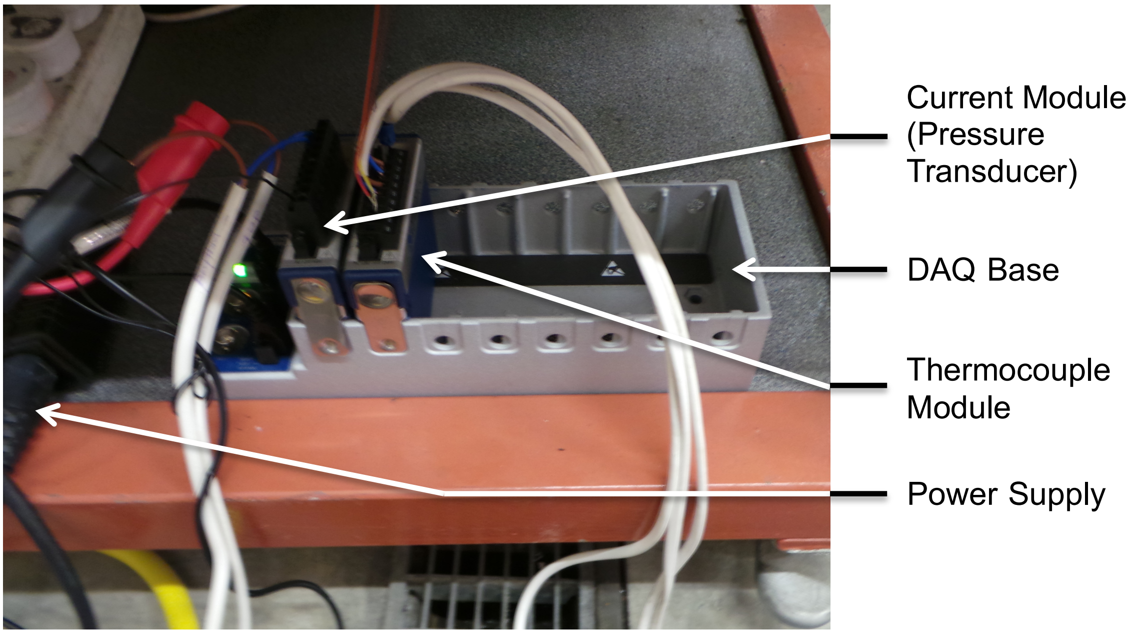

Figure 4-10 NI compactDAQ chassis with integrated I/O analog modules

Some of the main specifications of the compactDAQ chassis are detailed in Table 4-3. For the thermocouples, a thermocouple input module NI 9211 was used which is capable of accommodating four thermocouples at a rate of 14 samples per second. The pressure transducers were connected to a different input module that is the 16-Bit analog current input module NI 9203. The NI 9203 has a sampling rate of 200 kS/s (Sine.ni.com 2013).

Table 4-3 NI compactDAQ Specifications (Sine.ni.com 2013)

| NI compactDAQ Specifications | |
|---|---|
| Number of Input Channels | *8 analog / digital* |
| Sampling Rate | *1Hz to 50KHz*<br>*(Determined by I/O module used)* |
| Voltage Range | *-15V to 20V* |

The signals that are processed by the DAQ are then displayed graphically on a computer screen using National Instruments own data-logging software, which is National Instruments SignalExpress as shown in Figure 4-11.

SignalExpress is capable of acquiring, and presenting data simultaneously (Ni.com 2013).

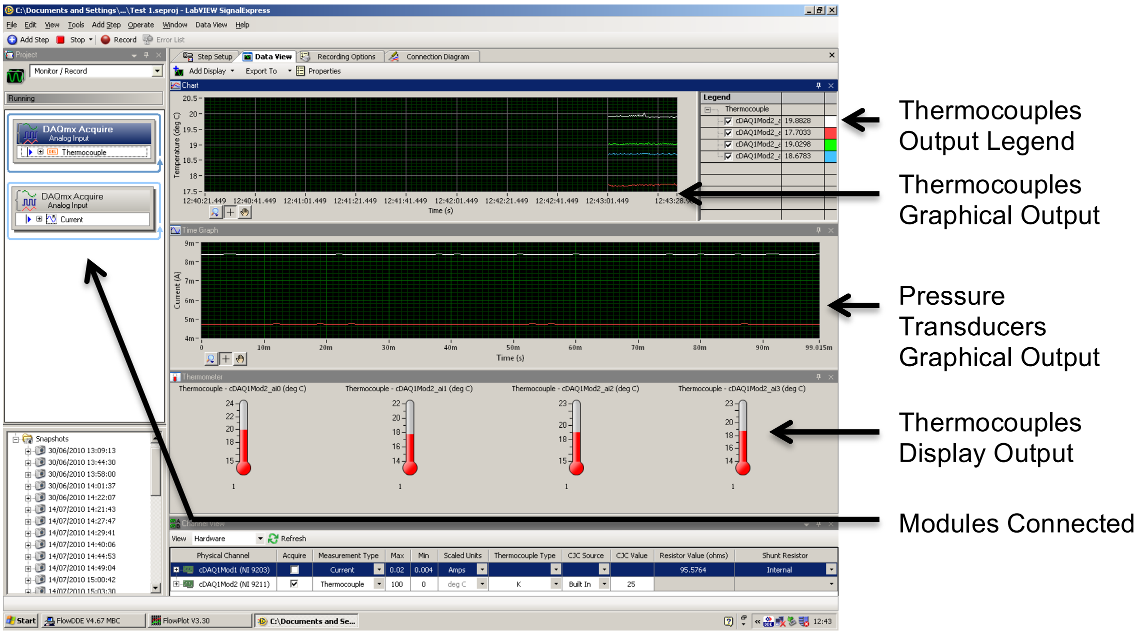

View: Hardware

| Physical Channel | Acquire | Measurement Type | Max | Min | Scaled Units | Thermocouple Type | CJC Source | CJC Value | Resistor Value (ohms) | Shunt Resistor |
|---|---|---|---|---|---|---|---|---|---|---|
| cDAQ1Mod1 (NI 9203) | ☐ | Current | 0.02 | 0.004 | Amps | | | | 95.5764 | Internal |
| cDAQ1Mod2 (NI 9211) | ☑ | Thermocouple | 100 | 0 | deg C | K | Built In | 25 | | |

Figure 4-11 NI SignalExpress screenshot

## 4.4 Phase Doppler Anemometry

Laser Doppler Anemometry (LDA) is an optical technique ideal for non-intrusive 1D, 2D and 3D point measurement of velocity and turbulence distribution in both free flows and internal flows. Phase Doppler Anemometry (PDA) systems, which is an extension to LDA measure the size, velocity and concentration of spherical particles, droplets or bubbles suspended in gaseous or liquid flows (Dantec-Dynamics 2006). A very common application is the analysis of atomized liquids (sprays) in fuel injection, spray painting, liquid metal spray and pharmaceutical sprays. In this case it will be described here in relation to spray in a vacuum. The operating principles will be explained.

### 4.4.1 Phase Doppler Anemometry Operational Theory

PDA is a non-intrusive absolute technique for measuring the velocity and diameter of spherical droplets simultaneously in a liquid spray (Soo 1999; Xu 2002; Zhang 2010). The PDA measurements technique can be used to measure gas bubbles characteristics within a liquid stream and can measure liquid droplets characteristics within a gas stream. Particle concentrations and mass flux can also be measured using the PDA (Aísa et al. 2002).

Two coherent laser beams (shifted and non-shifted) intersect to form an elongated control volume indicated in Figure 4-12. The intersecting coherent laser beams interfere with each other creating interference fringes within the control volume as shown in Figure 4-13. The droplet characteristics are measured inside the elongated control volume.

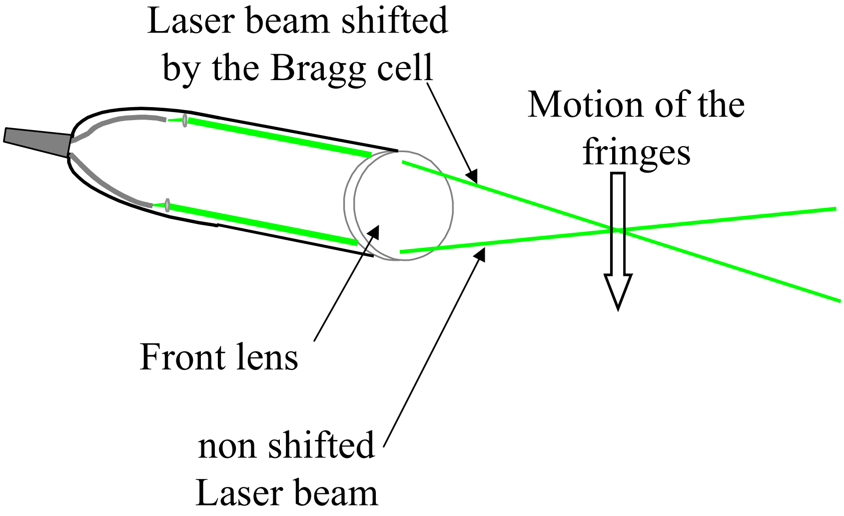

Figure 4-12 Schematic of the laser shifted and non-shifted beams (Dantec-Dynamics 2006)

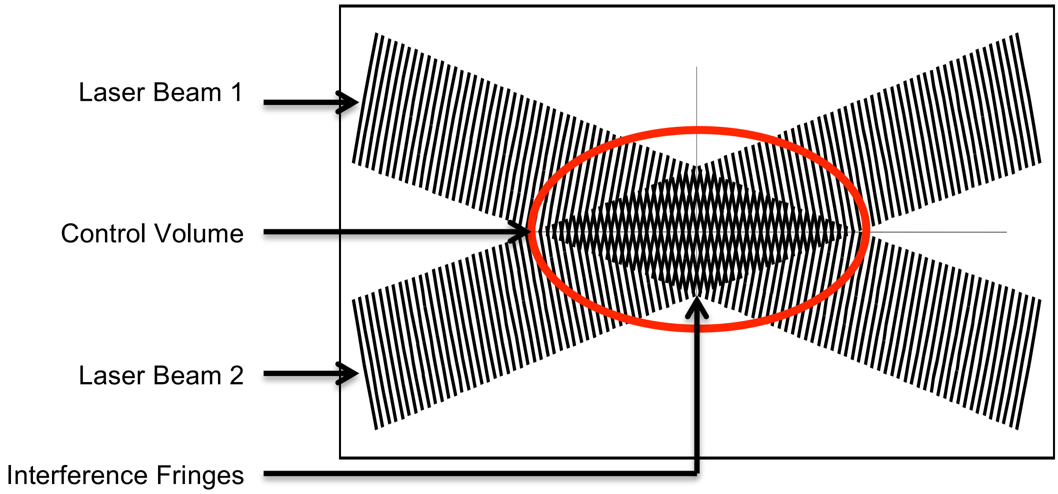

Figure 4-13 Interference fringes within the control volume

The main principle of the PDA measurement technique is the scattering of plane light waves induced by the incident beams by spherical particles (gas bubbles or liquid droplets). Therefore when a liquid droplet intersects the control volume, it scatters light from the two incident laser beams; both scattered light waves interfere and create a signal with a known frequency, which is proportional to the velocity of the liquid droplet. The detectors then receive this signal with different phases and the phase shift between the two signals is proportional to the diameter of the liquid droplet, presented in Figure 4-11.

Light waves hitting a spherical object are scattered in all directions in different manners. These scatters are composed of diffraction, reflection, refraction and absorption. There are dominant scatters, which will give the strongest signals, and therefore they are used to collect the data. The dominant scatter to be used is identified by the angle calculated which is demonstrated by Figure 4-15.

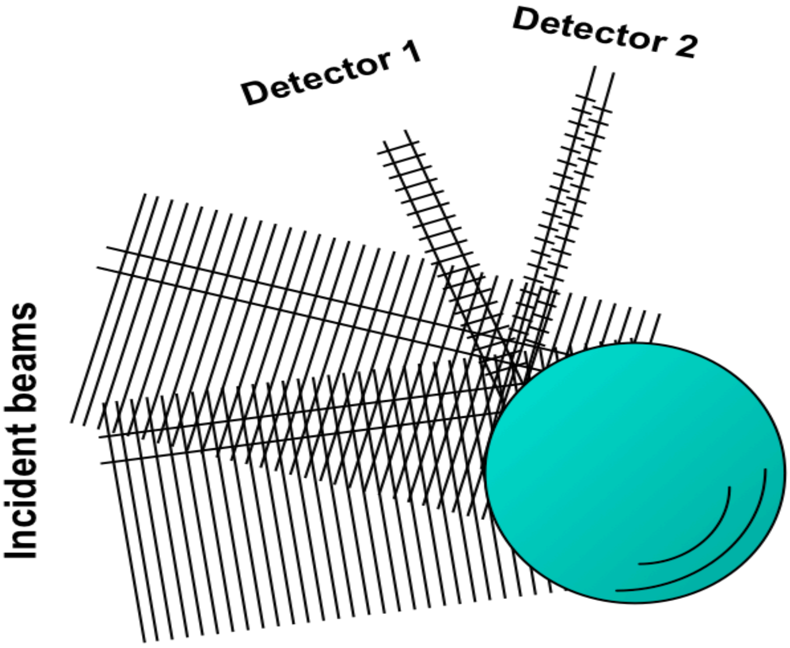

Figure 4-14. Light scattered by droplet intersecting control volume (Dantec-Dynamics 2006)

To overcome directional ambiguity, a frequency phase shift to one of the laser beams using a Bragg cell, which is a type of acousto-optical modulator, is done. This will allow positive and negative velocity to be distinguished from each other as shown in Figure 4-12. Hence a droplet intersecting the control volume in the direction of the fringe movement will result in a burst with a lower Doppler frequency than if the droplet was intersecting the control volume in the opposite direction.

In the experiments attempted, a dual PDA (2D PDA) system was used which comprises  a green laser beam (514.5nm) and a blue laser beam (488nm) that are both shifted as shown in Figure 4-16. This type of system helps in eliminating measurement errors due to trajectory and slit effects and also rejects non-spherical droplets. It also improves mass flux measurements and is optimized to deal with transparent droplets.

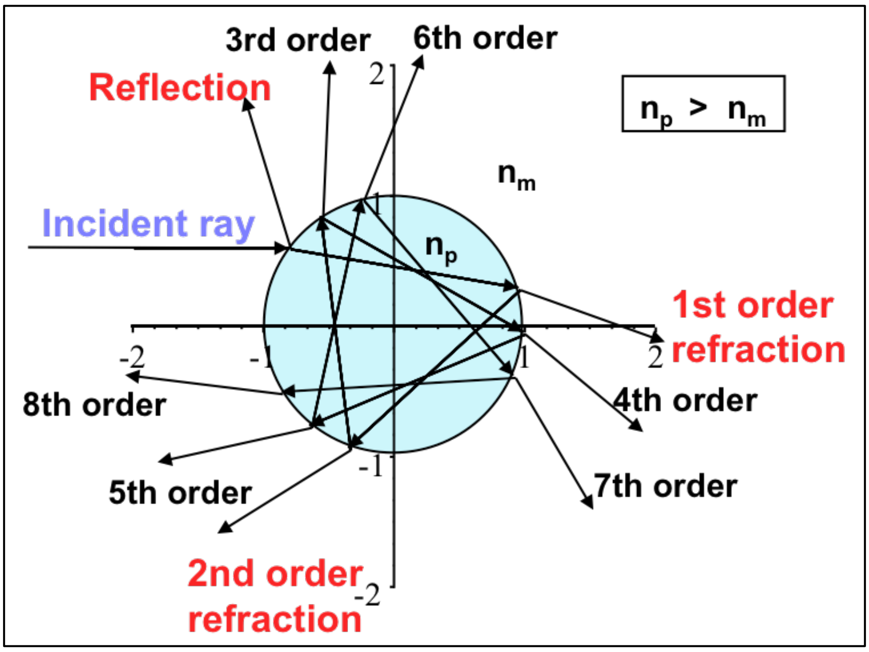

Figure 4-15. Scattering behaviors of a water droplet suspended in air with the dominant scatters in red (Dantec-Dynamics 2006)

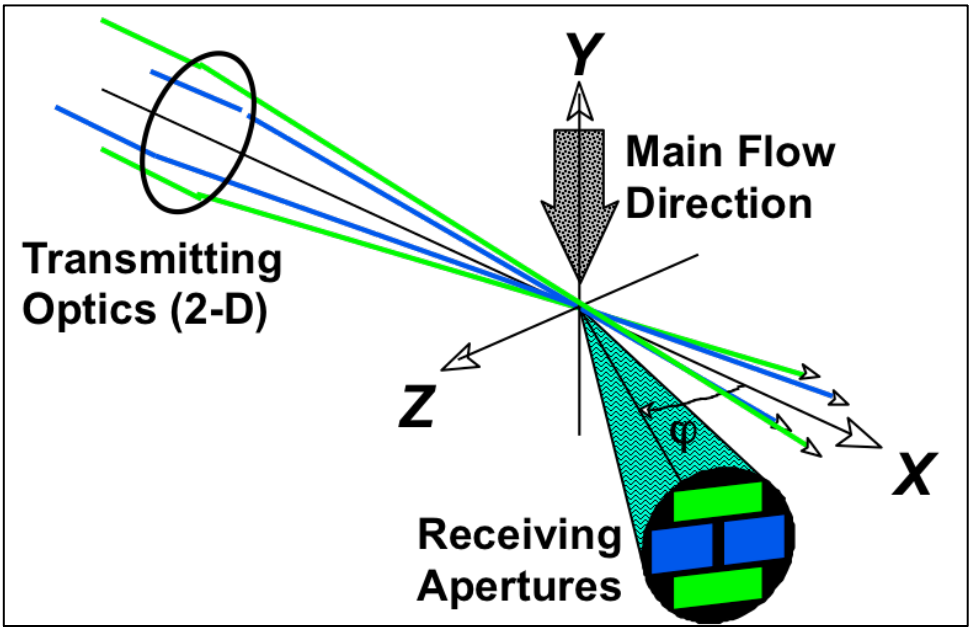

Figure 4-16 Configuration of the DualPDA

### 4.4.2 PDA System Used

DANTEC DYNAMICS provided the PDA system package used in the experimental procedure. The PDA package comprised of a transmitter, a Fiber PDA detector unit, a Particle Processor and BSA P60 Flow software. A Multiline Coherent Innova 70-5 Series Argon-Ion laser was used as shown in

Figure 4-17, which was setup at a 2W power output (Konstantinov 2012).

As the laser beam enters the Bragg cell, it is split into two beams which are the un-shifted and the shifted beams (40 MHz); this is done to overcome the directional ambiguity as described in section 4.3.1. Then it enters into a colour splitter which will split the pair of beams into three colours, namely green, blue and violet, each with 514.5 nm, 488 nm and 476.5 nm respectively. The pair of green beams were used to measure velocity in the y-axis and the pair of blue beams were used to measure velocity in the z-axis, as shown in Figure 4-16.

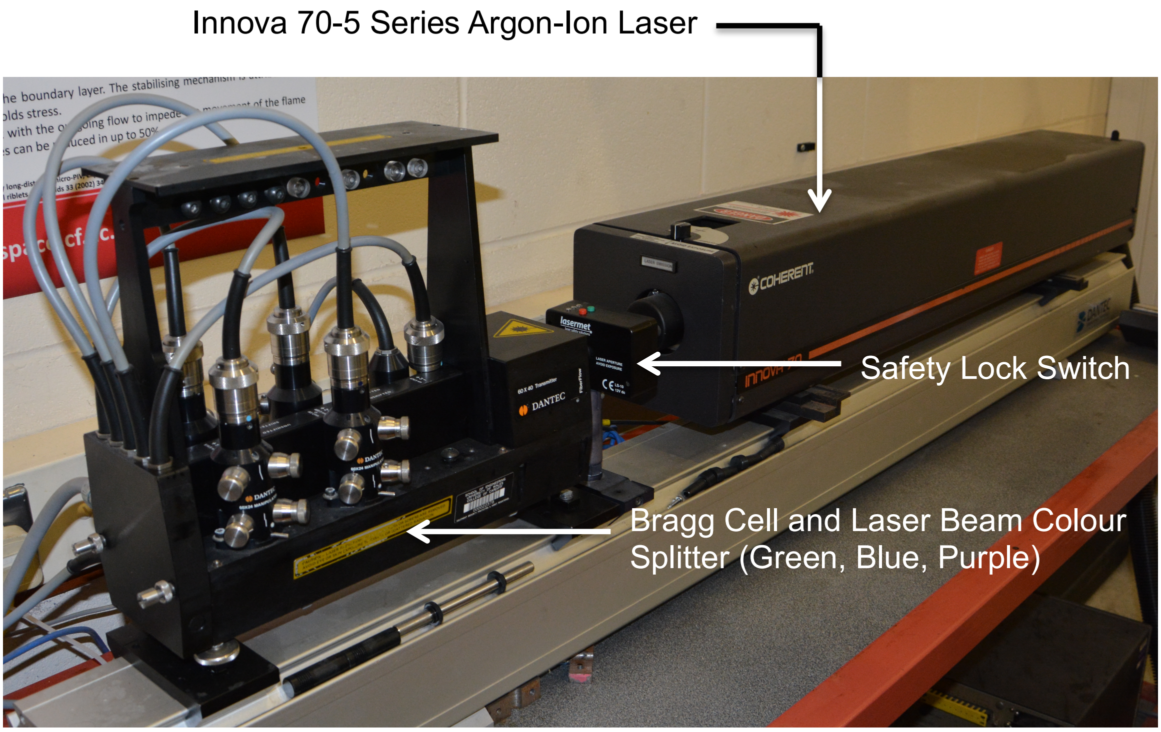

Figure 4-17 Innova 70-5 Series Argon-Ion laser

The pair of purple beams were not used for dual PDA testing, however they were used in aligning the green and blue laser beams to produce a control volume and therefore ensuring an optimum set-up. The two pair of laser beams used were then directed to a 112 mm Fiber PDA transmitting optic with a beam spacing of 74mm and nominal beam diameter of 1.5mm spacing (Dantec-Dynamics 2006).

To capture the first order refraction for the water and glycerol solution droplets in the gas medium, the transmitting optics and the receiving optics are integrated on the same plane with an offset of 70° from the forward scatter. This was achieved by mounting both the transmitting and receiving optics on a traverse system that is controlled by the software provided with the PDA package. The traverse enabled the transmitting optics to be moved in a three dimensional pattern with a 500mm of travel length.

### 4.4.3 PDA Setup

Critical steps were followed to insure that the PDA hardware is setup in the correct manner and is working as it is intended to by the manufacturer. These steps were carried out by the aid of the BSA software manual, which involved lots of aligning steps. The steps are as follows:

1. Aligning the green and the blue laser beams from the transmitting optics and the atomizer so that they are in the same plane.
2. Aligning the green and blue laser beams to make sure they intersect each other at the same point creating the control volume using a photocell and a software package.
3. Controlling and regulating the power of the laser beams to insure both laser beam pairs (shifted and un-shifted) have the same power.
4. Aligning and focusing the receiver optics with the control volume using a mist / spray from a controlled nebulizer with known spray

characteristics using the traverse system.

5. Using the software provided to check that all the setup was done correctly by running the PDA software in repetitive mode and comparing the results with the given characteristics of the nebulizer spray.
6. If required, fine-tuning to the hardware could be done to insure that the results match the given characteristics. Also adjusting the software parameters such as the voltage signals and the optics setup helped in setting up the PDA.

Following the steps listed above can produce particle size readings from 0.05 µm to over a couple of millimeters. Also comparatively high data rates up to 250 kHz and supersonic velocities of 343 m/s (Nasr et al. 2002). Throughout this study, droplet size ranges of 0.1 µm to 600 µm, and velocities up to 100 m/s were measured; data rates of over 10000 droplets per seconds were recorded.

## 4.5 Experimental Procedure

### 4.5.1 PDA Working Steps

A limited and relatively small control volume is produced when the pair of laser beams intersect each other, therefore the measuring area within the control volume could be considered to be just a few microns in width. Using this information it is clear that a sampling grid system is essential to acquire droplet measurements in different locations within the liquid spray. This technique will help in getting good comparative results of different liquid sprays. Figure 4-18 illustrates the sampling grid chosen for the experiments in this study.

The sampling grid chosen investigates the spray quality in the y-axis, which is downstream from the nozzle and the z-axis, which is the radial direction. Some studies show that measurements start at 150 mm in the y-axis and with 5 mm intervals in the z-axis up to 50 mm from the nozzle centerline (Chin and Lefebvre 1995). No suggestions were specified about what axial or radial portion of the spray should be sampled to ensure adequate data collection. Break-up was expected at 200-300 mm downstream from the nozzle orifice (Lefebvre 1989); this point was taken into consideration when choosing the sampling grid.

Therefore a decision was made to measure the maximum area possible viewed by the receiving optics. Hence measuring up to 250 mm in the y-axis from the nozzle tip in 50mm intervals and 2mm intervals in the z-axis was done. The z-axis maximum sampling point varied for each y-axis interval, and this aspect was determined by using Pythagoras theorem. The discharge angle and the y-axis are constant in each interval, as illustrated clearly in Figure 4-18. This was also verified by the drop of data rate at the edge of the spray by at least 10%. The sampling grid chosen thus insures that the number of sampling points are enough to capture considerable spray qualities in the y-axis and z-axis.

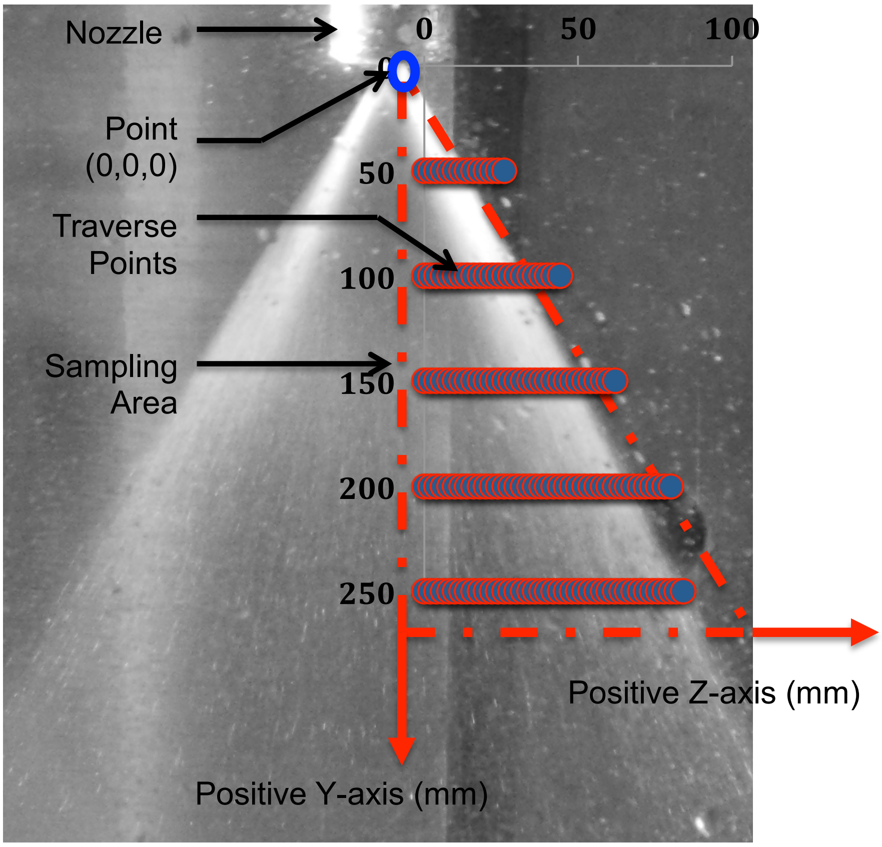

Figure 4-18 Schematic diagram of the liquid spray with the sampling area and the sampling traverse points within a specific grid plane.

The sampling grid chosen was then imported to the BSA software provided by DANTEC to control the traverse system with the integrated transmitting and receiving optics. The BSA software was setup to sample each point on the grid for five second in order to overcome the time limitation discussed in chapter 3.

Although the time limitation was an issue, it did not affect the data rate of the droplets collected, as data rates were relatively high. The minimum sample size was expected to contain about 5000 droplets to the nearest 100. This insured that the estimated spray quality lays within ± 5% of the true value (Lefebvre 1989).

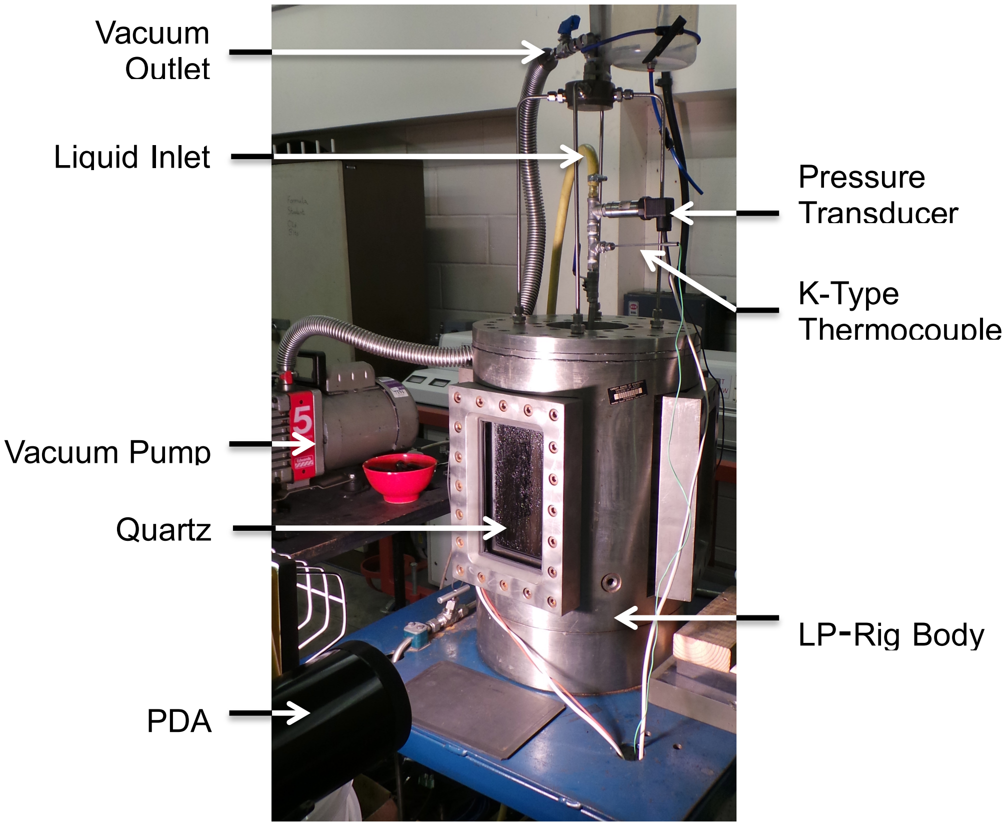

Figure 4-19 LP-Rig with integrated measurement and data logging components

### 4.5.2 LP-Rig Working Steps

The LP-Rig had to be regularly setup for each experimental run to ensure that the data collected is true and has high validation rate. The silica quartz windows were cleaned before each run to have a relatively high transparency factor to satisfy the requirements of the transmitting and receiving optics. The window also had to be treated with RainX® Anti-Fog after cleaning to prevent the fogging of the spray on the windows, which minimizes the receiving optics data collection and also causes a disturbance to the transmitting optics while producing a control volume.

The RainX® Anti-Fog is applied to the windows in small amounts using a cotton cloth to form a film on top of the window glass from the inside of the LP-Rig as presented in Figure 4-20. This treatment helped to obviate the fogging effect that affected the transmitting and receiving optics. The RainX® Anti-Fog film was observed to not have any effect on the transmission of the laser beams through the quartz glass.

Each nozzle is dismantled and cleaned by water before each experimental run to remove any debris that might clog the nozzle orifice and disturb the data collection process. Then the nozzles are attached to the LP-Rig and tightened to stop any leaks into the LP-Rig during test runs.

In the vacuum test runs, the LP-Rig is made airtight by securing all windows and by making sure they are tight enough by using a torque wrench to screw on the bolts, explained in Figure 4-20. Then the vacuum pump, in Figure 4-4, is turned on for 30 minutes to warm up before closing the outlet valve. The vacuum pressure is monitored and when it reaches the required pressure, the experiment is set to start.

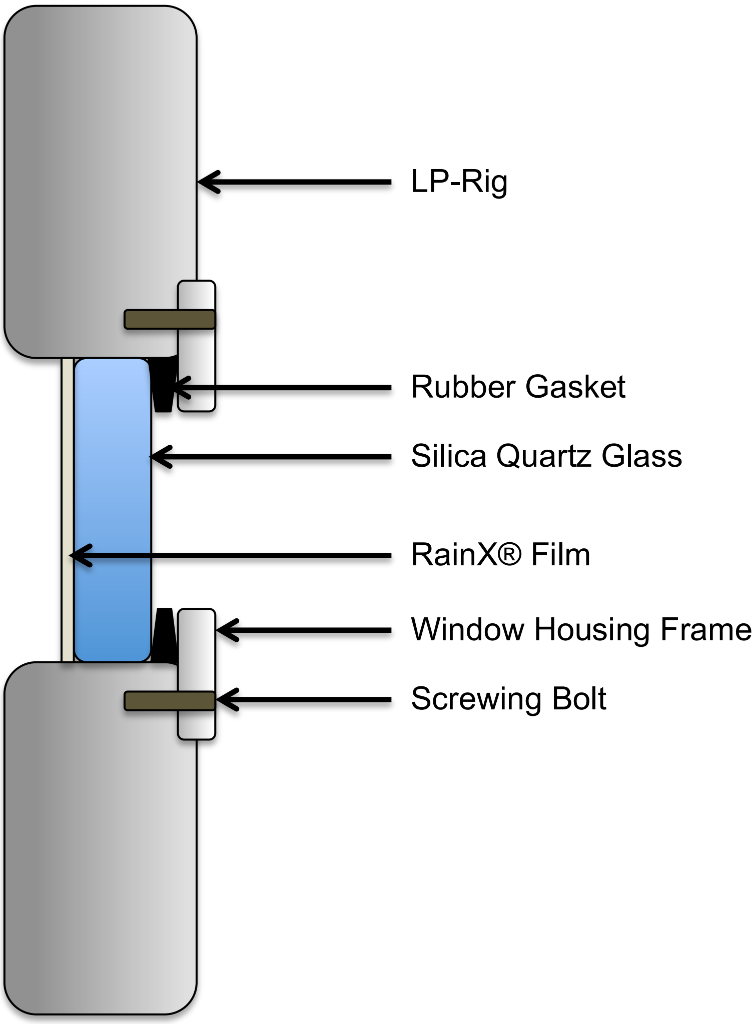

Figure 4-20 Cross-section of LP-Rig window fittings showing RainX® Film

## 4.6 Summary

This chapter details the LP-Rig setup and the specifications of the components attached to it. It also describes how the components are integrated and mounted into the LP-Rig. This chapter also points out the method by which the liquid spray data would be collected and processed in a high quality manner and high validity points.

# 5 Results

## 5.1 Introduction

This chapter analyses the results of the experiments carried out to examine the effect of a vacuum on solutions undergoing pressure jet atomization at a variety of viscosities and surface tensions. To begin with water is used as a solution to test a nominal or 'baseline' condition from which other solutions can be compared against. After establishing a benchmark using this nominal condition the same tests are run using different solutions with different known viscosities. Then an additive is added to the viscous solutions to alter the surface tension between the air-liquid interface and the same tests are repeated.

The results are then analyzed and the effect of the different variables identified in Chapter 3 are discussed and compared with the established benchmark and against each other in order to demonstrate the effect of vacuum, nozzle geometry, viscosity and surface tension on the spray quality in terms of atomization and SMD. Appendices A-C will contain all graphical data while this chapter will only include the comparative data sets to demonstrate the effects of geometry, vacuum, viscosity, surface tension and the interaction between these parameters on spray quality (which is defined in terms of difference in SMD, velocity and spray density).

## 5.2 Analysis of the Nominal Condition

The nominal condition is considered in order to set a baseline from which other variables can be compared. Understandably, the choice of conditions to represent this baseline is not easy, since it is difficult to indicate a nominal condition where no such previous analysis of this phenomenon exists.

This nominal condition was chosen to represent water droplets undergoing pressure jet atomization, as water has a known density, viscosity and surface tension; in addition to this, there is a wealth of data in the literature concerning atmospheric atomization of water modified to variety of viscosities and surface tension(Ohnesorge 1936; Lin and Reitz 1998; Nasr et al. 2002).

Therefore it is common to have water as a benchmark for the upcoming tests. Each nozzle will be analysed individually to insure that there is a representable benchmark for the other tests as discussed in Chapter 3, Table 3-1.

### 5.2.1 Delevan WM104 at Nominal Condition

The Sauter Mean Diameter (SMD) under atmospheric (ATM) and vacuum conditions are analysed first. This will demonstrate the atomization quality, i.e. the effect of different variables in terms of SMD, velocity and spray density (droplet data rates) as discussed in Chapter 3.

Referring to Figure 5-1, the SMD of 50mm, 100mm and 150mm in the y-axis direction away from the nozzle tip shows an increase with the movement of the traverse in the z-axis direction, but only to peak and then a decrease is seen with increasing z-axis position. For the 200mm and 250mm planes the SMD has a semi-linear increasing trend. This is due to the break-up of the droplets by air resistance in the test rig. This is due to a high (fluid-side) Weber number enforced by the air encompassing the jet, which provides shear forces acting on the droplets (Kay 2006; Zhao et al. 2011).

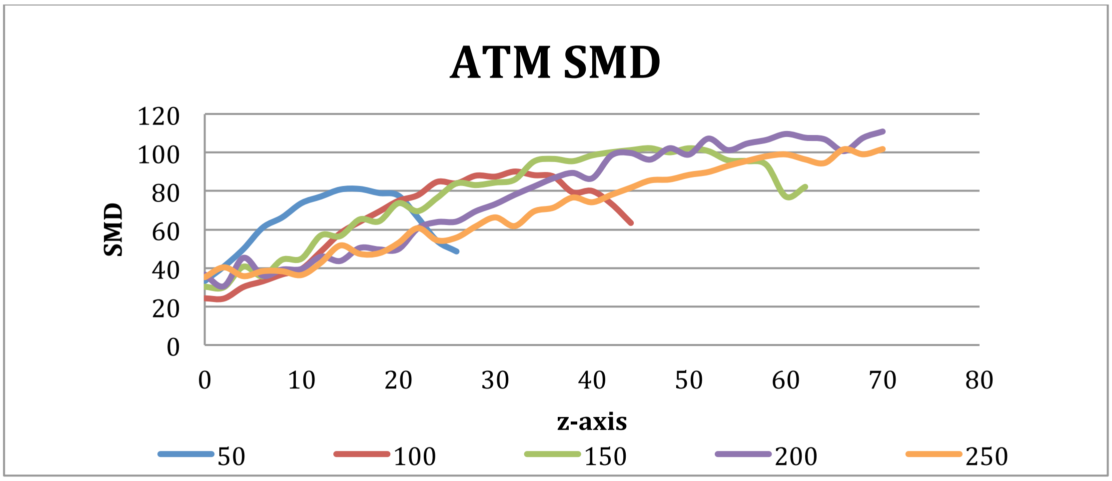

Figure 5-1 shows the SMD vs Z-axis points, for different y-axis traverse at atmospheric condition

Figure 5-2 shows the SMD vs Z-axis points, for different y-axis traverse at vacuum condition. When compared to the atmospheric condition, the vacuum SMD values tend to have similar values across the traverse points. This shows a significant reduced effect from secondary atomization due to the lack of air resistance that is observed in the atmospheric condition, which is responsible for the shear force in atomization. This is due to a lower Weber number present in a vacuum (Guildenbecher et al. 2009).

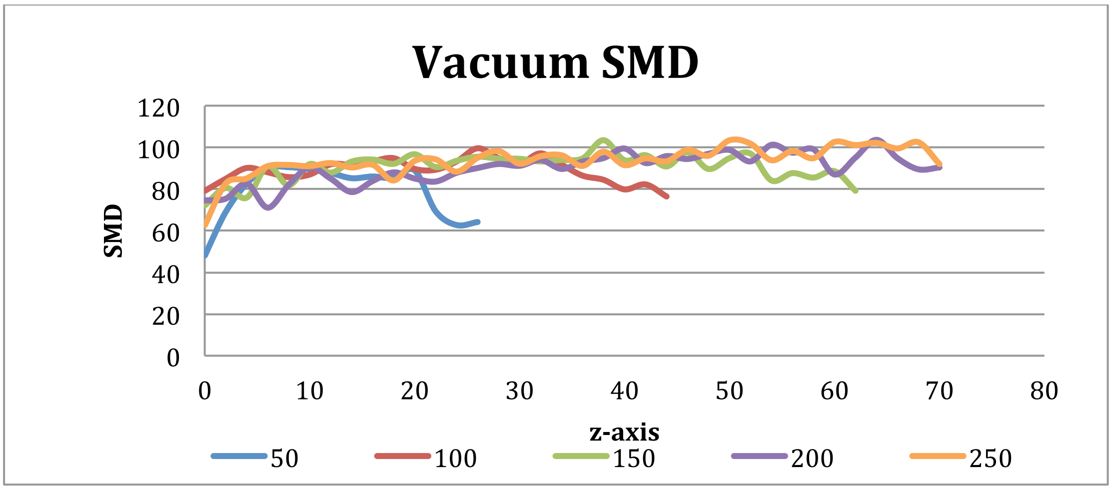

Figure 5-2 shows the SMD vs Z-axis points, for different y-axis traverse at vacuum condition

The velocity of the droplets under atmospheric and vacuum conditions is examined as this data aids in determining the effect of ambient air in the experiment system. Figure 5-3 shows the velocity vs z-axis points at the atmospheric condition. In the graph it is clear that a decrease in velocity is observed as the droplets move away from the nozzle in the y-axis direction (Figure 4-18 explains the positive y-axis direction) and z-axis. This is due to the resistance from the surrounding air acting on the spray and reducing the momentum of the droplets, which is consistent with the corresponding reduction in SMD.

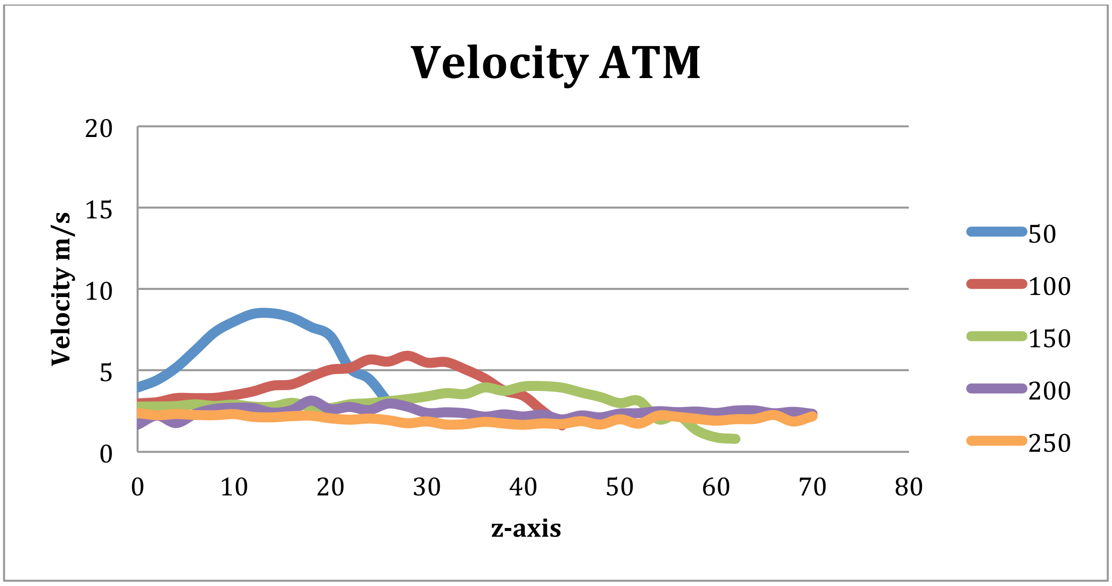

Figure 5-3 Velocity vs Z-axis points at atmospheric condition

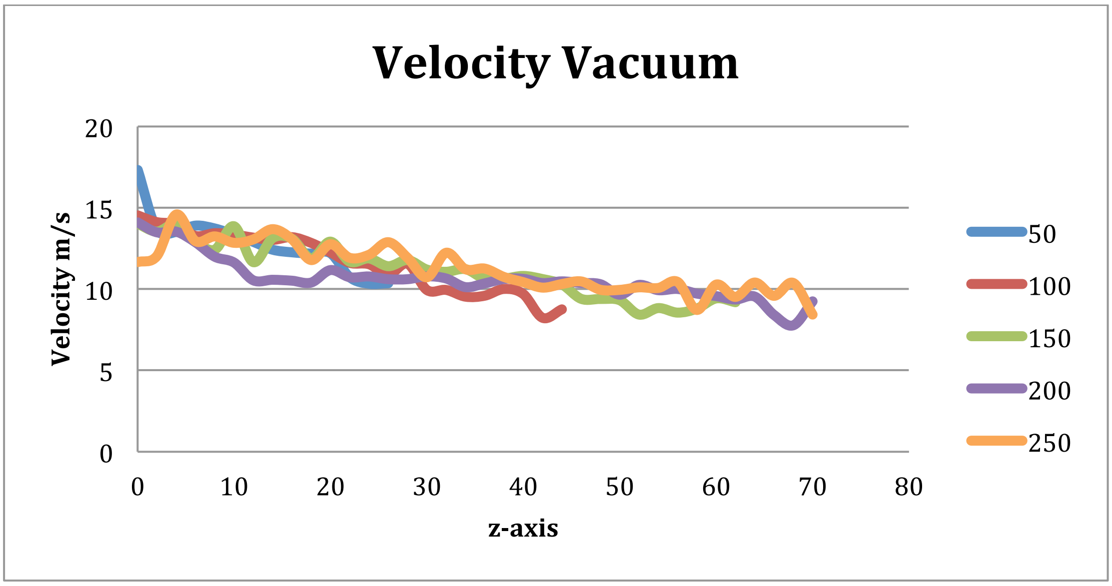

Figure 5-4 Velocity vs Z-axis points at vacuum condition

Figure 5-4 shows the velocity vs z-axis points at vacuum condition. The graph in Figure 5-4 shows a decrease in velocity as the droplets disperse and move away from the nozzle in the z-axis direction. The velocities of the droplets in the y-axis direction remain consistent to a certain point and do not decrease comparatively to the velocities of the atmospheric conditions in Figure 5-3. This is due to the lack of air resistance present in the test rig when operating under a vacuum.

Droplet Diameter Bubble Plot (DDBP) is a graphical representation of the droplet size distribution within the spray with the counts number plotted as a 3D graphical form. The size of the bubble at each point is proportional to the number of counts it represents at the sampled point. This type of representation helps to visualize the spray jet distribution and quantify the quality in terms of the droplets counts and distribution along the 2 dimensional axes.

Figure 5-5 is a DDBP graph that shows the counts number of the droplets of each point under ATM conditions. The size of the bubble represents the number of counts with respect to the other points. The spray can be clearly seen to cover a wider area although the nozzle used WM104 is a hollow cone spray nozzle. The blue lines added to the DDBP represent the borders of the real data, which will be implemented on the rest of the graphical results as shown in Figure 5-7 and Figure 5-8, and this can be inferred to be the zone enclosed by the spray, these lines were derived by using the data rate results.

The counts number of the droplets of each point under vacuum conditions in Figure 5-6 shows the effect of the vacuum on the spray distribution of the droplets. The spray in this figure is more of a hollow cone shaped spray, which is outlined by the blue lines, which are shaped according to the low data rates achieved at those points. This phenomenon is due to the lack of air present in the experimental rig system, which in term reduces the shear effect on the spray to atomize.

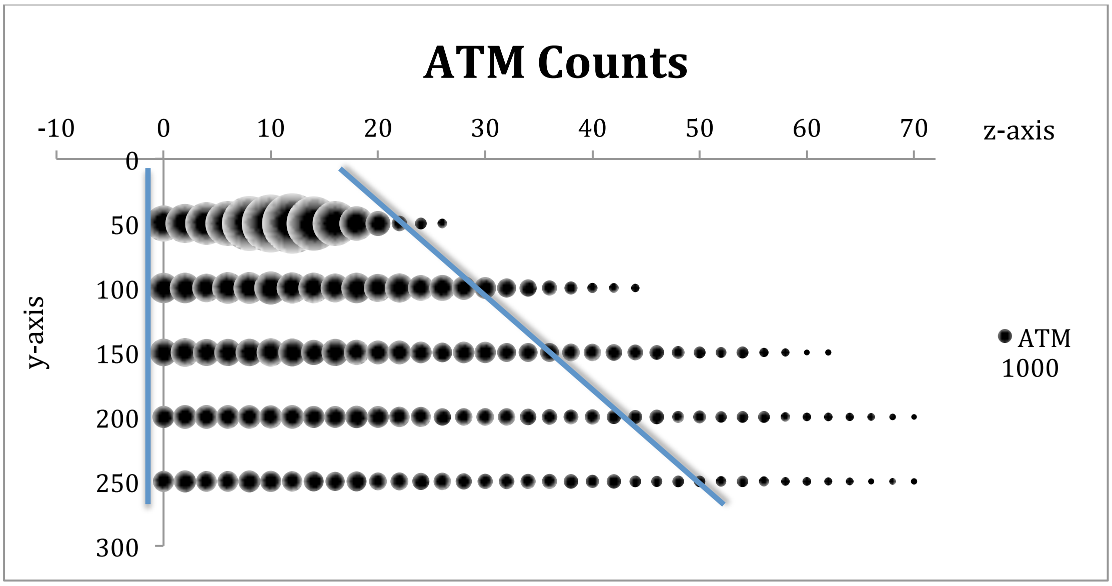

Figure 5-5 DDBP that shows the counts number under ATM condition of the droplets of each sampled point, enclosed by the blue lines is the zone of spray

Using the data from Figure 5-5 and Figure 5-6 and implementing them into the data from Figure 5-1 and Figure 5-2 the results are shown in Figure 5-7 and 5-8 respectively. These implementations will trim off data with counts less than 1000 for ATM condition and 200 for Vacuum condition. This is applied to all data in this chapter to get a clear view of the characteristics of the spray under different conditions.

Comparing Figure 5-1 and Figure 5-2 with Figure 5-7 and Figure 5-8 respectively clearly explains the need to systematically trim data to have a better understanding of the effects of the vacuum on the spray quality and spray distribution throughout the sampled area identified in Figure 4-18.

The SMD under ATM conditions is clearly decreasing in the y-axis direction as pointed out in Figure 5-7, while under vacuum conditions it remains significantly less affected as shown in Figure 5-8.

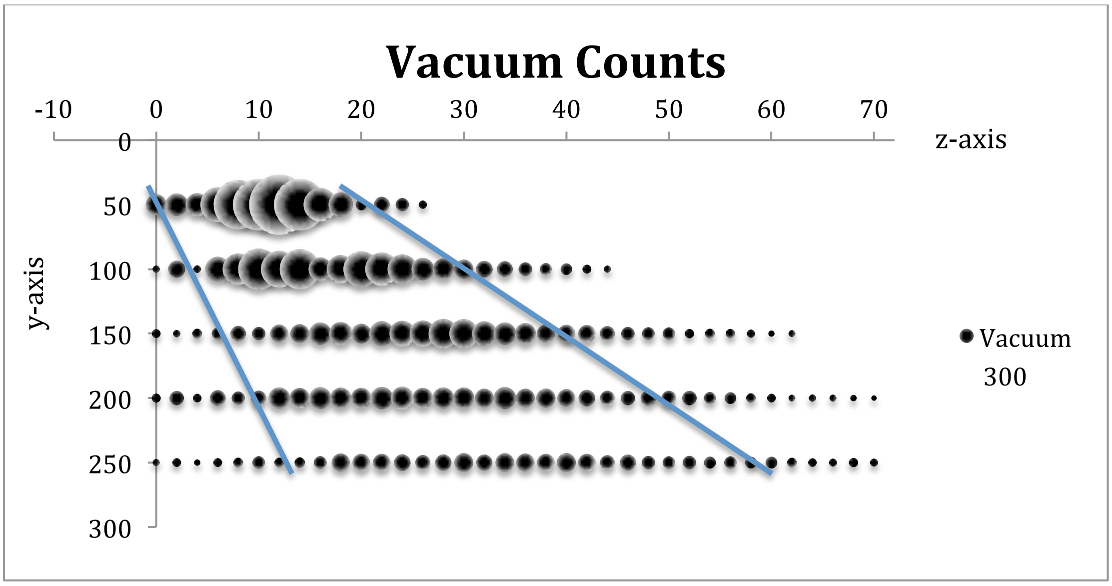

Figure 5-6 DDBP that shows the counts number under Vacuum condition of the droplets of each sampled point, enclosed by the blue lines is the zone of spray

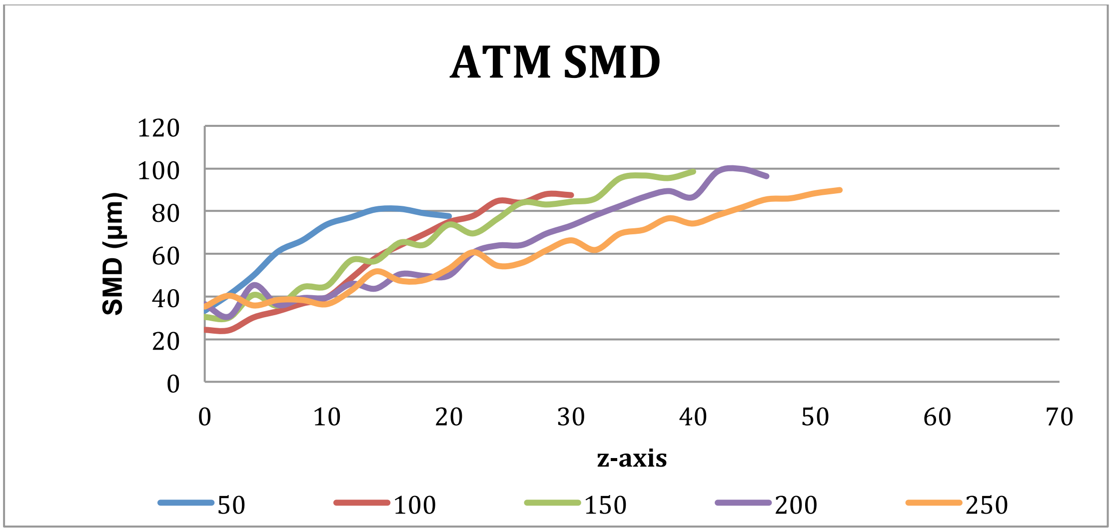

Figure 5-7 shows the SMD vs Z-axis points, for different y-axis traverse at ATM condition with real data points

Droplet diameter frequency distributions for both ATM and vacuum conditions are demonstrated in Figure 5-9. By number of counts the frequency of ATM condition peaks at approximately 15µm with the majority of the droplet diameters being less than 50µm.

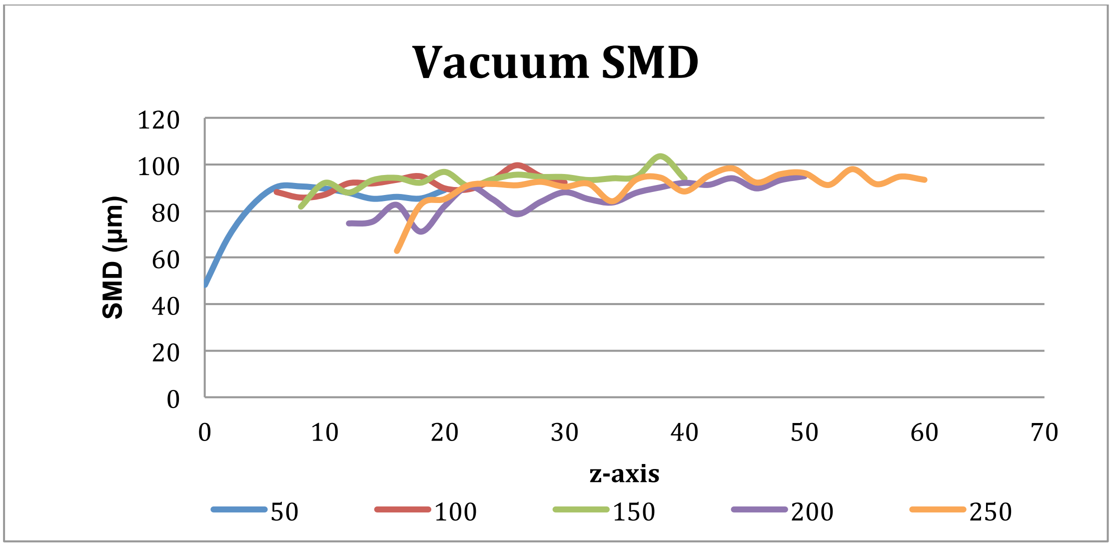

Figure 5-8 shows the SMD vs Z-axis points, for different y-axis traverse at vacuum condition with real data points

The frequency of the vacuum condition peaks at approximately 40µm with the majority of the droplets in the higher range of the scale 50µm and above. Therefore under vacuum conditions the droplet diameters are 62.5% larger than, when compared to their diameters at ATM conditions at the peak point.

This is a result of the poor atomization quality in the vacuum condition experiment due to the lack of air present in the system, which in turn leads to a lower shear force on the spray compared to the shear force present at ATM condition.

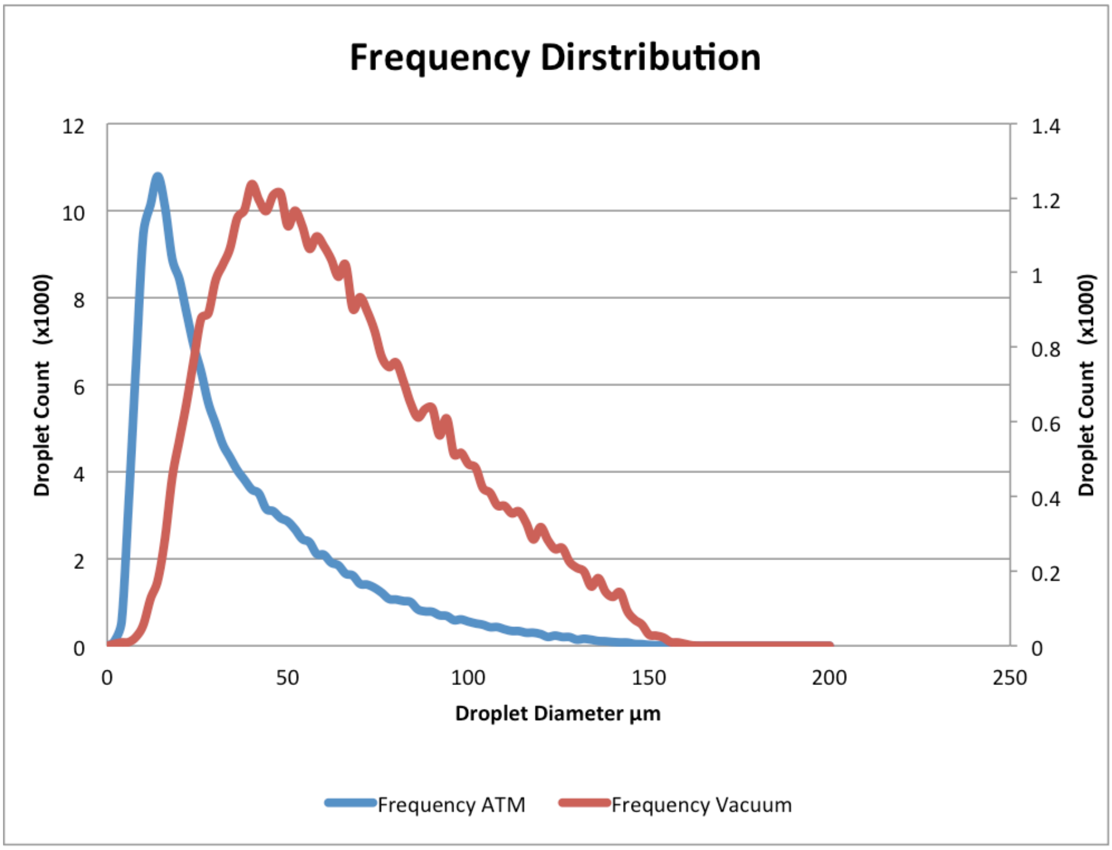

Figure 5-9 Droplet frequency distribution plot

Table 5-1 summarises the operating conditions and the spray characteristics of the tests carried out at the nominal condition. Equation 5-1 is used to calculate Reynolds number and Equation 5-2 to calculate Weber Number Ohnesorge number was calculated using Equation 3-1 and Equation 3-2. Dantec Dynamics BSA Software calculates the $D_{32}$ and the $D_{21}$ values.

$$Re = \frac{\rho_l U_{av} d_{10}}{\mu_l}$$ ***Equation 5-1***

$$We = \frac{\rho_l U_{av}^2 d_{10}}{\sigma_l}$$ ***Equation 5-2***

Table 5-1 Summary of nominal condition test and spray characteristics

| **Test** | **ATM** | | | **Vacuum** | | |
|---|---|---|---|---|---|---|
| | **WM 054** | **WM 104** | **WM 1154** | **WM 054** | **WM 104** | **WM 1154** |
| **Water Pressure (bar)** | 3.73 | 3.73 | 3.73 | 3.73 | 3.73 | 3.73 |
| **Rig Pressure (bar)** | 1.01 | 1.01 | 1.01 | 0.03 | 0.03 | 0.03 |
| **ΔP (bar)** | 2.72 | 2.72 | 2.72 | 3.7 | 3.7 | 3.7 |
| **Re Liquid** | 79.53 | 106.36 | 380.60 | 605.86 | 728.00 | 285.15 |
| **We Liquid** | 1.24 | 3.27 | 23.35 | 74.66 | 103.32 | 28.66 |
| **Oh Liquid** | 0.01398 | 0.01700 | 0.01270 | 0.01426 | 0.01396 | 0.01877 |
| **SMD, $D_{32}$ (μm)** | 82.41 | 71.94 | 89.42 | 81.93 | 88.16 | 60.22 |
| **$D_{21}$ (μm)** | 72.06 | 50.47 | 79.34 | 69.71 | 70.91 | 45.10 |

## 5.3 Comparative Results at Nominal Condition

In this section a comparative analysis of the different nozzle geometries will be examined. The 150mm downstream plane in the y-axis direction from the nozzle tip is studied to be the comparative data series. This particular plane was chosen because it is the furthest plane that had a consistent reading by the PDA system. This was due to the limitations that where discussed in Chapter 4.

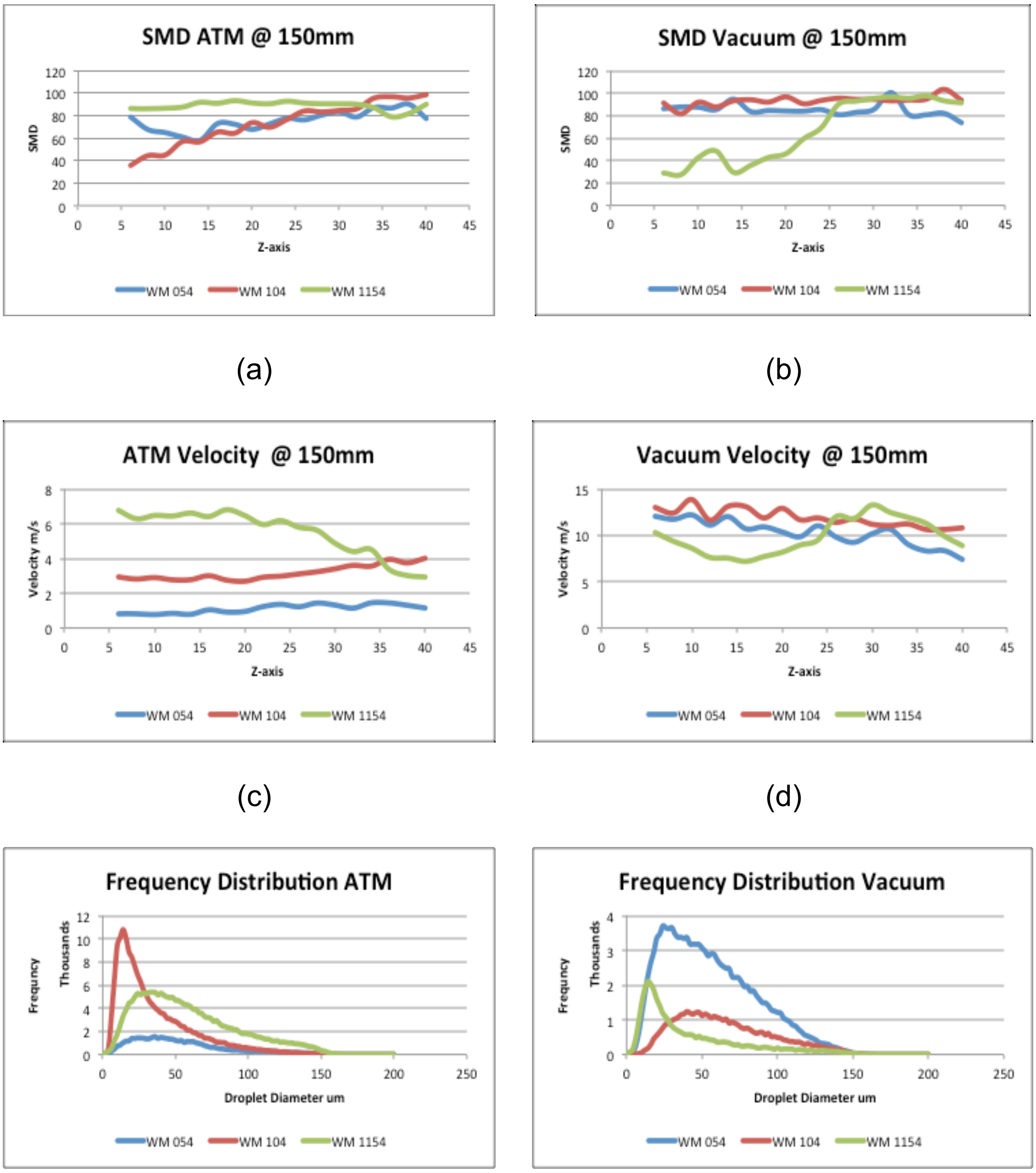

(a) (b)

(c) (d)

(e) (f)

Figure 5-10 (a) SMD at ATM, (b) SMD at vacuum, (c) Velocity at ATM, (d) Velocity at vacuum, (e) Frequency distribution at ATM, (f) Frequency distribution at vacuum.

In Figures 5-10 (a) to (f) the nozzles selected according to Table 4-1 are represented in different colours to provide an understanding of the effects of geometry on the spray. Figures 5-10 (a) and (c) clearly show that the nozzles with a bigger orifice has a higher SMD and a higher flow rate compared to nozzles with smaller orifice (Lefebvre 1989). This is also shown in Figure 5-10

(b) and (d) when the sampling points pass the 25mm mark in the z-axis, and this can be explained by looking at the 150mm plane in Figure 5-6. The concentration of droplet data series starts at the 25mm point in the z-axis, hence the corresponding SMD and velocity display a predicted outcome.

The vacuum conditions in the experimental tests as discussed previously produce an almost perfect hollow cone, and as the sampling points reach the edge of the hollow cone spray, it is noticed in the results displayed in figures 5-10 (a) and (b).

In figures 5-10 (e) and (f) the frequency distribution of the water droplets` diameters for the three nozzle types chosen for the experiment are plotted in ATM and vacuum conditions respectively. The quality of the spray atomization is lower in terms of spray counts and droplet diameter in the vacuum condition by an average of 59.6% (using peak to peak comparison of the WM 104 nozzle) through the different nozzles.

From this data it is proven that under vacuum conditions the atomization quality is poor in both the number of droplets produced and the SMD. This is due to a lower Reynolds number in the vacuum condition compared to the ATM condition (Lefebvre 1989; Cengel and Boles 2007), which in turn means that there is a lack of inertia forces such as the shear forces that act on the spray to produce atomization.

It is interesting to note at this stage from the data given that the relative contribution from the vapour pressure of water evaporating in near-vacuum conditions clearly has a far lower magnitude than the secondary breakup accused by the shear forces acting between the water and air in the atmospheric case. Hence it can be inferred that under the current times and temperatures considered (analogous to the conditions within the absorption refrigeration system) droplet breakup is controlled via primary atomization, immediately downstream of the nozzle orifice.

## 5.4 Analysis of Viscous Solutions

Referring to table 3-2 the viscosity tests are carried out in two different viscosity values. The first test condition was carried out using 20% glycerine by volume solution (0.00286609 kg/ms) and the second test condition was carried out using 50% glycerine by volume solution (0.0064178 kg/ms). The main justification of this is to simulate the effect of adding lithium bromide salt to the water (as is the practice in absorption refrigeration systems).

### 5.4.1 Viscous Solution First Condition

#### *5.4.1.1 Operating Conditions and Results*

Table 5-2 summarises the operating conditions and the spray characteristics of the test carried out using 20% glycerine by volume solution (0.00286609 kg/ms). The pressure is displayed in 2 d.p. Through all the tests carried out ΔP was maintained at a pressure of 2.72 ± 3% bar for ATM and 3.7 ± 3% ATM for Vacuum.

Table 5-2 Summary of viscous solution first condition test and spray characteristics (0.00286609 kg/ms)

| Test | ATM | | | Vacuum | | |
|---|---|---|---|---|---|---|
| | **WM 054** | **WM 104** | **WM 1154** | **WM 054** | **WM 104** | **WM 1154** |
| **Water Pressure (bar)** | 3.73 | 3.73 | 3.73 | 3.73 | 3.73 | 3.73 |
| **Rig Pressure (bar)** | 1.01 | 1.01 | 1.01 | 0.03 | 0.03 | 0.03 |
| **ΔP (bar)** | 2.72 | 2.72 | 2.72 | 3.7 | 3.7 | 3.7 |
| **Re Liquid** | 92.15 | 123.24 | 165.89 | 194.62 | 364.46 | 230.36 |
| **We Liquid** | 9.94 | 20.31 | 33.40 | 50.21 | 170.19 | 75.99 |
| **Oh Liquid** | 0.03421 | 0.03557 | 0.03484 | 0.03641 | 0.03680 | 0.03784 |
| **SMD, D32 (μm)** | 100.67 | 92.07 | 93.91 | 93.36 | 83.40 | 88.09 |
| **$D_{21}$ (μm)** | 89.07 | 79.24 | 84.28 | 79.89 | 76.06 | 75.01 |

### *5.4.1.2 Spray Droplet Size Distribution*

The droplet diameter count frequency distributions indicated in Figure 5-11 appear to have similar shapes, with different droplet counts. The peak values for each nozzle tend to be different as well with the Delevan WM 104 having the smaller diameter peak of 16μm, which states that there are larger numbers of droplets having a smaller diameter.

According to droplet counts, the droplet diameters for all the nozzles are between 2μm and 150μm, with the majority of droplets lying between 12μm to 65μm.

The flow rate and the cone angles had a clear affect on the amplitude of the peaks, which are shown to be varying from one nozzle to the other (Nasr et al. 2002). The fluctuation of the peaks corresponds to the sample size of the droplets in each test. In Figure 5-13, the effect of the vacuum on the sample size can be observed.

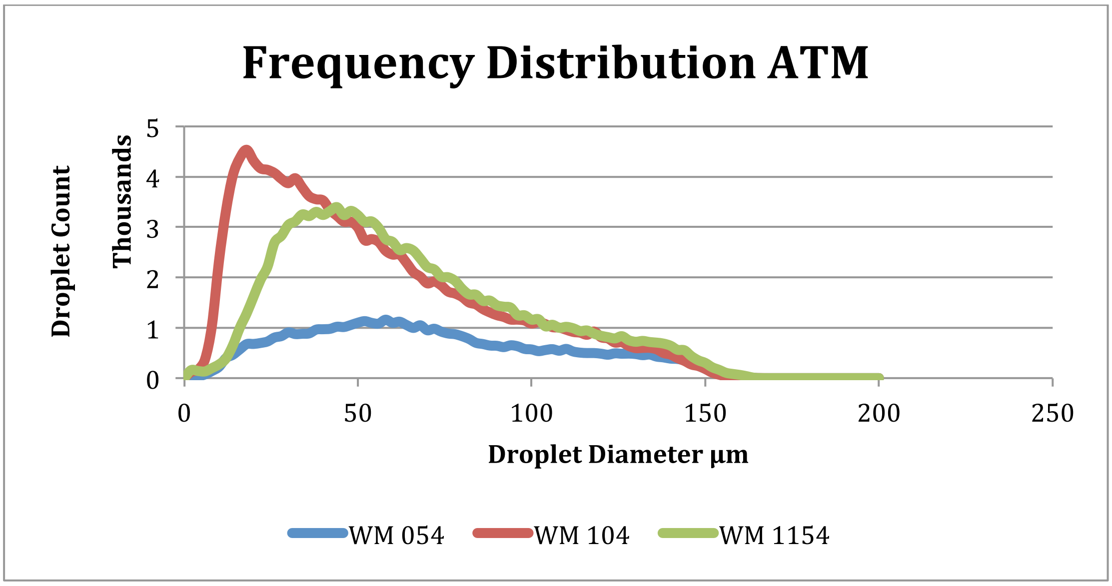

Figure 5-11 Frequency distribution by droplet count ATM (0.00286609 kg/ms)

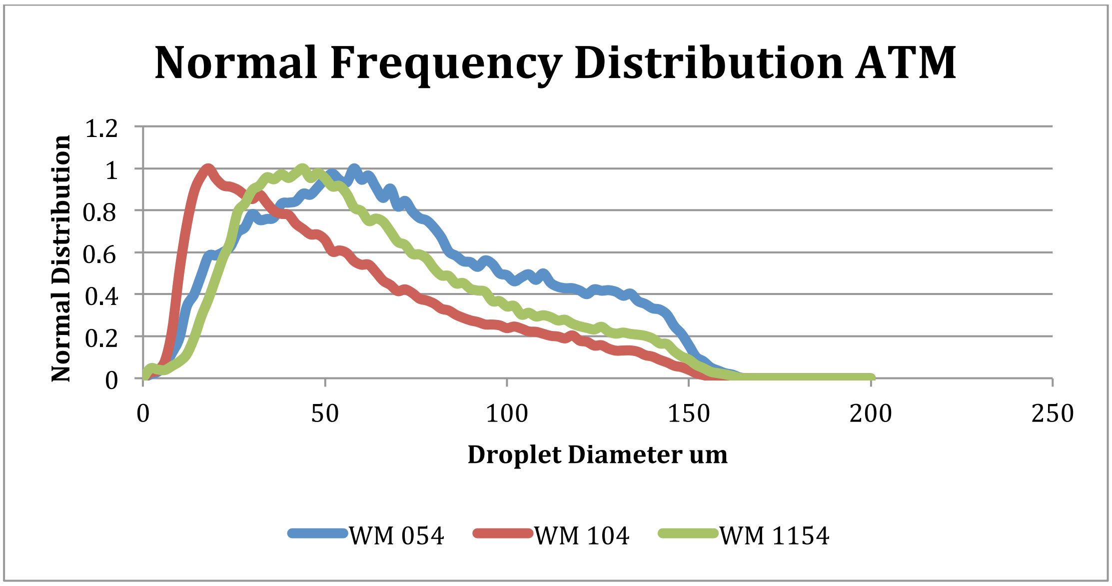

Figure 5-12 Normal Frequency distribution to peak value ATM (0.00286609 kg/ms)

The droplet diameter count frequency distributions indicated in Figure 5-13 have more of a flat shape curve rather than the normal distribution curve. A peak value is not easily distinguished for each of the nozzle.

Comparing the peak value for Delevan WM 104 under ATM condition having a 16μm diameter with vacuum condition having 54μm diameter, a 70.4 % increase in size at the vacuum condition with the first condition viscosity is realised, clearly having a large effect on the LiBr solution characteristics.

This huge increase comes at no surprise, as the Ohnesorge number is 0.0355 at atmospheric condition and the Ohnesorge number is 0.0368 at vacuum condition. A larger Oh indicates a greater influence of the internal forces acting on the liquid spray (Ohnesorge 1936; Aliseda et al. 2008).

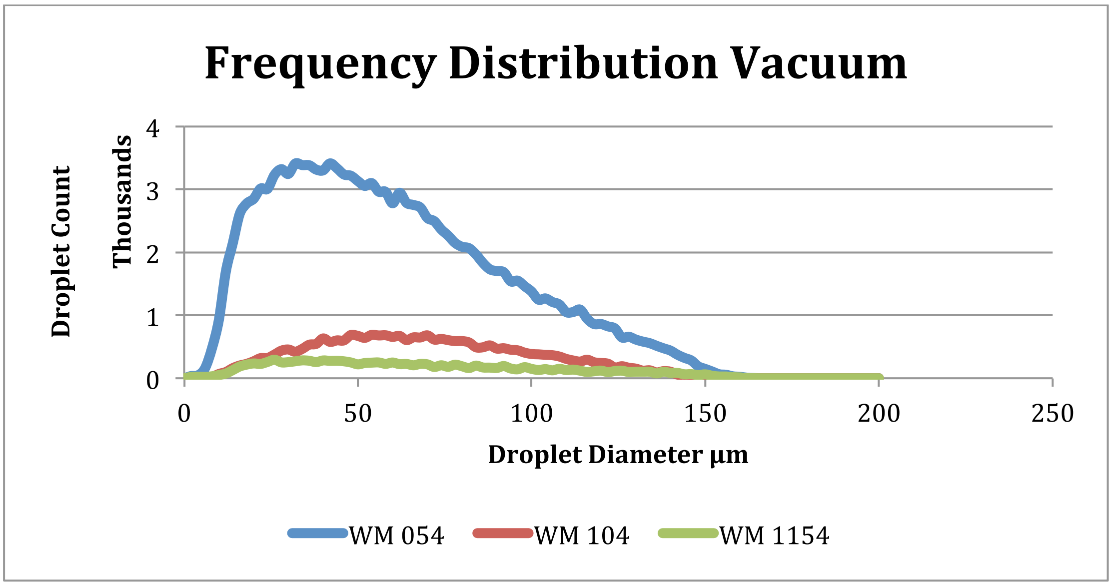

Figure 5-13 Frequency distribution by droplet count vacuum (0.00286609 kg/ms)

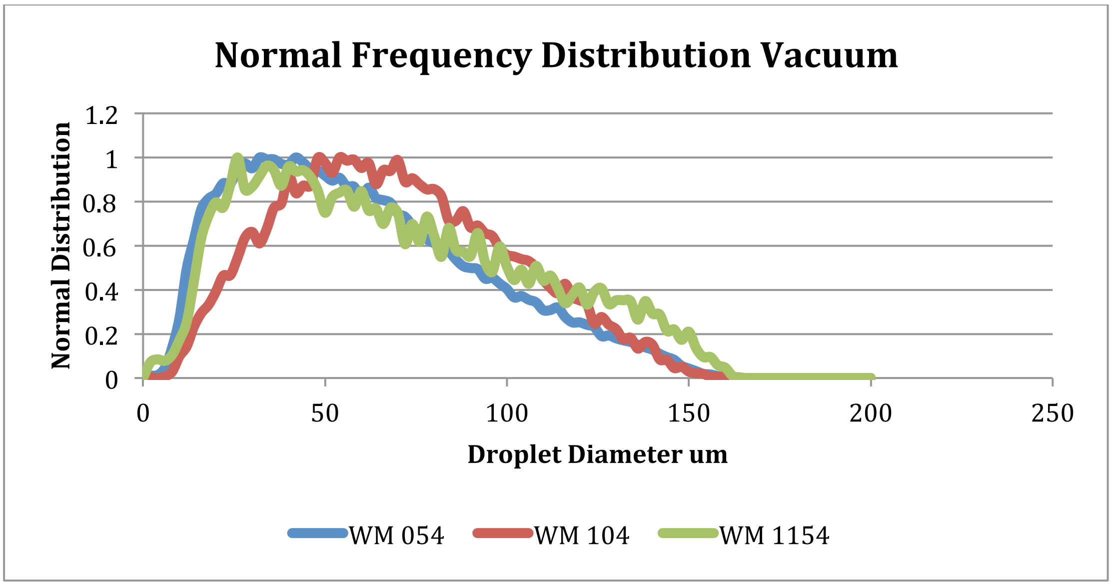

Figure 5-14 Normal Frequency distribution to peak value vacuum (0.00286609 kg/ms)

### *5.4.1.3 Droplet Data Rate*

The droplet data rate graphs presented in Table 5-3 show higher data rates closer to the nozzle tip at 50mm downstream compared to the planes further downstream in the y-axis direction, implying that the spray density in the discrete region surrounding the nozzle is higher. These clusters of data gradually decrease as the droplets travel further downstream in the y-axis direction. This is expected as the spray jet starts to atomize further downstream and the droplets start to spread out i.e. the spray gets wider downstream.

Under ATM conditions, an even spread of droplets data rates are achieved moving downstream; the data rates are significantly concentrated at the center axial position and start to dissipate moving to the edge of the spray in the z-axis direction. Although the nozzles used are hollow cone nozzles, this is not shown in this case; in fact the spray behaves more like a solid cone of droplets, which implies that the additional viscosity under the conditions is inhibiting the primary breakup mechanism (Santangelo and Sojka 1995).

Table 5-3 Droplet data rate with varying nozzles (0.00286609 kg/ms)

<table>
<tr><th colspan="2">Droplet Data Rate</th></tr>
<tr><th>ATM</th><th>Vacuum</th></tr>
<tr><td>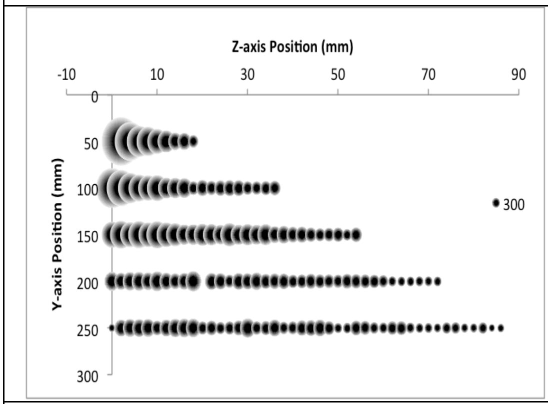
</td><td>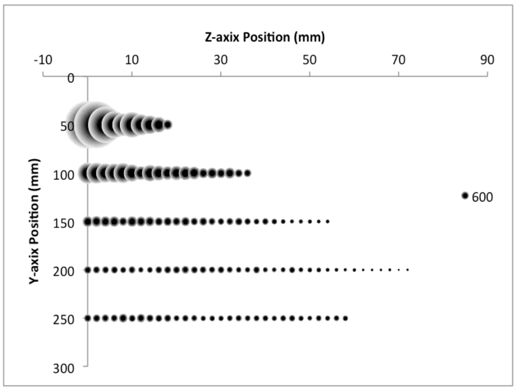
</td></tr>
<tr><td colspan="2">Delevan WM054</td></tr>
<tr><td>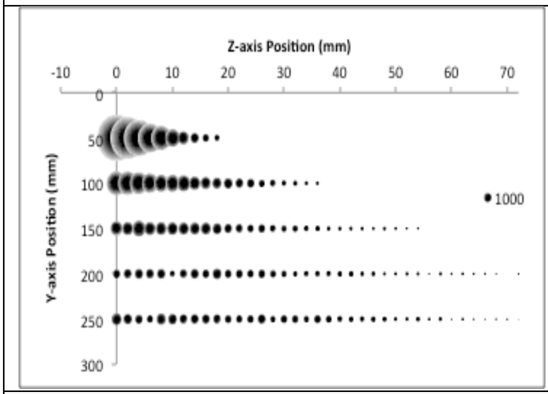
</td><td>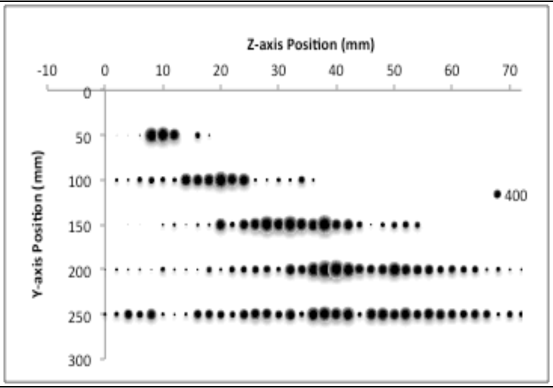
</td></tr>
<tr><td colspan="2">Delevan WM104</td></tr>
<tr><td>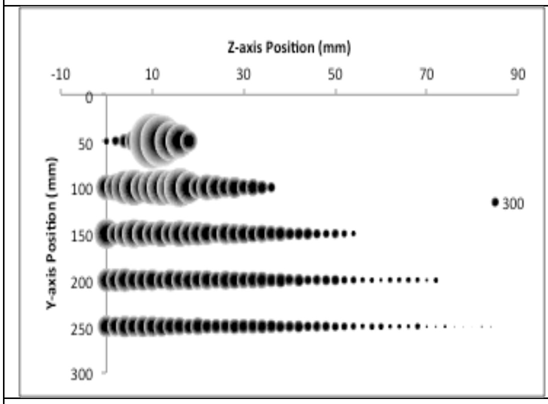
</td><td>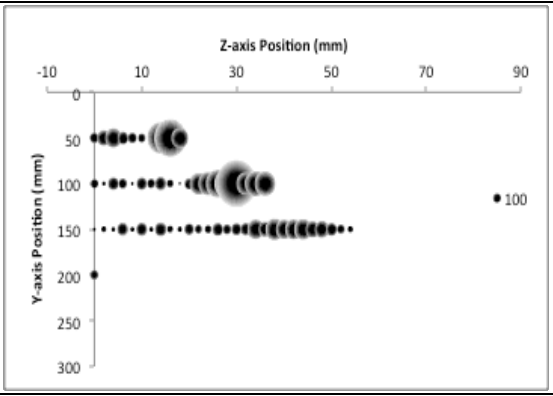
</td></tr>
<tr><td colspan="2">Delevan WM1154</td></tr>
</table>

Under vacuum conditions the hollow cone shape can be visually seen. The Delevan WM104 data rate clearly shows the hollow cone shaped spray throughout the spray sample area. As the spray travels downstream in the y-axis direction the spray also tends to shift away from the centerline in the z-axis direction. This occurs due to the lack of ambient air present in the test rig and the increased viscosity of solution when compared to the baseline condition.

The Delevan WA1154 shows a larger cone angle compared to the other nozzle used. The concentration of data clusters starts 10mm from the central axis, which indicates a cone angle of 22.6° under ATM conditions and a 22.6% increase in the cone angle at vacuum condition to 29.2°.

#### *5.4.1.4 Droplet Velocity*

The droplet velocities are plotted in Figure 5-15 for ATM condition and Figure 5-16 for vacuum condition. The plots only show the sampled points at the 150mm plane in the y-axis downstream from the orifice of the nozzle. The geometry of the nozzles, which is represented by the orifice diameter size clearly affects the droplet velocities, hence the increase in flow rate is proportional to the increase in orifice diameter.

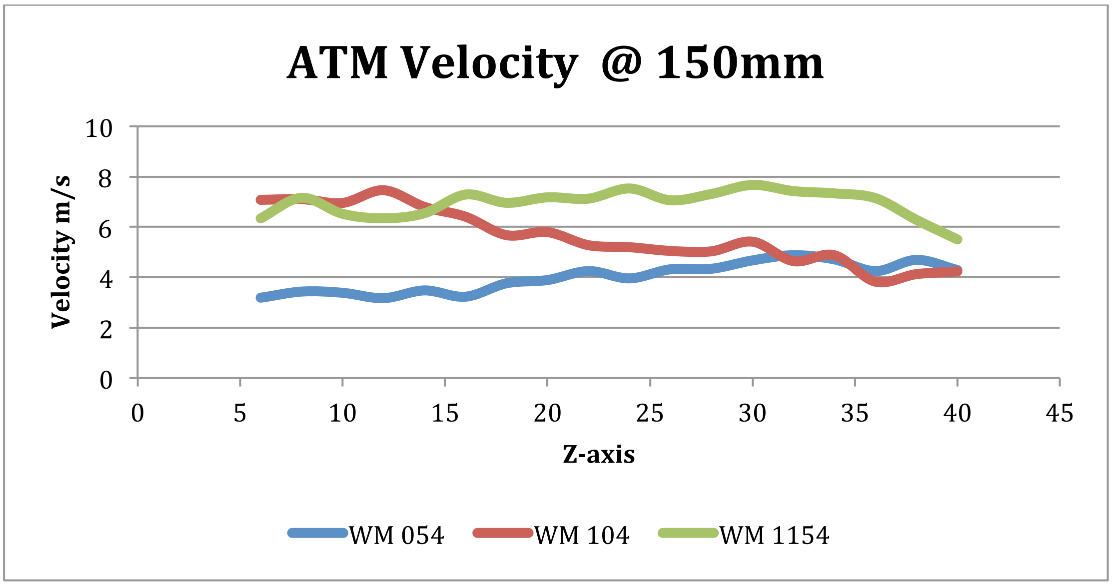

Figure 5-15 Average droplet velocity at 150mm point in y-axis for ATM condition (0.00286609 kg/ms)

Observing the Delevan WM104 nozzle at the 30mm point on the z-axis direction, an increase in velocity from 5.4 m/s at atmospheric condition to 17.1 m/s at vacuum conditions, equivalent to a 68.4% increase at equivalent positions within the spray field is evident. This is associated with the air resistance encountered by the droplets under ATM conditions, while the droplets under vacuum conditions encounter significantly less resistance. It should also be noted that in a wide cone angle with greater dispersion of the spray, the average bulk velocity of the fluid would be reduced.

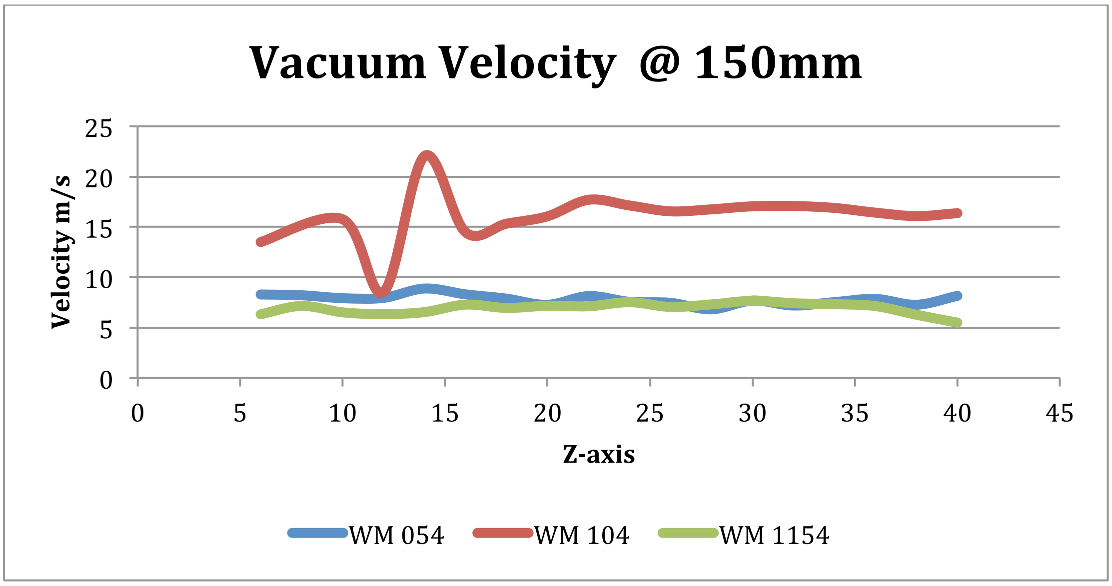

Figure 5-16 Average droplet velocity at 150mm point in y-axis for vacuum condition (0.00286609 kg/ms)

#### *5.4.1.5 Droplet SMD*

Figures 5-17 and 5-18 display the SMD for the nozzles chosen in Table 3-2. Taking into consideration that viscosity is a stabilizing force, which provides an opposing force on fluid distortion and liquid atomization, the SMD graphs show that increasing the viscosity produces a poorly atomized spray compared to the nominal condition graphs displayed in Figures 5-10 (a) and (b).

The spray quality at ATM conditions in Figure 5-17 is balanced throughout the z-axis direction with a fluctuation of 5-10%. This shows that the quality of the spray with a viscosity of 0.00286609 kg/ms is still able to atomize under ATM conditions as there is a slight increase in Reynolds number compared to the nominal conditions, which in turn suggests a minute effect of viscosity on the SMD.

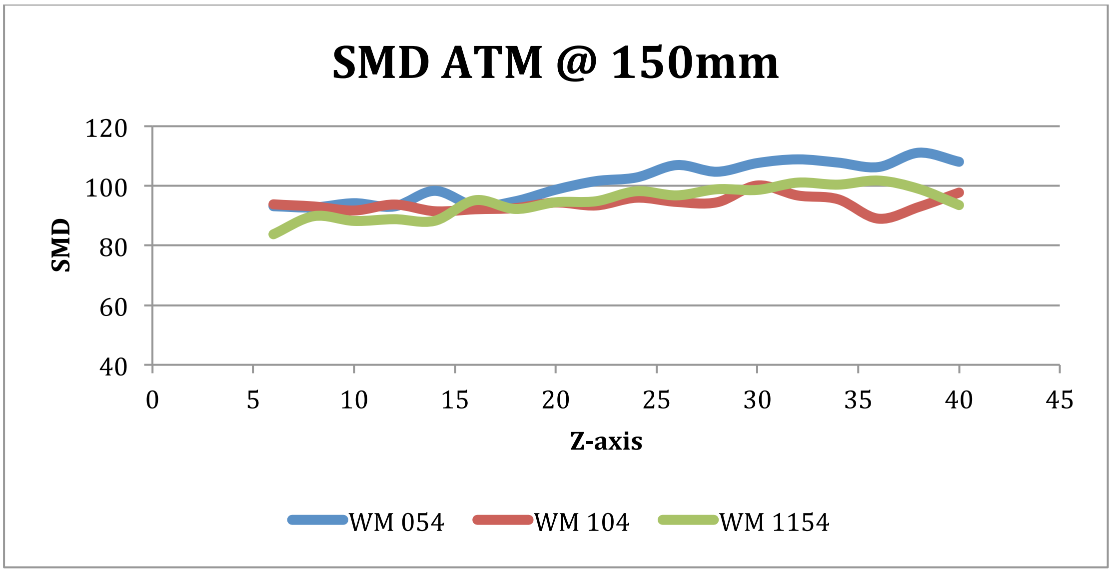

Figure 5-17 SMD at ATM condition with different nozzles (0.00286609 kg/ms)

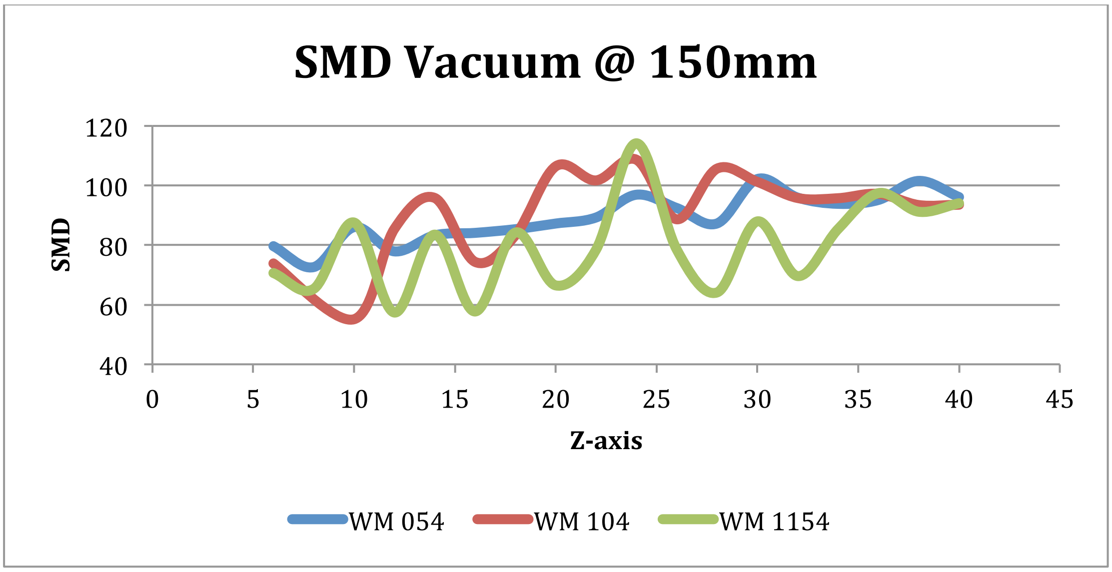

Figure 5-18 SMD at vacuum condition with different nozzles (0.00286609 kg/ms)

Looking at the SMD in Figure 5-18, it is observed that there is instability in the SMD throughout the spray in the z-axis direction for all the nozzles. This instability is produced either by a small number of large droplets at the point of measurements along the z-axis or by un-atomized spray areas. The small Reynolds number of the nozzles relative to the nominal conditions supports this theory (Lefebvre and Wang 1987; Lin and Reitz 1998). In the atmospheric condition, this phenomenon is not noticed as there are external forces that affect the atomization of the droplets as shown in Figure 5-17.

## 5.4.2 Viscous Solution Second Condition

### *5.4.2.1 Operating Conditions and Results*

Table 5-3 summarises the operating conditions and the spray characteristics of the test carried out using 50% glycerine by volume solution, which corresponds to resultant viscosity of 0.0064178 kg/ms.

Table 5-4 Summary of viscous solution second condition test and spray characteristics (0.0064178 kg/ms)

| **Test** | **ATM** | | | **Vacuum** | | |
|---|---|---|---|---|---|---|
| | **WM 054** | **WM 104** | **WM 1154** | **WM 054** | **WM 104** | **WM 1154** |
| **Water Pressure (bar)** | 3.73 | 3.73 | 3.73 | 3.73 | 3.73 | 3.73 |
| **Rig Pressure (bar)** | 1.01 | 1.01 | 1.01 | 0.03 | 0.03 | 0.03 |
| **ΔP (bar)** | 2.72 | 2.72 | 2.72 | 3.7 | 3.7 | 3.7 |
| **Re Liquid** | 48.90 | 48.99 | 70.86 | 62.06 | 153.47 | 177.59 |
| **We Liquid** | 11.34 | 13.74 | 30.16 | 36.43 | 139.44 | 184.08 |
| **Oh Liquid** | 0.06887 | 0.07567 | 0.07750 | 0.09726 | 0.07695 | 0.07640 |
| **SMD, D32 (μm)** | 96.67 | 95.31 | 87.78 | 74.67 | 90.59 | 91.77 |
| **$D_{21}$ (μm)** | 93.00 | 82.86 | 77.56 | 40.55 | 78.43 | 79.83 |

### *5.4.2.2 Spray Droplet Size Distribution*

The effect of increasing the viscosity can be observed in the droplet diameter count frequency distributions Figures 5-19 and 5-21. Comparing the peak value of Delevan WM 104 at ATM 42μm and 56μm at vacuum conditions with the peak values of the nominal condition 15μm and 40μm for atmospheric condition and vacuum conditions respectively, it is proven that viscosity has a greater influence on spray quality in terms of droplet diameter and breakup, which is not surprisingly agreed with the literature available (Aliseda et al. 2008; Warnakulasuriya and Worek 2008).

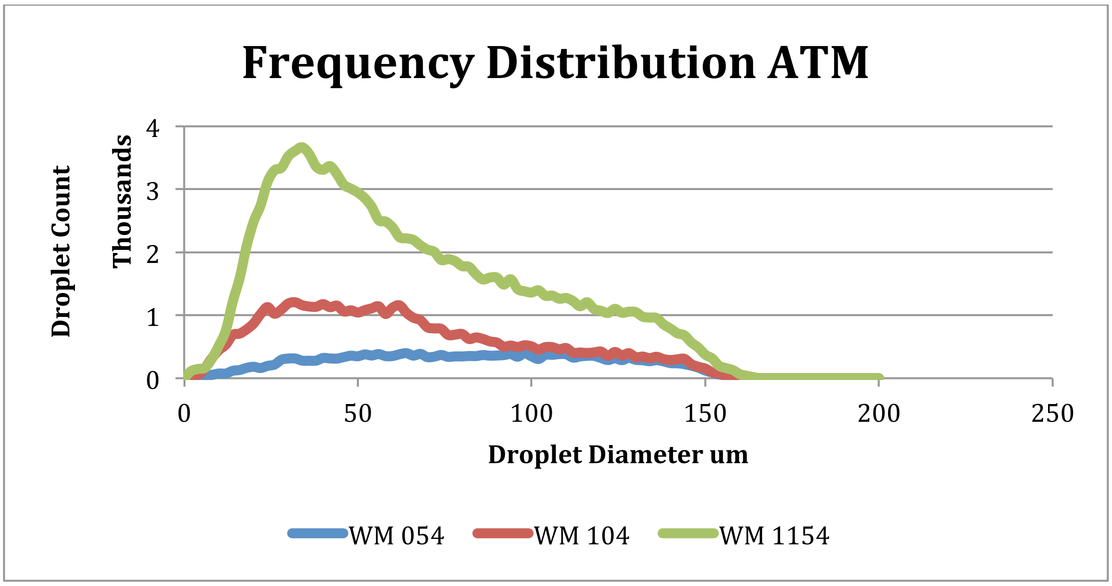

Figure 5-19 Frequency distribution by droplet count ATM (0.0064178 kg/ms)

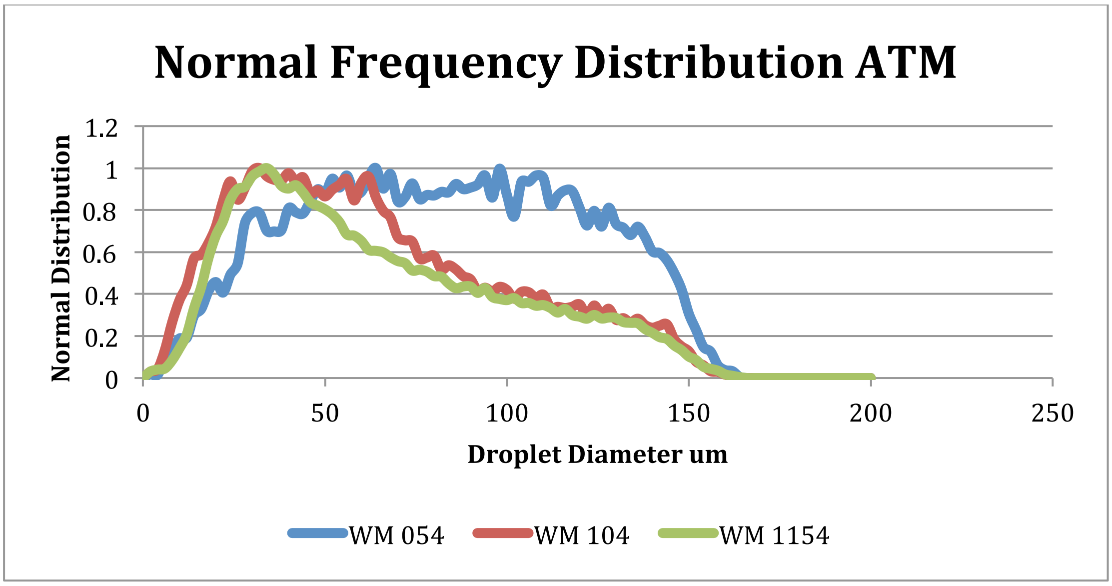

Figure 5-20 Normal frequency distribution to peak value ATM (0.0064178 kg/ms)

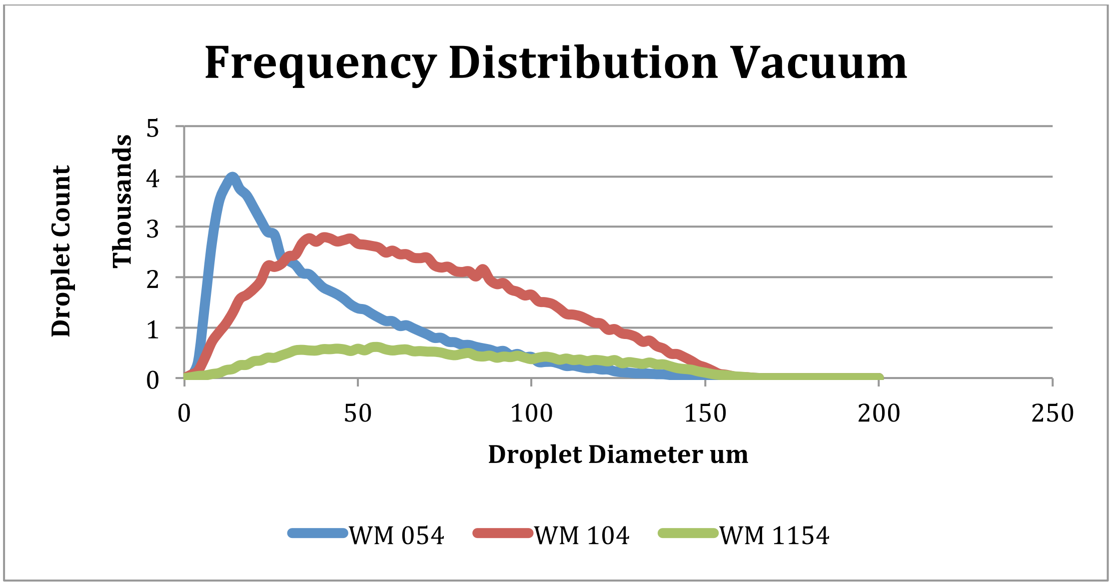

Figure 5-21 Frequency distribution by droplet count vacuum (0.0064178 kg/ms)

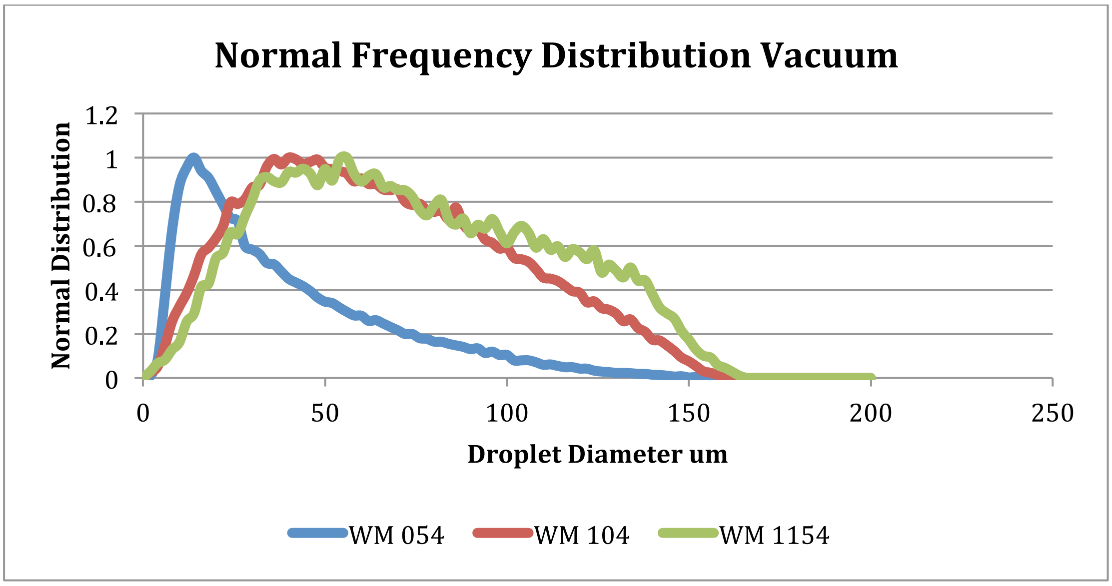

Figure 5-22 Normal frequency distribution to peak value vacuum (0.0064178 kg/ms)

The atomization quality of Delevan WM054 nozzle at the vacuum condition is relatively higher than the ATM condition, which can also be observed to have a peak point at lower diameter of 12µm. This is due to the higher ΔP that corresponds to a higher flow rate compared to the atmospheric condition. Nevertheless this observation can be deemed to be unsatisfactory as the WM054 nozzle failed to atomize completely. It was observed to reach the tulip stage as described by Lefebvre (1989), Table 5-5 also confirms this phenomenon as it shows a uniform distribution of clusters along all the planes for the WM054 nozzle at the vacuum condition. Figure 5-23 is a physical representation of the WM054 tulip stage spray.

#### *5.4.2.3 Droplet Data Rate*

All the droplet data rate graphs presented in Table 5-5 show higher data rates closer to the nozzle tip at 50mm downstream compared to the planes further downstream in the y-axis direction, implying that the spray density in the discrete region surrounding the nozzle is higher, which was also observed earlier in Section 5.4.1.3.

Under atmospheric conditions it is noted that the spray clusters for WM054 and WM104 tend to stay to the centerline throughout the planes downstream; this is mostly due to the stabilizing forces that have increased with the increasing viscosity.

On the other hand it is not the case for WM1154; it is observed that the spray clusters have an even spread of droplets moving downstream throughout the planes and they also show a slight outline of a hollow cone spray. The higher flow rate through the nozzle and the aero-dynamical forces acting on the spray are responsible for this act.

Under vacuum conditions the hollow cone shape can be visually seen for WM104 and WM1154 nozzles. Comparing the data rate plot for the WM104 under vacuum condition with 20% glycerol by volume and 50% glycerol by volume it is noticed that there is a lower quality of atomization, which is caused by the increase in viscosity and a relative decrease in the Reynolds number as indicated by Tables 5-2 and 5-4.

Figure 5-23 Delevan WM054 tulip stage spray characteristic

The spray angle is also relatively larger when comparing the different nozzles under vacuum conditions; as discussed earlier this is due to the higher flow rates achieved under vacuum conditions (Warnakulasuriya and Worek 2008).

Table 5-5 Droplet data rate with varying nozzles (0.0064178 kg/ms)

| Droplet Data Rate | |
|---|---|
| ATM | Vacuum |
| 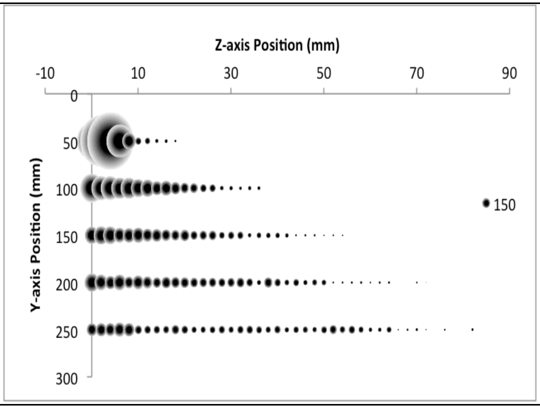 | 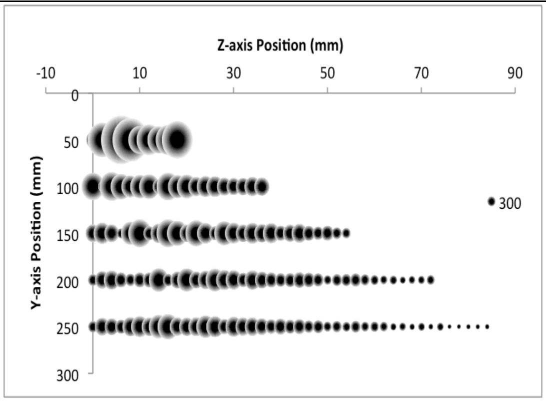 |
| WM 054 | |
| 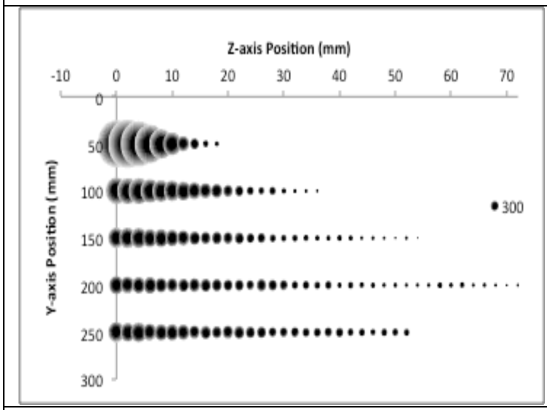 | 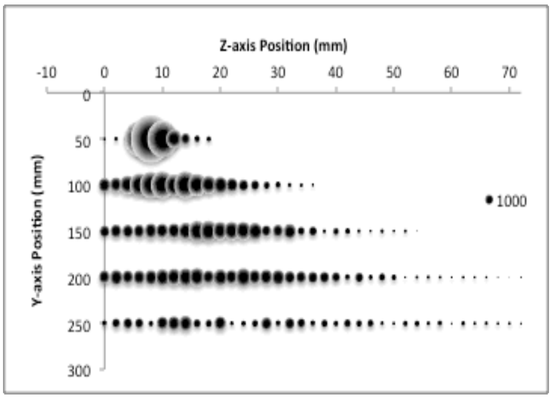 |
| WM 104 | |
| 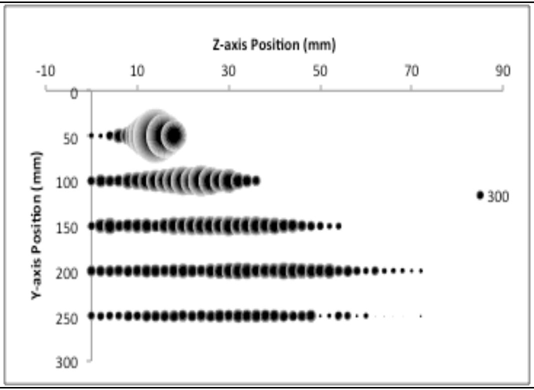 | 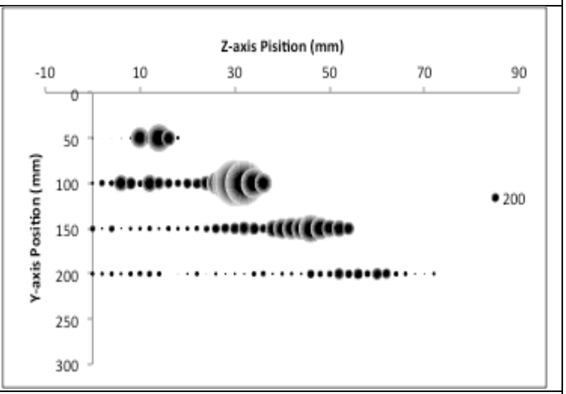 |
| WM 1154 | |

#### 5.4.2.4 Droplet Velocity

As stated earlier, the velocity graphs are plotted for atmospheric condition and vacuum condition and are shown in Figures 5-20 and 5-21 respectively.

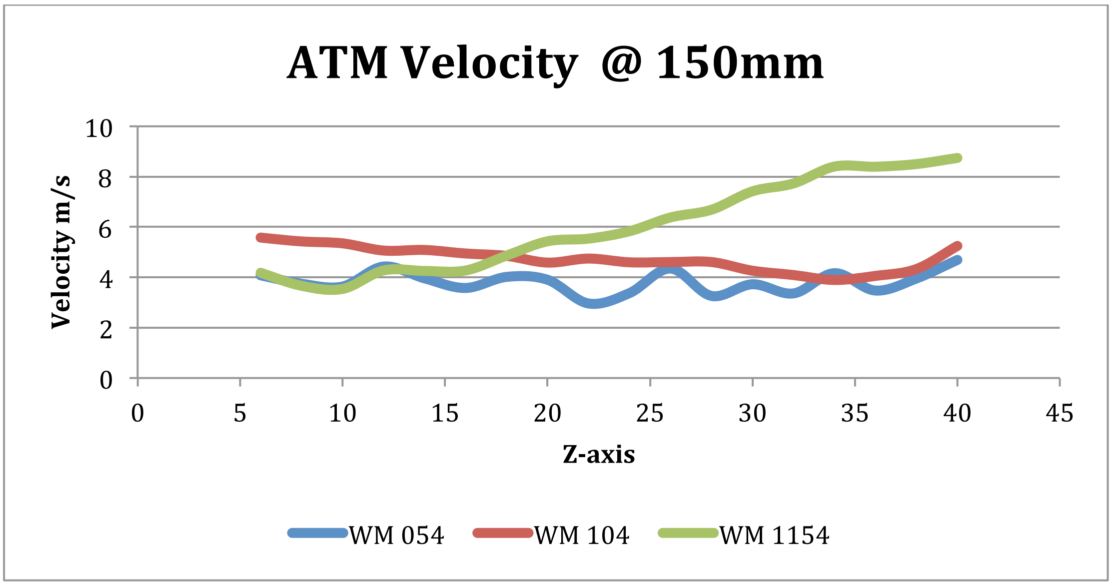

Figure 5-24 Average droplet velocity at 150mm point in y-axis for ATM condition (0.0064178 kg/ms)

Looking at the 30mm point on the z-axis direction in both Figures 5-24 and 5-25, it is noticed that the velocity of the WM104 nozzle is higher at the vacuum condition. The velocity at atmospheric condition is 4.2 m/s and at vacuum condition it is 14.7 m/s, which exhibits an increase of 71.4% at equivalent positions within the spray field.

From the above statement, it is noted that the increase in viscosity has got a minimal effect on the velocity when compared to the velocity value of 20% by volume viscosity. Therefore the increase in velocity is mostly due to the pressure difference through the nozzle.

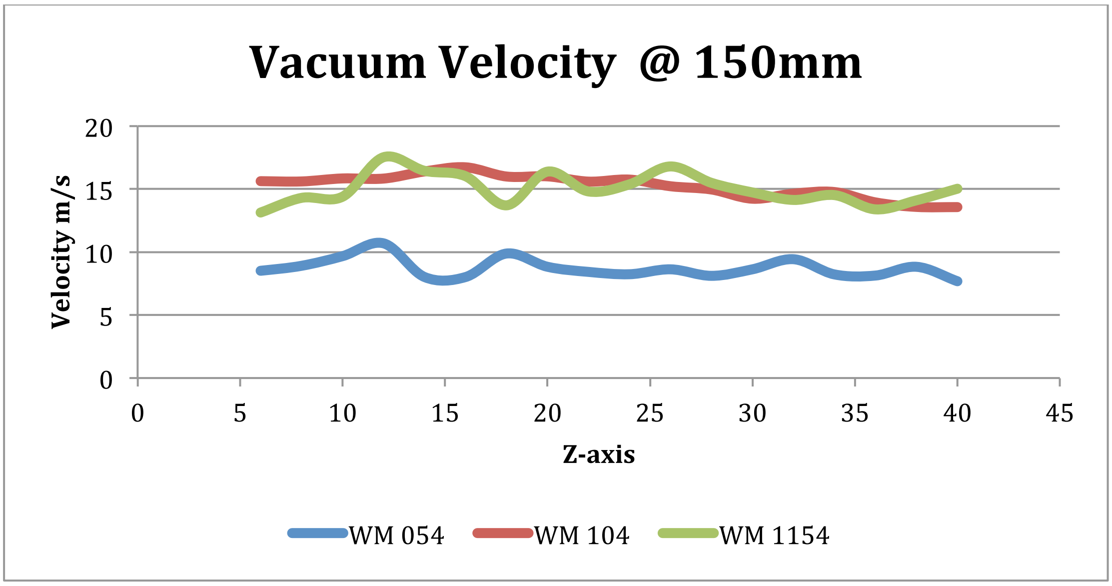

Figure 5-25 Average droplet velocity at 150mm point in y-axis for vacuum condition (0.0064178 kg/ms)

#### *5.4.2.5 Droplet SMD*

Figures 5-26 and 5-27 which display the SMD for the different nozzles used in the experiments at the two conditions, atmospheric and vacuum. In the light of the results of the WM054 nozzle, being not fully atomized as discussed in previous sections of this chapter, it is noted that the nozzle with the larger orifice had better SMD values throughout the 150mm plane at atmospheric and vacuum conditions.

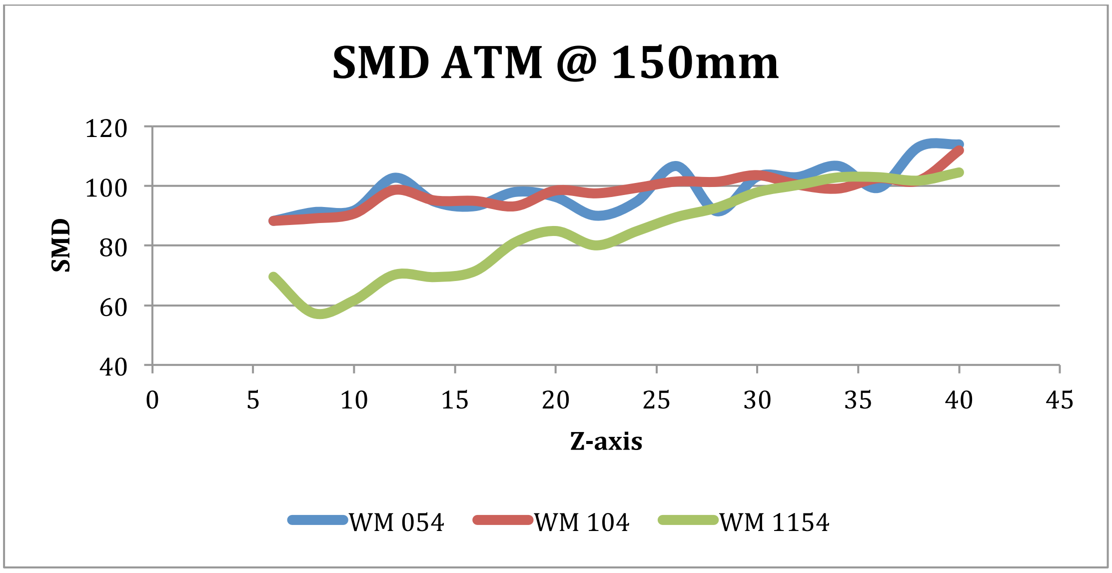

Figure 5-26 SMD at ATM condition with different nozzles (0.0064178 kg/ms)

With higher viscosity the geometry of the nozzle clearly has great effect on the spray quality in terms of SMD and droplet distribution. The results also indicate that the nozzle has a greater effect at the vacuum condition. Taking a common point in the sample area, which is 30mm on the z-axis, the difference in SMD between WM104 and WM1154 is 5.6% in favour of the WM1154 nozzle, while at vacuum condition it is 23.9% in favour of the WM1154. This is not only the effect of the nozzle geometry of having a relatively larger orifice diameter but also of having a higher mass flow rate (Reitz and Bracco 1986; Warnakulasuriya and Worek 2008).

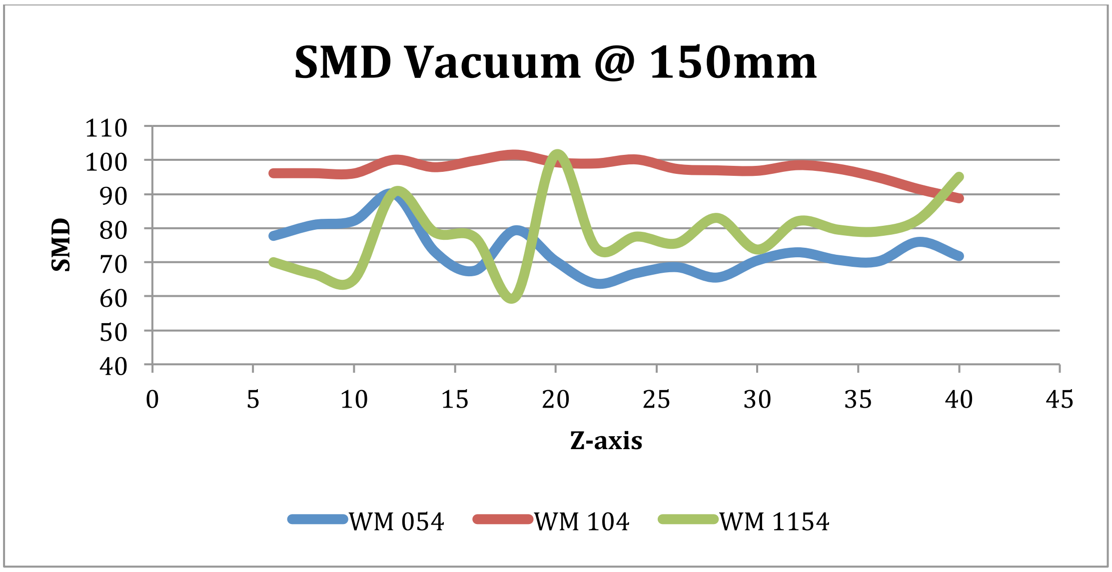

Figure 5-27 SMD at ATM condition with different nozzles (0.0064178 kg/ms)

Looking at the Reynolds number of the WM104 nozzle at atmospheric and vacuum conditions, 48.99 and 153.47 respectively, it is clear that the viscosity force i.e. internal forces or stabilizing forces of the liquid have a large effect on atomization. The Reynolds number of this experiment is significantly smaller than the nominal condition displayed in Table 5-1 and the 20% by volume concentration of glycerol solution displayed in Table 5-2, hence the greater effect of internal forces on the liquid spray.

## 5.5 Analysis of Viscous Solutions with Additive

Referring to Table 3-3 the viscosity tests are carried out in two different viscosity values with the same amount of additive added. The first test condition was carried out using 20% glycerine by volume solution and a 50% by mass 2-ethyl-1-hexanol additive (0.0024808 kg/ms) and the second test condition was carried out using 50% glycerine by volume solution and a 50% by mass 2-ethyl-1-hexanol additive (0.0067579 kg/ms).

The literature suggests using additives to enhance the absorption rate, by reducing the surface tension of the liquid spray used. Other literatures also propose using additives or surfactants to overcome the crystallization in the absorption refrigeration systems. In this study the additives are used to measure and quantify the reduction in SMD and enhance spray quality in terms of dispersion of droplets (Kim et al. 1999; Yoon et al. 1999).

### 5.5.1 Viscous Solution with Additive First Condition

#### *5.5.1.1 Operating Conditions and Results*

Table 5-6 summarizes the operating conditions and the spray characteristics of the viscous solution with the additive enhancement first condition, which are 20% by volume glycerol and 50% 2EH by mass solution (0.0024808 kg/ms). It is expected that the additive or the so-called 2EH surfactant affect the Reynolds number, Weber number and Ohnesorge number since surface tension is a major player in calculating those dimensionless numbers.

Table 5-6 Summary of viscous solution with additive first condition test and spray characteristics (0.0024808 kg/ms)

| **Test** | **ATM** | | | **Vacuum** | | |
|---|---|---|---|---|---|---|
| | **WM 054** | **WM 104** | **WM 1154** | **WM 054** | **WM 104** | **WM 1154** |
| **Water Pressure (bar)** | 3.73 | 3.73 | 3.73 | 3.73 | 3.73 | 3.73 |
| **Rig Pressure (bar)** | 1.01 | 1.01 | 1.01 | 0.03 | 0.03 | 0.03 |
| **ΔP (bar)** | 2.72 | 2.72 | 2.72 | 3.7 | 3.7 | 3.7 |
| **Re Liquid** | 24.19 | 54.47 | 101.72 | 63.10 | 80.48 | 220.69 |
| **We Liquid** | 1.91 | 9.35 | 30.08 | 19.62 | 37.09 | 160.48 |
| **Oh Liquid** | 0.05706 | 0.05614 | 0.05392 | 0.07020 | 0.07568 | 0.05740 |
| **SMD, D32 (μm)** | 45.08 | 54.43 | 72.26 | 41.12 | 33.04 | 81.47 |
| **$D_{21}$ (μm)** | 49.18 | 50.46 | 59.67 | 32.87 | 27.86 | 54.26 |

#### *5.5.1.2 Spray Droplet Size Distribution*

The droplet diameter count frequency distributions, indicated in Figure 5-28, appear to have similar peak diameters throughout the different nozzles, while having different droplet counts frequency. The droplet`s diameter also tends to shift towards the smaller diameter values compared to the viscous solution first condition test, shown in Figure 5-11.

The flow rate and the nozzle geometry as discussed in previous sections have a clear effect on the amplitude of the peaks, which are shown to be varying from one nozzle to the other (Nasr et al. 2002).

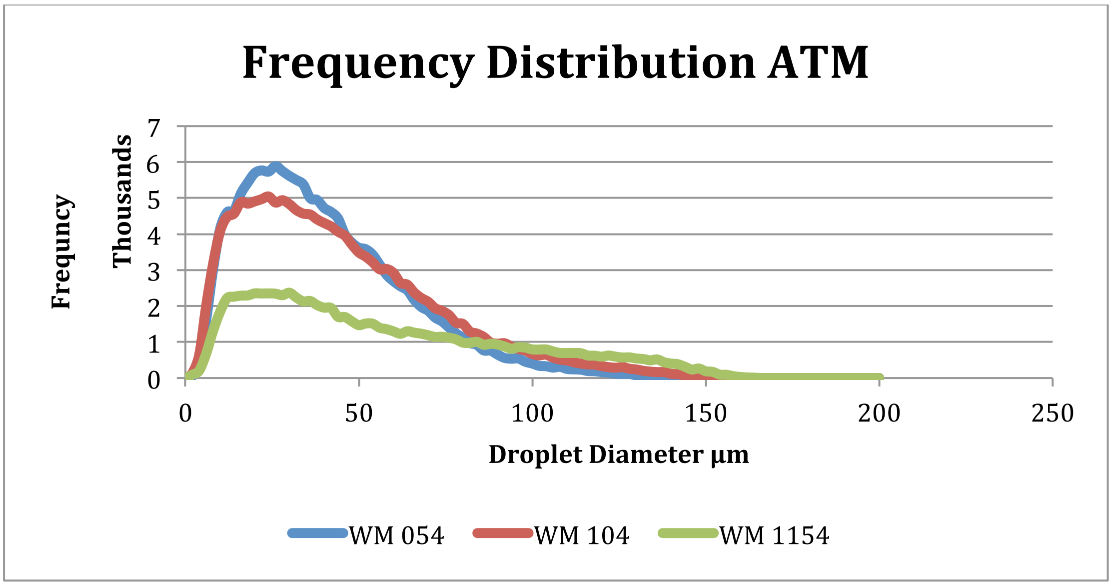

Figure 5-28 Frequency distribution by droplet count at atmospheric condition

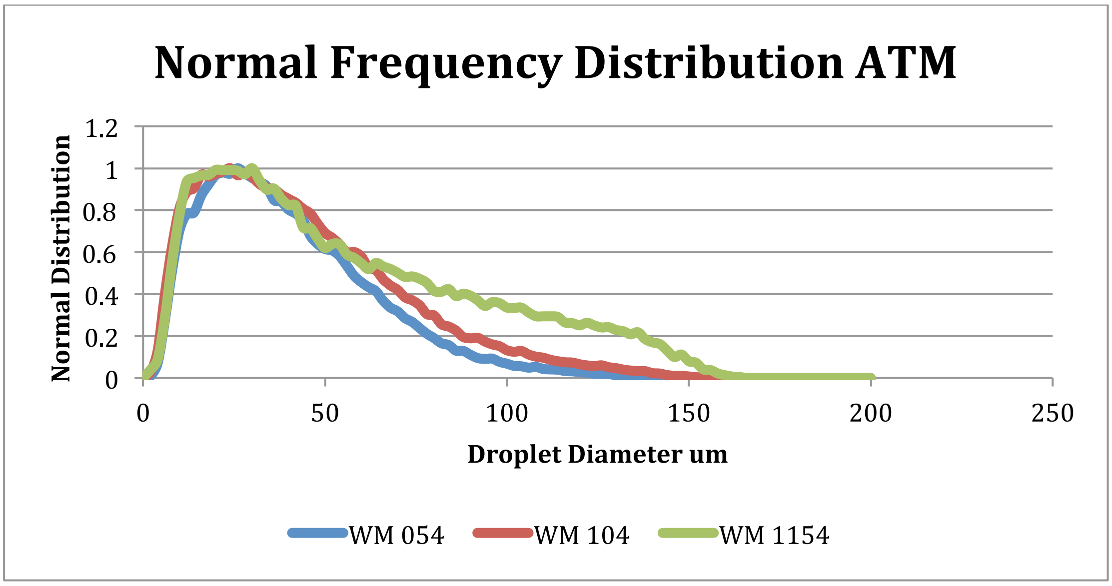

Figure 5-29 Normal frequency distribution to peak value at atmospheric condition

Although the peak value of the WM104 nozzle with the additive under atmospheric conditions is 22µm, it is slightly higher compared to the same nozzle with no additive under atmospheric conditions, that is 16µm.

According to the peak value, it indicates that the additive did not have any effect on the spray quality, which is not the actual case. The additive did have a great effect although it did not have a smaller peak; however it has the majority of the droplets distributed between the 8µm and the 50µm.

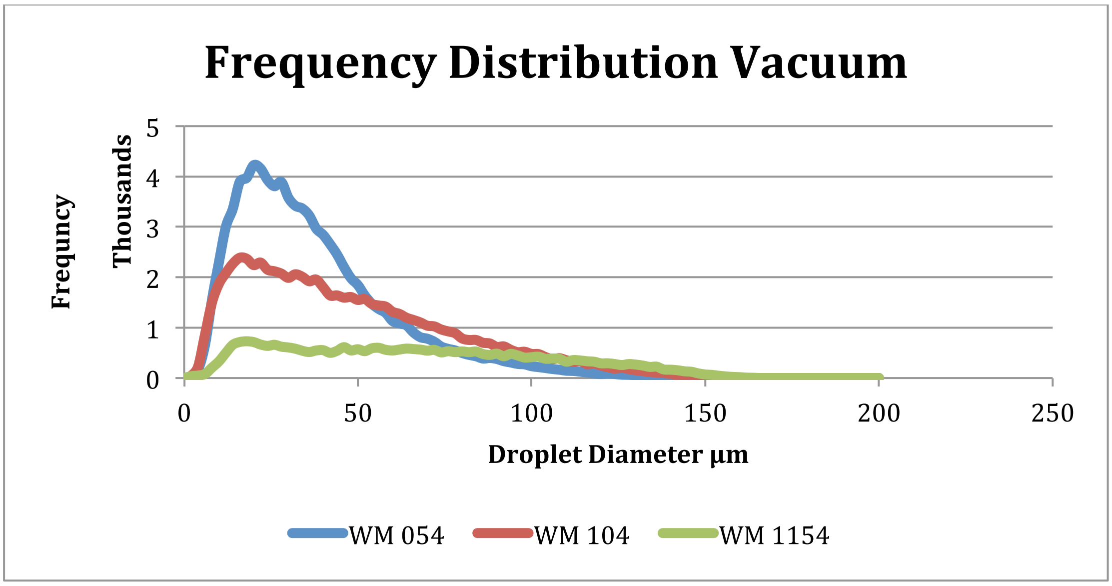

Figure 5-30 Frequency distribution by droplet count at vacuum condition

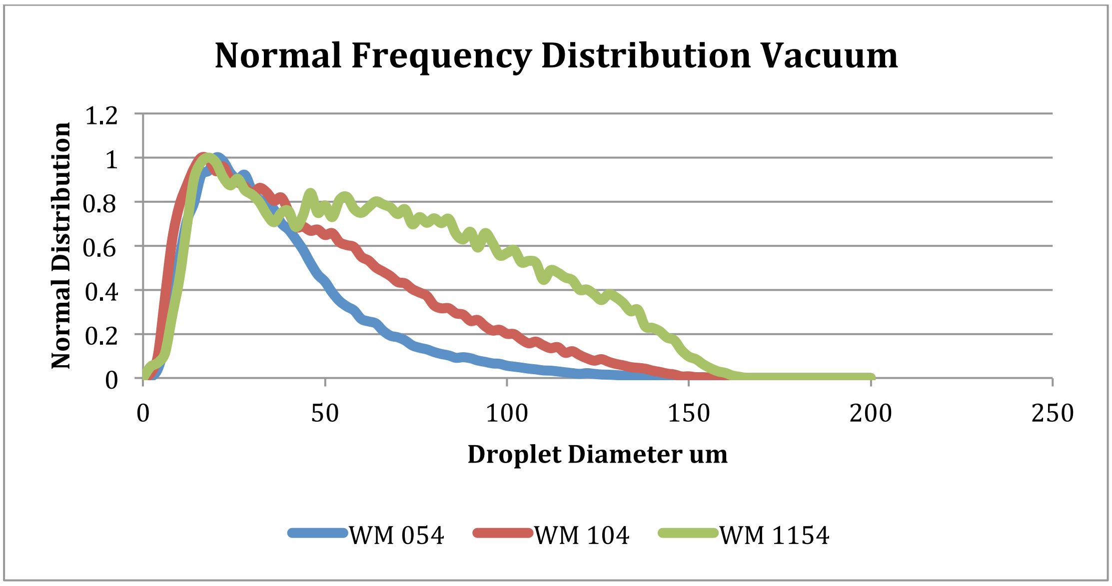

Figure 5-31 Normal frequency distribution to peak value at vacuum condition

The results under vacuum condition are far more interesting because in the vacuum the major forces that affect atomization are the internal or stabilizing forces and by adding the additive it has an immense effect on disturbing these stabilizing forces.

The peak value of the WM104 nozzle is decreased from 54µm to 14µm, which resembles a great drop of 74%. The decrease of the Webber number and the increase of Ohnesorge number compared to the viscous solution with no additive explain this phenomenon. These numbers are available in Table 5-6 and Table 5-2.

#### *5.5.1.3 Droplet Data Rate*

The droplet data rate plots presented in Table 5-7 show a larger spray angle compared to the spray angle of Table 5-3. The spray angle is 37.6° which is just shy of the maximum spray angle achievable by the nozzles 40°. These findings support the influence of the additive when compared to the spray angle achieved by the viscous solution of 29.2°.

The hollow cone spray features are also visible in the DDRP in Table 5-7 in both the atmospheric and vacuum conditions. Under atmospheric conditions the data rate is relatively higher and better dispersed throughout the planes downstream, compared to the vacuum conditions. This is due to the aid of the aero-dynamical forces acting on the spray and is enhanced with the additive, which decreases the effect of the stabilizing forces acting within the fluid.

Table 5-7 Droplet data rate with varying nozzles for the additive first condition

<table>
<tr><th colspan="2">Droplet Data Rate</th></tr>
<tr><th>ATM</th><th>Vacuum</th></tr>
<tr><td>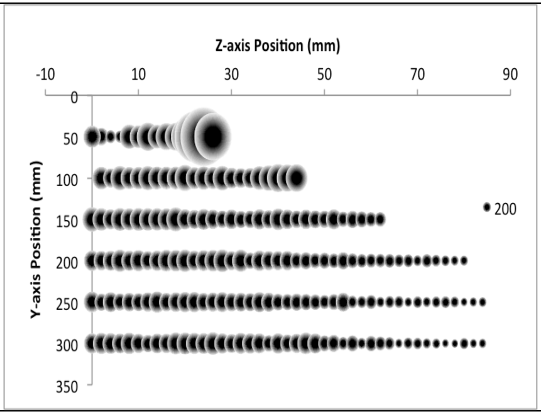 </td><td>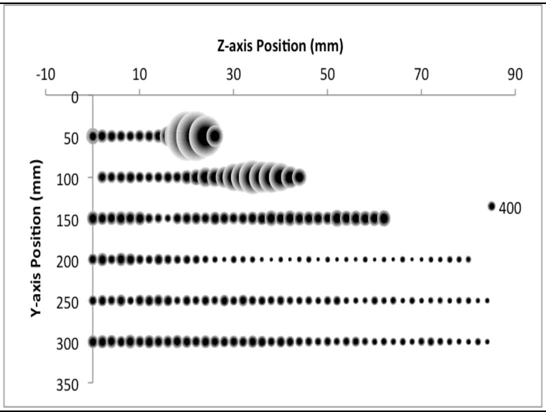 </td></tr>
<tr><td colspan="2">WM 054</td></tr>
<tr><td>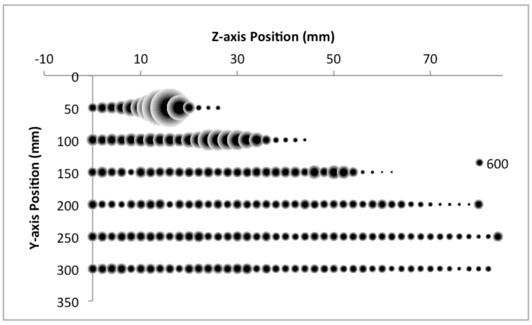 </td><td>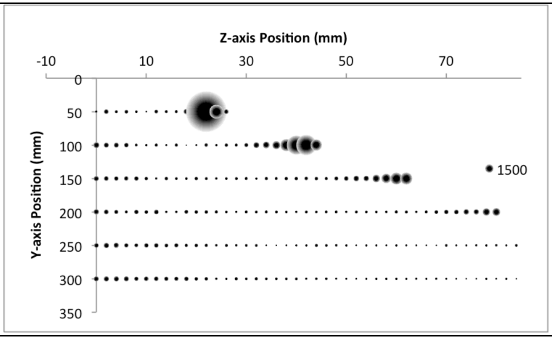 </td></tr>
<tr><td colspan="2">WM 104</td></tr>
<tr><td>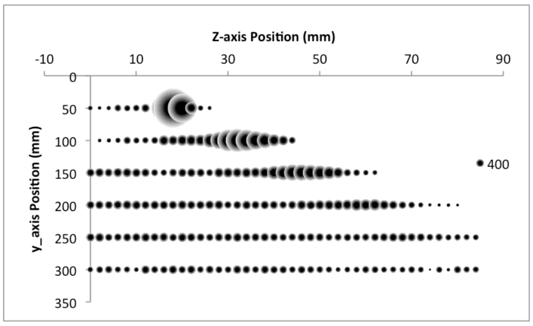 </td><td>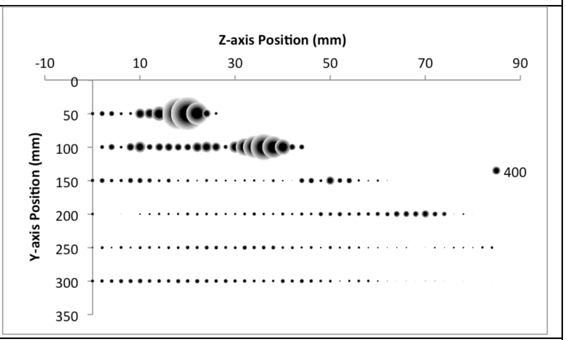 </td></tr>
<tr><td colspan="2">WM 1154</td></tr>
</table>

#### *5.5.1.4 Droplet Velocity*

As discussed from the previous section, the spray angle is relatively larger and the spray is physically a hollow cone spray, therefore the real data in Figure 5-32 starts at 30mm point in the z-axis direction, and 40mm in Figure 5-33.

In Figure 5-32 the nozzle geometry effect is shown as the nozzle with the larger orifice has a relatively higher velocity, and the viscosity is not affecting the flow rate as it is shown in Figure 5-15.

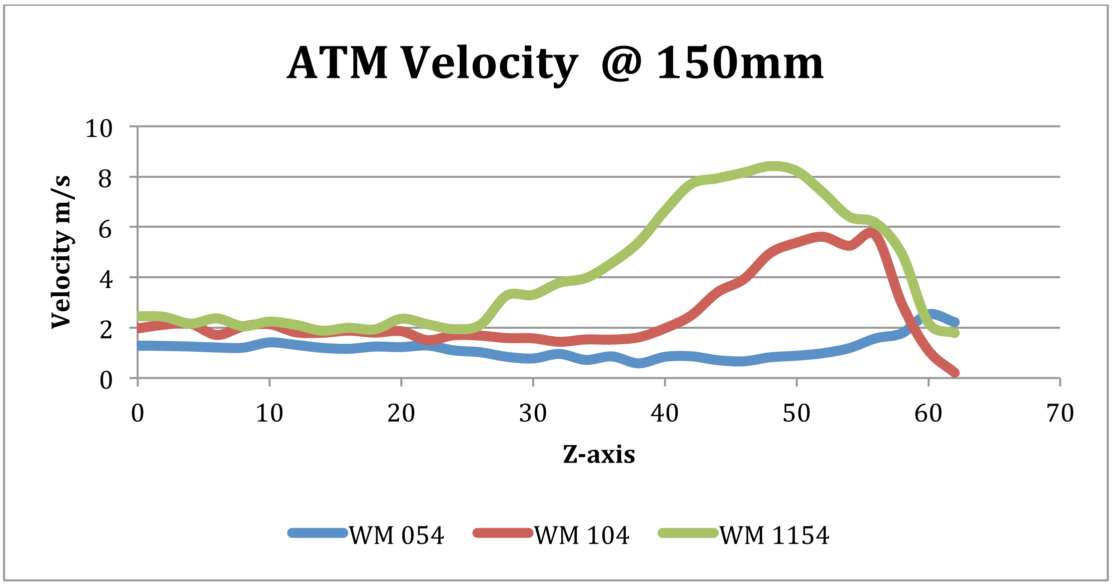

Figure 5-32 Average droplet velocity at 150mm point in y-axis for ATM condition

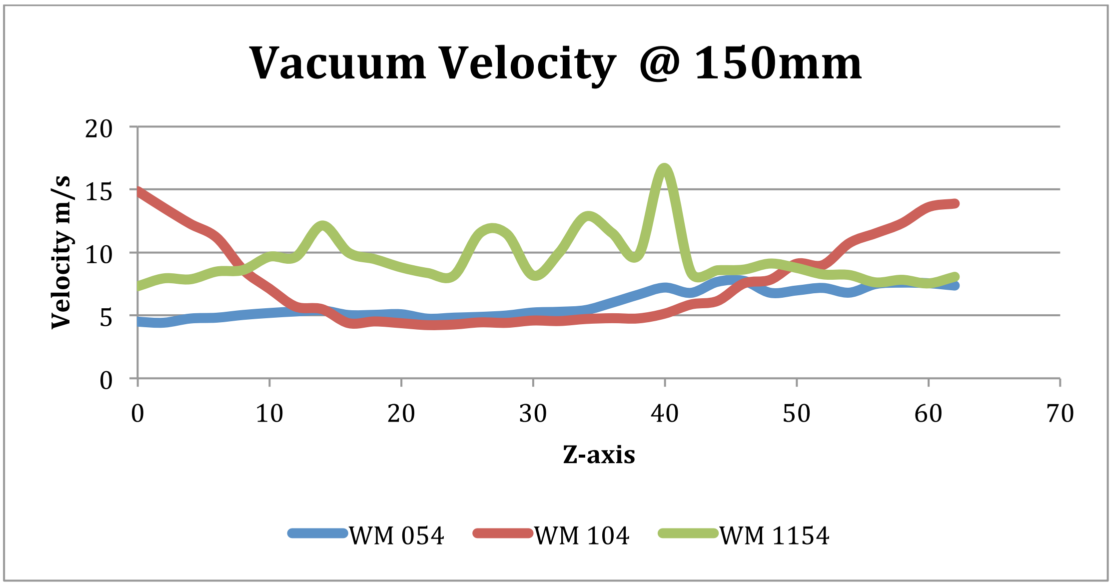

Figure 5-33 Average droplet velocity at 150mm point in y-axis for vacuum condition

Figure 5-33 shows the velocity at the 150mm plane downstream from the nozzle orifice at the vacuum conditions. The vacuum condition has got a relatively greater pressure difference, which causes the increase in velocity and is also assisted by the lack of air resistance in the test rig.

#### 5.5.1.5 *Droplet SMD*

The SMD values in Figure 5-34 show a steady development prior to the 30mm point on the z-axis. After the 30mm point we can see the increasing SMD values for all the nozzles that are tested. This is as detailed earlier due to the hollow cone configuration of the nozzles. This is also visible in Figure 5-35 that has the starting point of real data at the 40mm point in the z-axis.

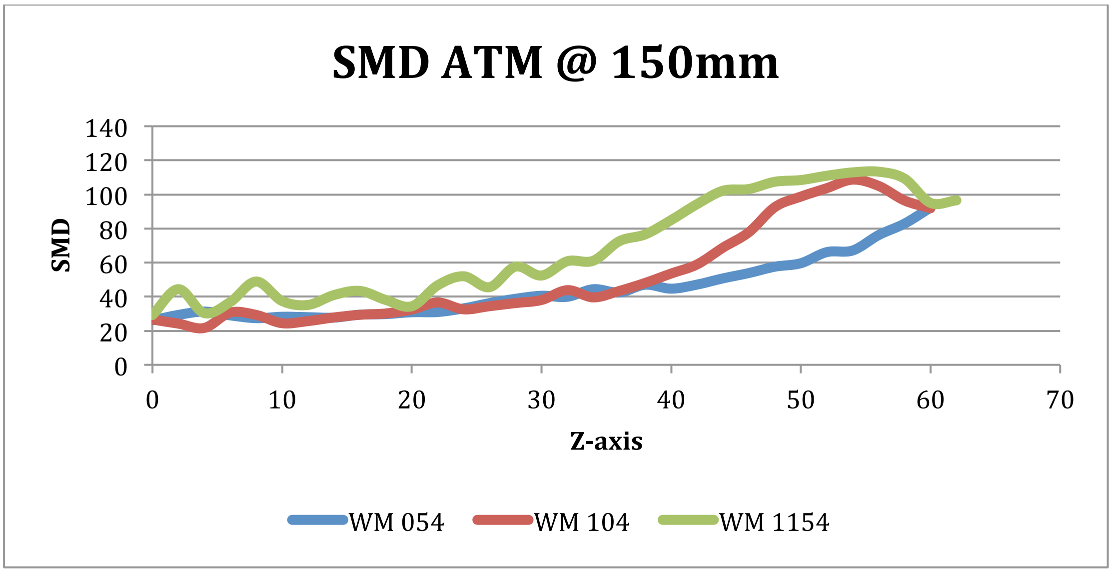

**Figure 5-34 SMD at ATM condition with different nozzles**

Looking at WM104 nozzle to compare the SMD of the viscous solution with and without the additive, it is noted that at 40mm point in the z-axis direction under vacuum condition, the SMD drops from 94.0μm to 22.0μm for the 20% viscous solution by volume with additive.

The Weber number and Reynolds number values support the large drop in SMD value, which are smaller than the Weber number and Reynolds number of the viscous solution. This states that the surface tension is reduced that is proven by the Weber number and that the viscosity force or stabilizing force is reduced, which is proven by the Reynolds number.

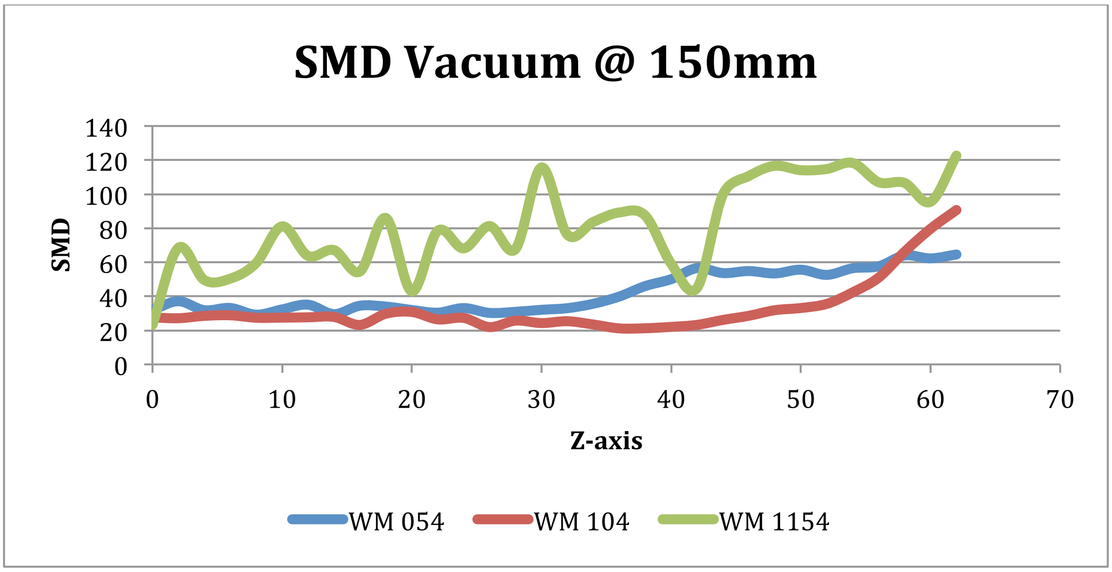

Figure 5-35 SMD at vacuum condition with different nozzles

## 5.5.2 Viscous Solution with Additive Second Condition

### *5.5.2.1 Operating Conditions and Results*

Table 5-8 Summary of viscous solution with additive second condition test and spray characteristics (0.0067579 kg/ms)

| **Test** | **ATM** | | | **Vacuum** | | |
|---|---|---|---|---|---|---|
| | **WM 054** | **WM 104** | **WM 1154** | **WM 054** | **WM 104** | **WM 1154** |
| **Water Pressure (bar)** | 3.73 | 3.73 | 3.73 | 3.73 | 3.73 | 3.73 |
| **Rig Pressure (bar)** | 1.01 | 1.01 | 1.01 | 0.03 | 0.03 | 0.03 |
| **ΔP (bar)** | 2.72 | 2.72 | 2.72 | 3.7 | 3.7 | 3.7 |
| **Re Liquid** | 11.88 | 19.38 | 54.27 | 10.45 | 20.63 | 126.69 |
| **We Liquid** | 2.48 | 6.10 | 47.20 | 3.44 | 11.76 | 227.55 |
| **Oh Liquid** | 0.13261 | 0.12746 | 0.12659 | 0.17764 | 0.16618 | 0.11907 |
| **SMD, D32 (μm)** | 56.57 | 60.78 | 84.66 | 33.28 | 41.69 | 88.72 |
| **$D_{21}$ (μm)** | 59.41 | 58.18 | 67.31 | 32.33 | 37.24 | 75.45 |

Table 5-8 summarizes the operating conditions and the spray characteristics of the viscous solution with the additive enhancement second condition, which are 50% by volume glycerol and 50% 2EH by mass solution (0.0067579 kg/ms). The Reynolds number, Weber number and Ohnesorge number are affected by the addition of the additive.

#### *5.5.2.2 Spray Droplet Size Distribution*

The frequency distribution graphs in Figure 5-36 shows that there are a large number of large droplets as well as a huge number of small droplets, which suggests that there is primary break-up and minor secondary break-up of the spray. This is also noted when comparing the 50% by volume viscosity with the 50% by volume viscosity with additive, which has a relatively higher SMD.

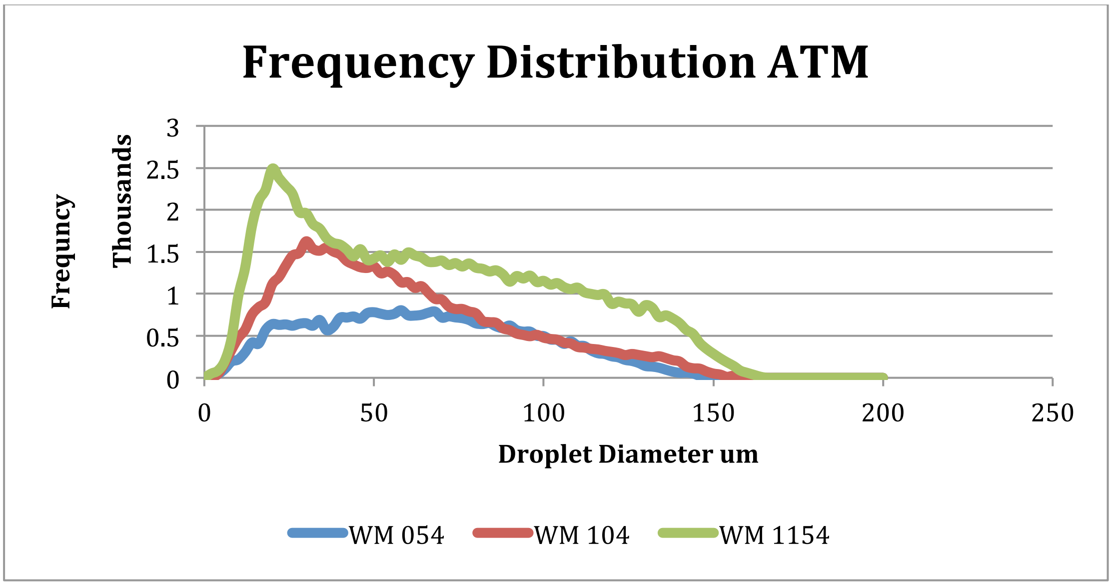

Figure 5-36 Frequency distribution by droplet count at atmospheric condition

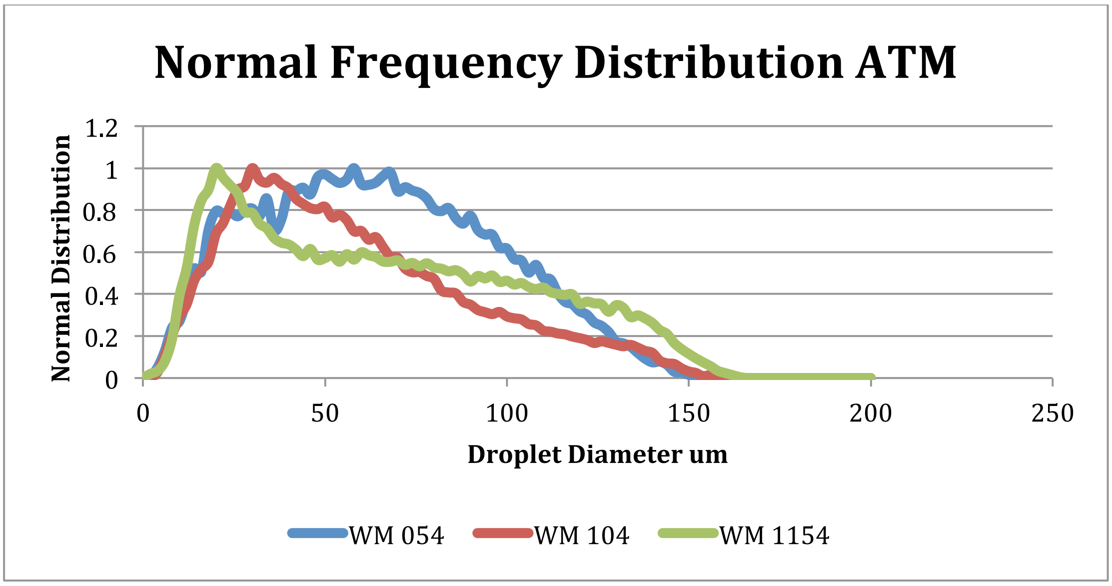

Figure 5-37 Normal frequency distribution to peak value at atmospheric condition

On the other hand, in the vacuum condition, shown in Figure 5-38, a different outcome is seen, which shows small droplets to be dominant, although it has got a lower data rate. This shows that there is better atomization in terms of SMD but not data rate. When looking back at Figure 5-21, the date rate is relatively higher but the SMD values are also relatively higher.

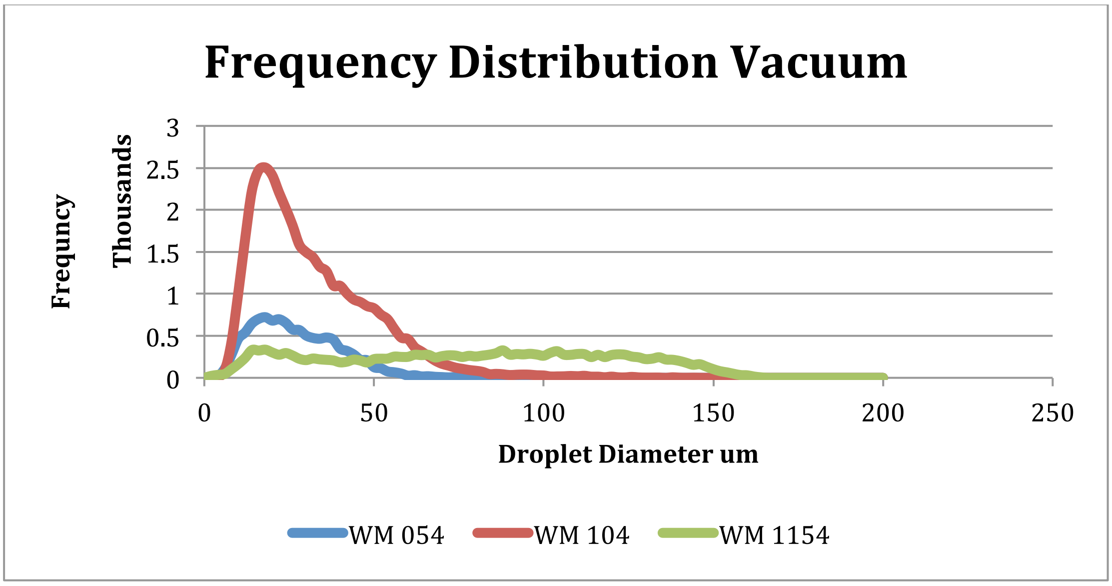

Figure 5-38 Frequency distribution by droplet count at vacuum condition

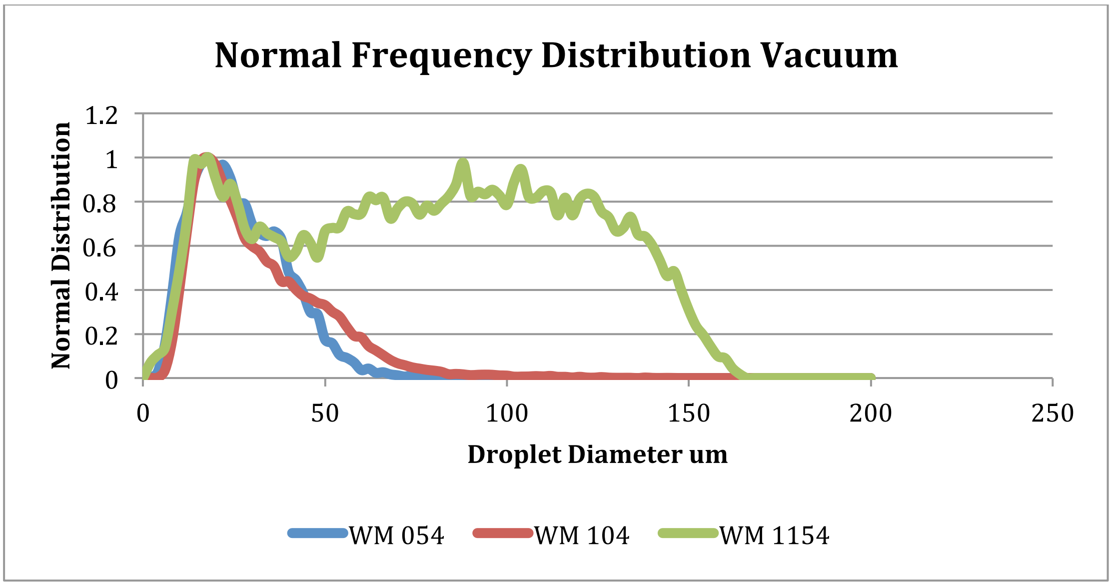

Figure 5-39 Normal frequency distribution to peak value at vacuum condition

Observing the dimensionless numbers (Re, We, Oh), they all satisfy the finding of this frequency distribution, as they are all significantly lower when compared to the nominal and the 50% viscosity by volume.

#### *5.5.2.3 Droplet Data Rate*

From Table 5-9, the WM054 nozzle results show that there is no atomization under the atmospheric condition; therefore it can be neglected. At the vacuum condition, although the results show a steady and a fine distribution of droplets throughout the planes it actually failed to atomize; therefore it can also be neglected from the results.

The WM104 nozzle, on the other hand, shows a similar distribution of droplets in both the atmospheric and vacuum conditions. They also do not show the hollow cone structure.

The WM1154 nozzle has got a hollow cone effect in both the atmospheric and vacuum conditions, and when compared to the viscous solution of 50% by volume with no additive, it is clear that it has a better atomization.

Table 5-9 Droplet data rate with varying nozzles for the additive first condition

<table>
<tr><th colspan="2">Droplet Data Rate</th></tr>
<tr><th>ATM</th><th>Vacuum</th></tr>
<tr><td>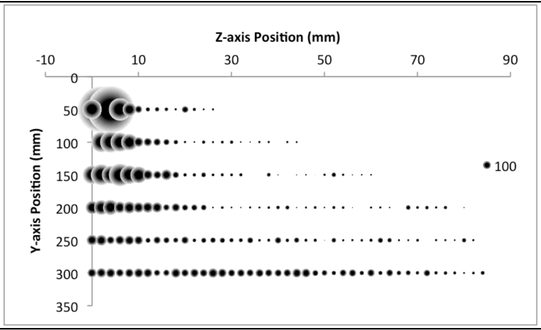 </td><td>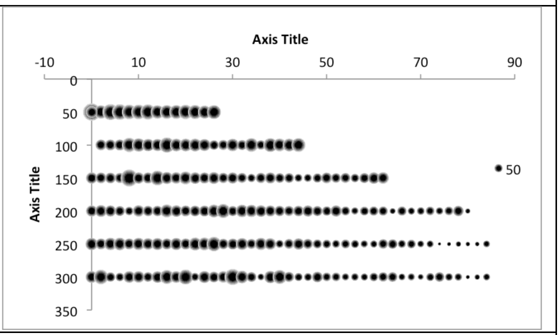 </td></tr>
<tr><td colspan="2">WM 054</td></tr>
<tr><td>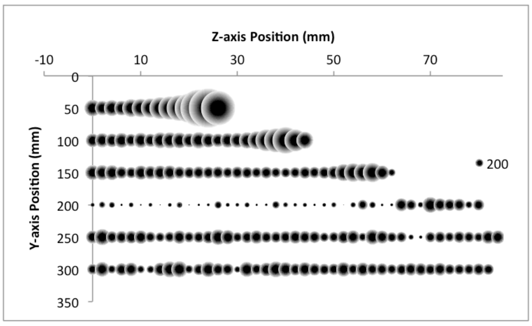 </td><td>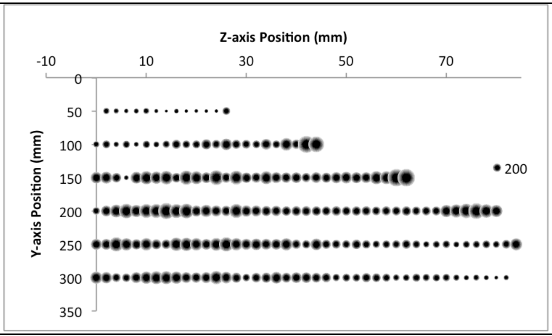 </td></tr>
<tr><td colspan="2">WM 104</td></tr>
<tr><td>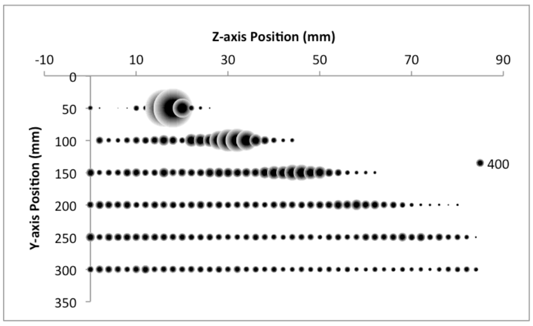 </td><td>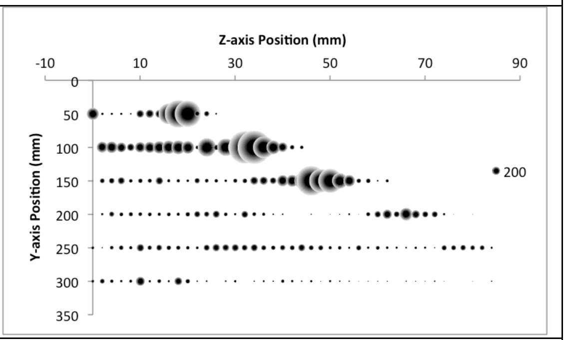 </td></tr>
<tr><td colspan="2">WM 1154</td></tr>
</table>

This is as stated due to the change in the liquid internal characteristics, which are the surface tension and viscosity forces. Observing the 150mm plane in the y-x direction, the tangible data is between the 40mm and the 60mm points in z-axis direction.

### *5.5.2.4 Droplet Velocity*

The velocity Figures 5-40 and 5-41 show that for WM1154, the velocity is two times higher than the WM104 nozzle. This explains why the hollow cone structure is visible in the WM11545 in Table 5-9.

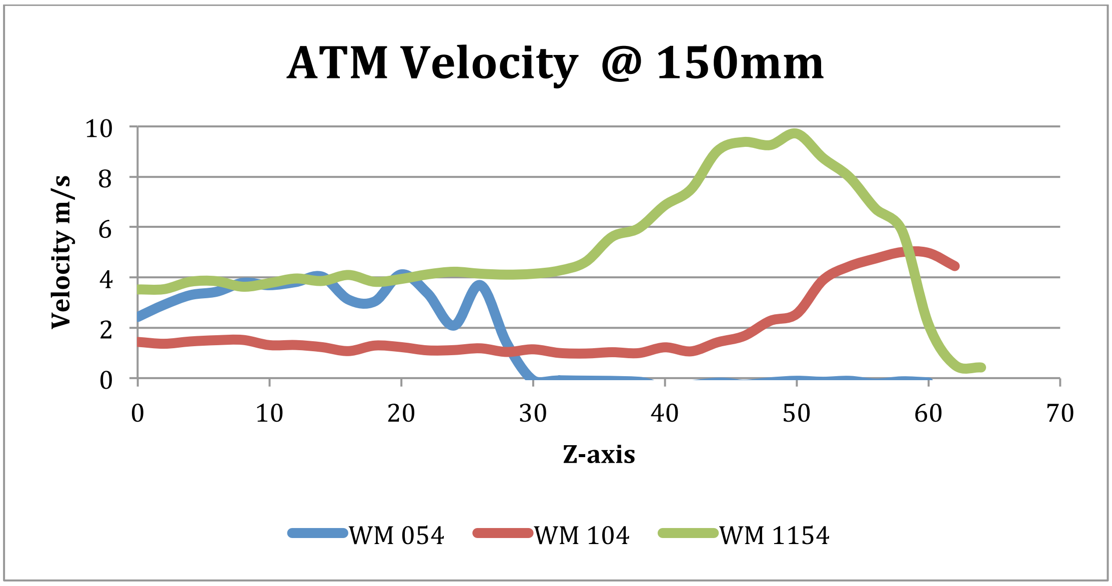

Figure 5-40 Average droplet velocity at 150mm point in y-axis for ATM condition

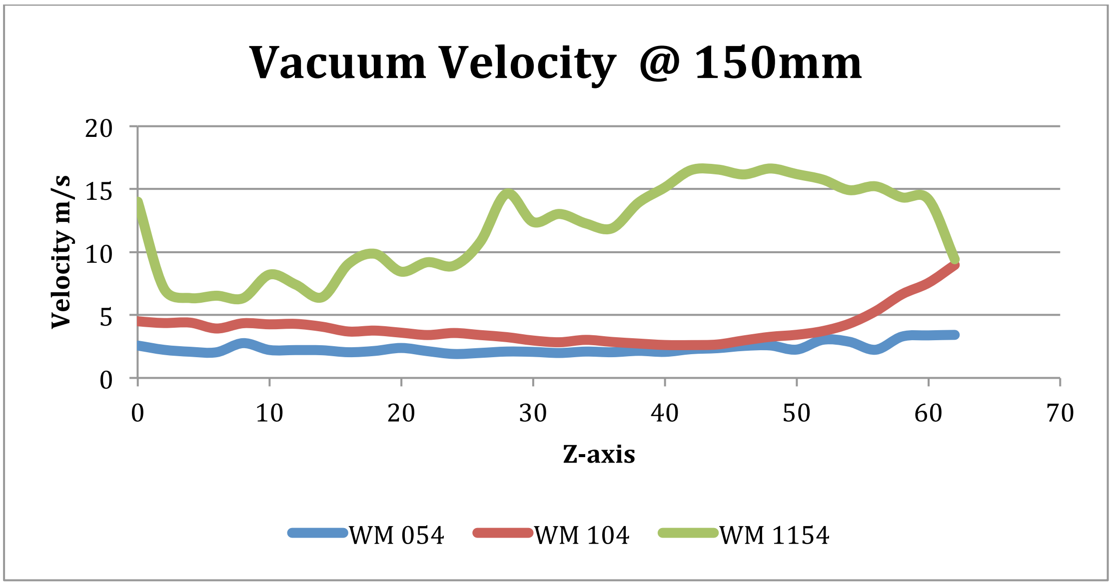

Figure 5-41 Average droplet velocity at 150mm point in y-axis for vacuum condition

#### *5.5.2.5 Droplet SMD*

In Figure 5-42, the SMD of WM104 nozzle is lower than the SMD of WM1154 nozzle, which shows that the WM104 nozzle has got a better atomization in terms of SMD. Looking at this result from a different angle, the data rate of the WM104 nozzle is relatively low compared to WM1154.

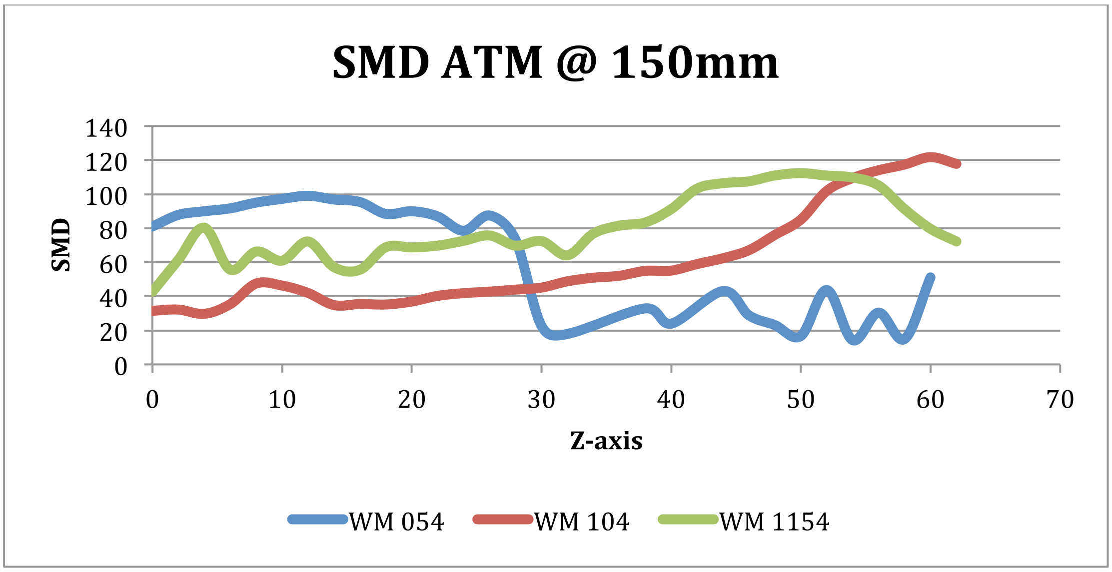

Figure 5-42 SMD at ATM condition with different nozzles

Using the point of 40mm in the z-axis direction, a comparison is made between the vacuum and the atmospheric condition. Comparing the atmospheric condition the WM104 nozzle has an SMD of 111.9µm for the 50% viscosity by volume solution and an SMD of 55.1µm for the 50% viscosity by volume and 50% additive by mass solution. This points to a decrease of 50.7%.

Comparing the same nozzle the WM104 under vacuum conditions, the SMD for the 50% concentration by volume is 88.7µm, and when adding the additive the SMD decreases to 34.1µm. This corresponds to a difference of 61.5%. The effect of the additive on the spray quality is clear and sound.

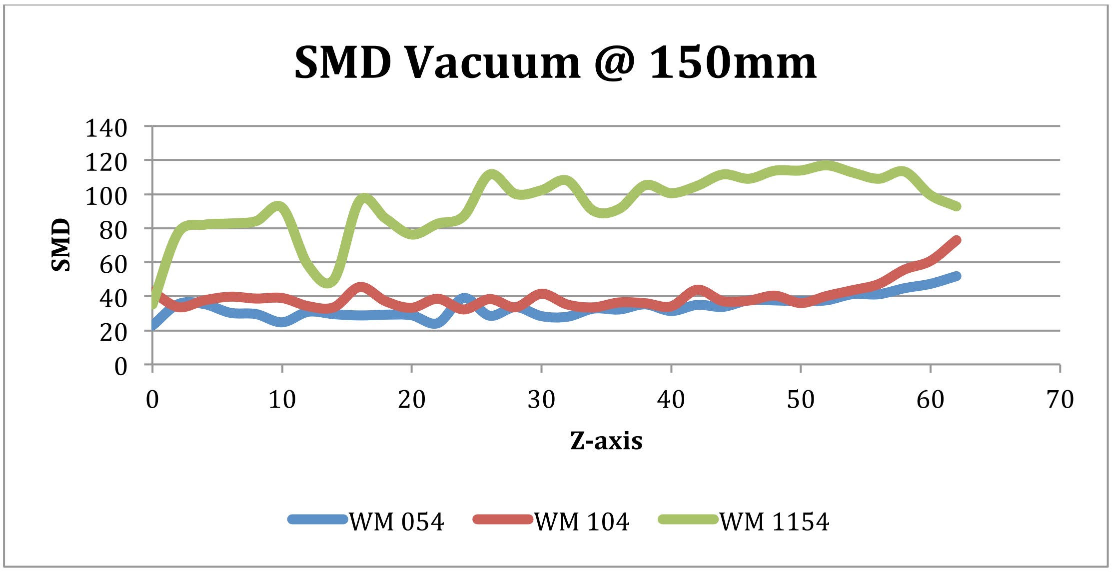

Figure 5-43 SMD at vacuum condition with different nozzles

## 5.6 Additive Effect

Figure 5-44 represents the data of WM104 from Section 5.4.1 and Section 5.5.1 to compare the effect of the 2EH additive on the spray quality in terms of SMD and droplet distribution.

This nozzle was chosen to study the effect of the additive because it depicted consistent results throughout the experiments. Sections 5.4.1 and 5.5.1 were chosen because they had the more consistent results of the sections.

The blue line represents the viscosity with no additive, and the red line represents the viscosity with additive. The two dotted lines represent the SMD of each solution used.

The average SMD is observed to decrease from 83µm to 33µm when the 2EH is present. Adding a surfactant has an effect on the properties of the surface of the liquid, thus making a significant influence on the break-up of the liquid during atomization (Michelson 1990).

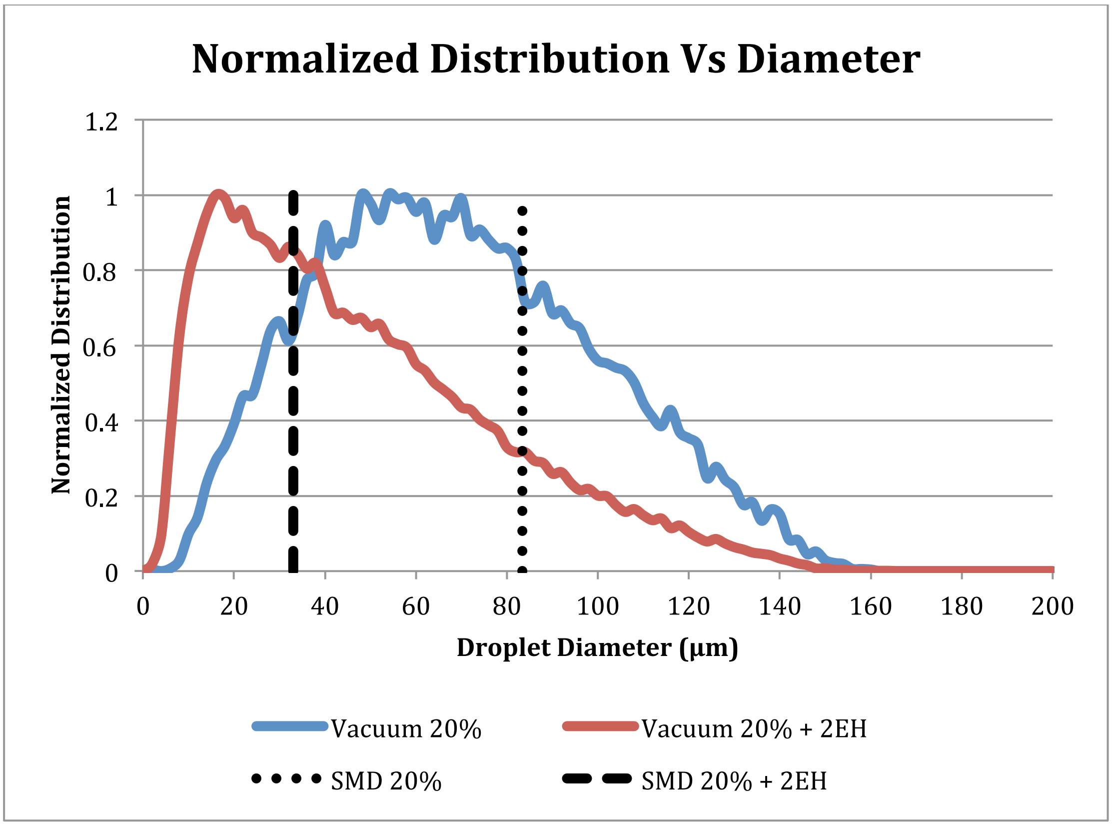

Figure 5-44 Normalized distribution to peak of WM104 nozzle, to compare the 2EH additive effect

## 5.7 Viscosity Summary

Figure 5-45 shows the viscosity vs SMD for of the WM104 nozzle. The point 0.001 kg/ms represents the viscosity of water, and the point 0.0028 kg/ms represents the viscosity of the 20% by volume.

The dotted line represents the lithium bromide viscosity, which is 0.0035 kg/ms (Wimby and Berntsson 1994) and the point 0.0064 kg/ms represents the 50% viscosity by volume.

The SMD difference between the atmospheric and vacuum conditions is minor compared to the atmospheric and vacuum conditions with the 2EH additive. It is also observed that the increase in viscosity of more than 0.004 kg/ms doesn`t have a great influence on SMD, as the SMD shows a trend of reaching a peak value on all conditions tested.

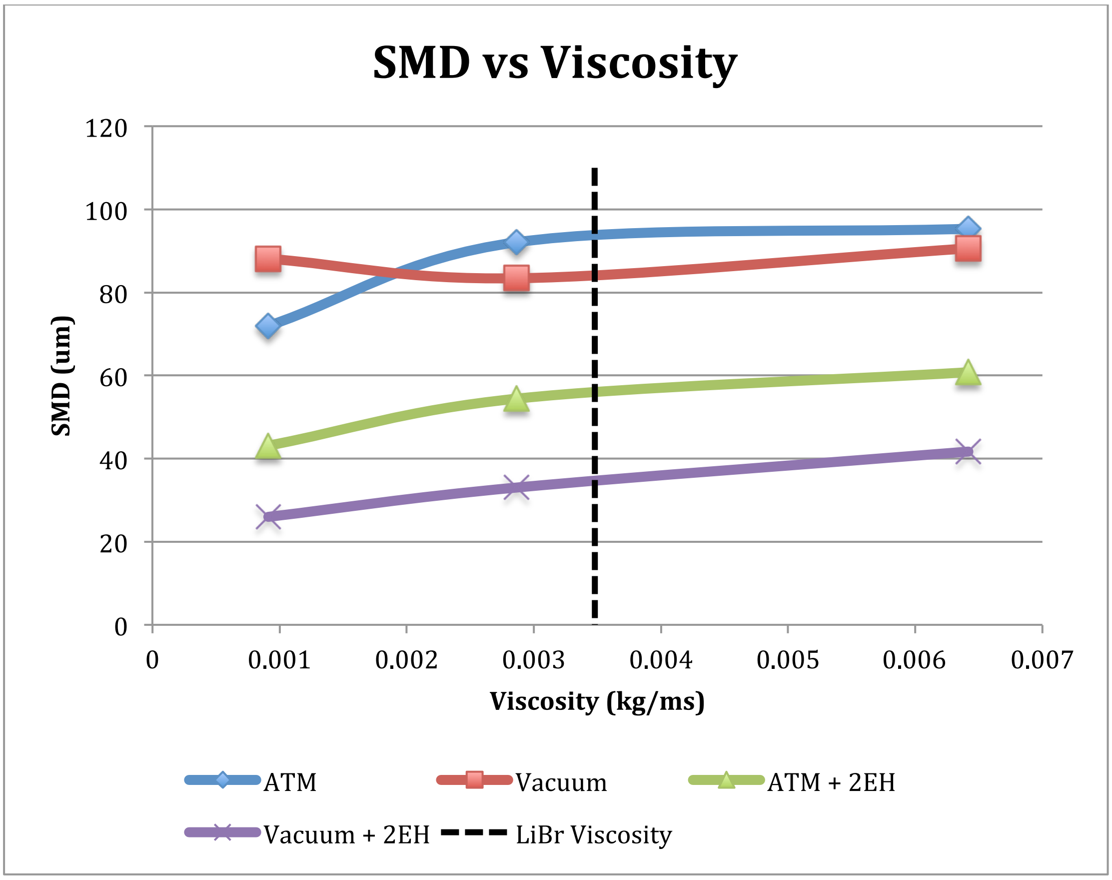

Figure 5-45 SMD vs viscosity for the WM104 nozzle

## 5.8 Evaporation Test

This experiment was conduct to eliminate the effect of evaporation on the spray droplets in the vacuum condition. Under a vacuum, the water boiling point is decreased such as in the experiment case so that when the pressure of the rig is 0.03 bar, the boiling point of water is 24°C.

This suggests that the droplets should flash atomize, but it was not the case as the droplets did not have the required resonance time to do so (Kim et al. 2001).

Table 5-10 Droplet evaporation test

| | |
|---|---|
| Initial droplets | 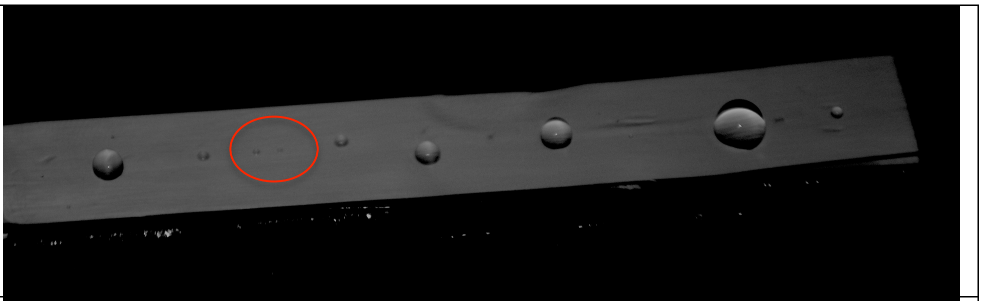 |
| Droplets after 30min vacuum run |  |

In Table 5-10 the initial droplet stage shows two droplets that are highlighted with the red circle. It took those two drops 30 minutes to evaporate under vacuum conditions (0.03 bar); it can be seen in Table 5-10, in the second picture, in the red circle the two drops are not visible, hence they have evaporated. Therefore the evaporation effect on the atomization in the vacuum condition could be neglected due to insufficient resonance time for the droplets.

## 5.9 Heat Test

The heat test was carried out to investigate the effect of increasing the input temperature on the SMD. The test was set on the 150mm plane in the y-axis downstream from the nozzle orifice. The nozzle used was the WM104 for the reasons mentioned earlier in this chapter. The PDA took reading of the 150mm plane nine times by increasing the input temperature simultaneously.

Figure 5-46 shows the SMD plotted in a polynomial format so that it would be possible to compare the results. The results indicate that at the minimum temperature input of 17°C, the maximum SMD is 83μm, while at the maximum input temperature of 41°C, the maximum SMD is 79μm.

There is a difference of 6μm, which lay in the ±5% range; therefore it is acceptable to state that the input heat does not significantly affect the spray quality in terms of SMD. On the contrary, the temperature has an effect on the viscosity of the solutions used in the jet-spray (Wimby and Berntsson 1994; Dorfner et al. 1995).

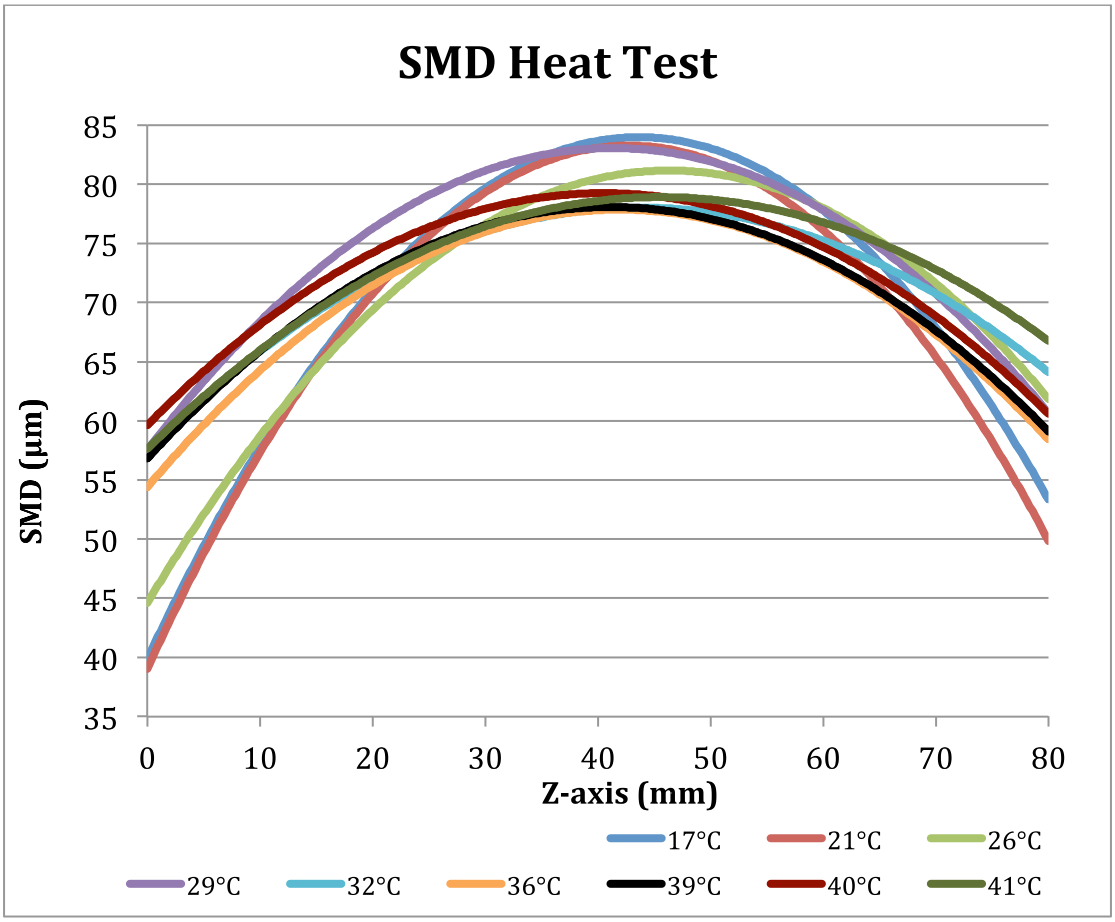

Figure 5-46 The effect of heat on SMD

## 5.10 Summary

A nominal condition was established to be the benchmark in comparing results of the other tests. It was found that the vacuum effect in the nominal condition SMD was sizeable. It increased the average SMD by 25μm.

Then the viscosity experiment tests were analyzed and it was clear from the results that increasing the viscosity will have a great influence in increasing the SMD of the droplets and hence affecting the quality of the atomization both in SMD values and droplet distribution. At the same time the liquid characteristics were affected as it was shown that there was a decrease in the Reynolds number.

Therefore from the SMD plots, it is observed that a reduction in atomization quality was continuing as viscosity was increased. The addition of 2EH to the solutions rapidly decreased the SMD numbers and had an improved atomization quality in both SMD and droplet distribution.

It was also shown that the droplet evaporation at the atomization stage was not sufficient to have a great effect on atomization as well as the input temperatures that were tested in this experiment and it had a minimal impact that could be neglected.

# 6 Qualitative Study - Industrial implementation of results

In this chapter the results of the experiments carried out in Chapter 5 are explained in relevance to its impact on the refrigeration systems industry and specifically the absorption refrigeration system. Recommendations will also be pointed out to enhance the performance of the absorption refrigeration systems, given that one of the aims of this work is to potentially facilitate the application of absorption refrigeration systems that are driven by solar energy.

## 6.1 Increasing the COP of Absorption Refrigeration Systems

One of the challenging issues with integrating absorption refrigeration system is the COP, which is very low compared to the compressor refrigeration system. Looking back to the literature, the COP of the single effect absorption refrigeration ranges from 0.38 to 0.7 (Aphornratana and Sriveerakul 2007), while for the compressor refrigeration system, the COP ranges from 3.5 to 4.0.

In the experiments that have been conducted in this test, the COP was not calculated as a numerical figure to compare it with the literature and the industrial absorption refrigeration systems. However other factors that influence the COP have been calculated and investigated which refer back to the absorber chamber in the absorption refrigeration system. COP enhancement will come from the following factors, which could be summarized as the droplet SMD, the surface area, the droplets distribution and flow rate of the refrigerant. Looking back at Figure 5-44 and Figure 5-45 a size reduction factor or an enhancement ratio was derived to be 2.4. this ratio can help in determining the influence on COP.

### 6.1.1 SMD of Droplets in the Absorber Chamber

The viscous solution of the concentrated lithium bromide at 52% concentration has a significant effect on the spray quality in terms of SMD. The experiment results show that the SMD values increase with increasing viscosity of the solutions, which agrees with the literature finding of Nasr et al. (2002). Therefore two main factors that were noted to have a significant effect on the SMD are the pressure difference and the use of additives. According to the results, when increasing the pressure difference through the nozzle, the atomization quality increases and the SMD values are significantly decreased in numerical value. Therefore a key point in increasing the COP is to increase the pressure difference through the spray nozzle while keeping the vacuum pressure as it is fundamental for the system to work.

The other finding, which was the core investigation of the experiments carried out, is using additives to aid in enhancing the spray quality. Using an eight-octanol additive, which is 2ethyl-1-hexanol, evidently proved this fact. The 2EH demonstrated a significant effect in the SMD values and is discussed in detail in Section 6.2.

Although the COP of the absorption refrigeration systems is low, it is compensated for by the energy saved in the long term of usage and the implementation of dissipated heat that is usually wasted, in this case, the solar energy (Fong et al. 2010).

### 6.1.2 Surface Area to Volume Ratio

The surface area is an important factor of the absorption rate of the water refrigerant by the concentrated lithium bromide solution, in the absorber chamber. The surface area is inversely proportional to SMD, therefore when reducing the SMD value, the surface area that absorption takes place increases, hence an increase in the absorption rate.

The absorption rate of the lithium bromide is not studied in this research, as it was not in the scope of the research. However it is a variable that needs to be improved to enhance COP of the system. Therefore the quality of the spray has to be addressed by the manufacturers of the absorption refrigeration systems.

### 6.1.3 Flow Rate and Distribution of Spray Droplets

Flow rate and the droplet distribution are the two variables that were effected in a negative manner as shown in the results. While having relatively smaller SMD values in the spray, the flow rate and distribution were low. This produces a relatively smaller number of droplets with relatively small number of SMD values, which will affect the surface area of the absorption surface.

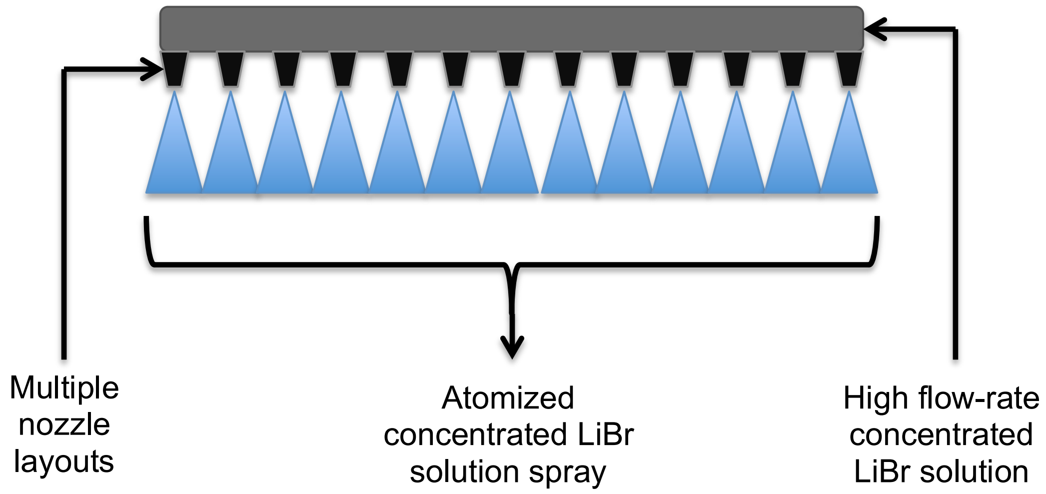

Figure 6-1 Multiple nozzle layout configuration

The recommendation from this research is to adopt a multiple nozzle strategy as demonstrated in Figure 6-1 that will overcome the issue of the flow rate and hence have relatively large number of droplets with relatively small SMD values.

## 6.2 Application of Surfactants

A key variable that has been investigated in this study and is the core of the research experiments is the application of surfactants. The integration of the 2EH additive to the glycerol solution (LiBr equivalent) in the test had a measurable impact as shown in the results chapter. The 2EH proved in the results that it could reduce the SMD by 60% - 80% of the viscous solution. On the other hand, the amount of additive required to reduce the SMD is prone to saturation at fairly low concentrations as stated by Wimby and Berntsson (1994) referring back to Figure 2-4. The effect of the additive is found to be most effective when the concentration used is equivalent to 120ppm, thereafter this effect is constant.

The attempt to add a higher concentration will not enhance the SMD values nor will it help the droplet distribution; in fact, it will reduce the absorption rate and will also affect the other processes in the absorption refrigeration system.

Hence a recommendation from this research is to use additives to enhance the quality of the spray and find the critical concentration of the additive used rather than simply increasing the surfactant concentration. Further developments of additive are also fundamental to further enhance spray quality and COP.

Looking into the development of new surfactants, which will have a significant effect on the spray quality, is an option that ought to be considered by manufacturers of absorption refrigeration systems as the surfactants have proved to produce significantly high effects on the spray quality in terms of SMD and spray distribution.

## 6.3 The Driving Pressure Effect on the System

The pressure difference is a core parameter in an absorption refrigeration system to work optimally. By implementing a greater pressure difference through the nozzle, a higher spray velocity is achieved and hence a larger flow rate through the nozzle. This is shown in the difference between the vacuum condition and the atmospheric condition test done, by keeping the partial vacuum pressure (Xie et al. 2006).

There is a critical pressure difference that could be reached, which will satisfy the maximum flow rate with the minimum effect on the evaporation of the spray droplets. Water molecules evaporate at 7°C when the saturation pressure is 0.001bar (Rogers and Mayhew 1992), therefore it is necessary to take these characteristics into consideration when designing absorption refrigeration systems.

## 6.4 Absorber chamber

Absorption refrigeration manufacturers have apparently overlooked the absorber chamber`s importance in the cooling operation, as they never mention the absorber chamber in their specifications catalogues.

It is apparent that research has also overlooked this part of the absorption refrigeration system, where a lot of the research talks about increasing COP by modifying other chambers within the system and external parts connected to the system.

Studies showed that adding additive to the lithium bromide solution enhanced the absorption rate, and also showed that using different nozzle geometries yielded different droplet SMD values.

The phenomenon that occurs in the absorber chamber requires both these studies and this is where this thesis research has proved that combining the studies will immensely help in improving the COP of the absorption refrigeration system.

By implementing the above strategies, the absorber chamber could be reduced in size and hence a reduction in the size of the absorption refrigeration system. It is then feasible to use absorption refrigeration systems for domestic uses as they are currently used in the industrial sectors where waste energy (steam, gas) is widely available.

## 6.5 Absorption Rate

The core finding falls around the absorption rate of water molecules by the concentrated lithium bromide solution. The lithium bromide solution has a great hygroscopic affinity to absorb water molecules (Wietelmann and Bauer 2000). In this process there is mass transfer and temperature transfer that are occurring at the same time.

To increase the COP, the absorption rate needs to be significantly high, and to achieve this, the results show that using surfactants will have two main effects, which are:

1. Increase the surface area to volume ratio of the spray droplets.
2. Enhance the absorption rate and mass – heat transfer by reducing the surface tension forces.

## 6.6 Lithium Bromide Concentration

The concentration of lithium bromide solution according to the literature was found to be around 60%. With this amount of viscosity, the SMD values were found to increase by increasing viscosity and the distribution was also affected. Therefore it is appealing to the manufacturers to decrease the concentration but this will cause a reduction in absorption rate, which is not the recommended output.

Therefore, implementing a surfactant or a number of surfactants will solve the concentration drawback in the spray quality and enhance the absorption rate.

## 6.7 Chamber Temperature

The absorption chamber temperature is of significant importance, as it was clearly discussed in the literature that reducing the absorbers temperature will increase the COP value of the absorption refrigeration system. On the other hand it was shown in the results that the input temperature has a very small effect on the SMD of the spray droplets. Therefore there is a substantial amount of temperature given that it could be investigated to compare COP of the system with existing absorption refrigeration systems.

# 7 Summary and Conclusion

This chapter recaps the work done and the experimental procedures followed by a summary of the outcome of the research. The chapter finalizes with the recommendations for further work to be carried out.

## 7.1 Summary of the Work

Lithium bromide absorption refrigeration systems are alternatives to electric combustion refrigeration systems as they are environmentally friendly and use non-toxic refrigerants such as water. These absorption refrigeration systems have a downside, which is a relatively low COP compared to the combustion system. The aim of this study is to increase the COP of the system by lowering the SMD, which will increase the surface area to volume ratio of lithium bromide, concentrated solution to enhance the absorption of the refrigerant which is water, hence the name absorption refrigeration system.

As industry is searching for alternative and renewable energy to replace the fossil fuel domination, harnessing the solar energy dissipated by the sun can be used by the absorption refrigeration system, thus harnessing energy that is usually wasted.

The literature on solar absorption refrigeration systems is found wanting in the study of the absorber chamber`s effect on COP. The absorber chamber uses spray technology, which has replaced the falling film to increase the surface area to volume ratio. Therefore this research has focused on the spray technology in a partial vacuum and on how to enhance the SMD of the droplets.

To study the characteristics of the spray, a pressure vessel was modified to be used as a vacuum chamber (LP-Rig). A Phase Doppler Anemometry system was also used to measure and quantify simultaneous droplet size and velocity measurements.

Operating parameters were identified and put into a matrix of operating tests. These parameters include the pressure difference through the nozzle, the geometry of the nozzles used in terms of exit orifice and the fluid characteristics, which is represented by the viscosity and surface tension. The lithium bromide solution was substituted by glycerol, because of the corrosive nature of lithium bromide.

To be able to run the experiments, some gadgets needed to be used and integrated into the LP-Rig. These gadgets come in the form of calibrated pressure transducers, K-type thermocouples and flow rate measurement tools (coriolismeter). To compute the viscosity measurements, a Cannon-Fenske Routine viscometer was used that has been calibrated by the supplier. The PDA set-up was accomplished by the use of a medical nebulizer, which had an identified droplet diameter range of 80% to be less than 5μm.

A nominal condition test was carried out to establish a benchmark for the other test to compare with. The nominal condition had water as the spray liquid. Two viscosities, namely, a 20% by volume and 50% by volume glycerol solutions were tested. In order to enhance the droplet SMD values, 2-ethyle-1-hexanol surfactant was added to the viscous solutions.

## 7.2 Conclusion

The research findings and outcomes:

- Using various nozzle geometries have yielded different spray qualities in terms of SMD and distribution. Flow rates were also affected and by using larger nozzle orifices, the flow rate increased.
- Under nominal conditions, the effect of the vacuum on the spray quality was investigated and was found to have increased the SMD values by 62% compared to the SMD values obtained under atmospheric conditions.
- A droplet diameter bubble plot showed that under vacuum conditions the droplet distribution of the spray features a hollow cone spray, while under atmospheric conditions the spray showed features of a solid cone.
    - The ambient air available in the LP-Rig had an impact on this phenomenon as the nozzles in use where hollow cone spray nozzles.
- The SMD measured under nominal conditions for the atmospheric conditions as shown in frequency distribution plots peak at 15μm and the vast majority of droplets are under 50μm.
- Adding the 20 % glycerol by volume to water has increased the SMD values compared to the nominal condition. The other interesting fact is that the number of large drops has increased in both the atmospheric and vacuum conditions. Therefore, shifting of the average SMD to the larger diameter ranges.

- Adding the 50% by volume glycerol to water has had a greater impact in increasing the SMD values. WM054 nozzle failed to atomize as shown in the results, due to the presence of large internal forces and the shear forces acting on the spray in the LP-Rig couldn`t overcome them. The high Reynolds number of the concentrated solution represents this phenomenon.
- When the 2-ethyle-1-hexanol was introduced to the system, the atomization quality was affected. The results show a huge decrease in the SMD values. The surfactant 2EH has altered with the internal forces of the fluid making them more vulnerable to the shear forces acting on the fluid within the LP-Rig.
- The WM104 nozzle achieved a 74% decrease in the peak droplet diameter with the 2EH surfactant, and looking at the Weber number it explains this huge decrease. Therefore a lower weber number shows that the shear forces are dominant.
- The surfactant had affected the spray quality in terms of SMD values as the average SMD for the 20% glycerol by mass solution with the 2EH surfactant, dropped from 83µm to 33µm.
- Increasing the viscosity more than 0.007 kg/ms doesn’t have a greater effect on SMD values as the SMD values start to maintain their value after 0.005 kg/ms.
- Evaporation is not considered to affect the spray quality under vacuum conditions as the droplets do not have the resonance time required to evaporate.

- The input temperature was also found to have a minimal effect on the spray quality and was not considered to be a factor that influences spray quality although the increasing temperature did reduce the SMD values but by 4%.

## 7.3 Further Work and Recommendations

Extend the analysis of the spray further downstream from the nozzle orifice and in the z-axis direction, to be able to use wider spray angles and higher driving pressures.

Further investigate the effects of the use of different surfactants or a mixture of surfactants. Also considerations in developing a surfactant for the absorption refrigeration system that will help avoid crystallization and enhance mass and heat transfer.

Examine different nozzle geometries as the literature and the thesis suggest on an actual absorption refrigeration system in order to compare actual COP values.

# 8 References

Administration, U. S. E. I. 2013. *International Energy Outlook 2013*. USA:

Aísa, L. et al. 2002. Particle concentration and local mass flux measurements in two-phase flows with PDA. Application to a study on the dispersion of spherical particles in a turbulent air jet. *International Journal of Multiphase Flow* 28(2), pp. 301-324.

Akorede, M. F. et al. 2012. Mitigating the anthropogenic global warming in the electric power industry. *Renewable and Sustainable Energy Reviews* 16(5), pp. 2747-2761.

Al-Alili, A. et al. 2014. Review of solar thermal air conditioning technologies. *International Journal of Refrigeration* 39(0), pp. 4-22.

Al-Karaghouli, A. et al. 1991. The solar energy research center building thermal performance evaluation during the summer season. *Energy Conversion and Management* [Online] 32(5). Available at: http://www.sciencedirect.com/science/article/pii/019689049190001Y [Accessed: 17 June 2011].

Al-Zubaydi, A. 2011. Solar air conditioning and refrigeration with absorption chillers technology in Australia-an overview on researches and application. *Journal of Advanced Science and Engineering Research* 1(1), pp. 23-41.

Ali, A. H. H. et al. 2008. Performance assessment of an integrated free cooling and solar powered single-effect lithium bromide-water absorption chiller. *Solar Energy* [Online] 82(11). Available at: http://www.sciencedirect.com/science/article/pii/S0038092X08001059 [Accessed: 18 March 2010].

Aliseda, A. et al. 2008. Atomization of viscous and non-newtonian liquids by a coaxial, high-speed gas jet. Experiments and droplet size modeling. *International Journal of Multiphase Flow* 34(2), pp. 161-175.

Alnaser, W. E. and Alnaser, N. W. 2011. The status of renewable energy in the GCC countries. *Renewable and Sustainable Energy Reviews* 15(6), pp. 3074-3098.

Alnaser, W. E. et al. 2004. First solar radiation atlas for the Arab world. *Renewable Energy* 29(7), pp. 1085-1107.

Anderko, A. and Young, R. D. 2000. Model for corrosion of carbon steel in lithium bromide absorption refrigeration systems. *Corrosion* 56(5), pp. 543-555.

Aphornratana, S. and Sriveerakul, T. 2007. Experimental studies of a single-effect absorption refrigerator using aqueous lithium–bromide: Effect of operating condition to system performance. *Experimental Thermal and Fluid Science* [Online] 32(2). Available at: http://www.sciencedirect.com/science/article/pii/S0894177707001124 [Accessed: 12 July 2011].

Balaras, C. A. et al. 2007. Solar air conditioning in Europe—an overview. *Renewable and Sustainable Energy Reviews* [Online] 11(2). Available at: http://www.sciencedirect.com/science/article/pii/S1364032105000456 [Accessed: 17 June 2011].

Barca, S. 2011. Energy, property, and the industrial revolution narrative. *Ecological Economics* 70(7), pp. 1309-1315.

Benedict, R. P. 1981. *Manual on the use of thermocouples in temperature measurement*. 3rd ed. Philadelphia: ASTM.

Bodas Freitas, I. M. et al. 2012. The Kyoto mechanisms and the diffusion of renewable energy technologies in the BRICS. *Energy Policy* 42(0), pp. 118-128.

Bourdoukan, P. et al. 2009. Experimental investigation of a solar desiccant cooling installation. *Solar Energy* [Online] 83(11). Available at: http://www.sciencedirect.com/science/article/pii/S0038092X09001881 [Accessed: 11 August 2011].

Bronkhorst-cori-tech.com. *mini CORI-FLOW Coriolis Mass Flow Controllers BCT-EN - Bronkhorst®* [Online]. Available at: http://www.bronkhorst-cori-tech.com/en/products/coriolis_meters_controllers/mini_cori-flow/mfcs/ [Accessed: 16 Jan ].

Cengel, Y. A. and Boles, M. A. 2007. *Thermodynamics An Engineering Approach*. 6th ed. London: McGraw-Hill Higher Education.

Cheng, W. et al. 2013. An experimental investigation of heat transfer enhancement by addition of high-alcohol surfactant (HAS) and dissolving salt additive (DSA) in spray cooling. *Experimental Thermal and Fluid Science* 45(0), pp. 198-202.

Chiari, L. and Zecca, A. 2011. Constraints of fossil fuels depletion on global warming projections. *Energy Policy* 39(9), pp. 5026-5034.

Chin, J. S. and Lefebvre, A. H. 1995. A Design Procedure for Effervescent Atomizers. *Journal of Engineering for Gas Turbines and Power* 117(2), pp. 266-271.

Comer, M. 1999. *Transient G-DI fuel spray characterisation.* University of Wales.

Dagoumas, A. S. et al. 2006. An economic assessment of the Kyoto Protocol application. *Energy Policy* 34(1), pp. 26-39.

Dantec-Dynamics. 2006. BSA Flow Software: Version 4.10 Installation & User's Guide. Skovlunde: Dantec Dynamics A/S.

Davies, P. A. 2005. A solar cooling system for greenhouse food production in hot climates. *Solar Energy* 79(6), pp. 661-668.

Delavan.co.uk. 2012. *Delavan Industrial Spray Nozzles for Spray Drying, Continuous Steel Casting, Air Atomizing, Two-Fluid Pulp and Industry* [Online]. Available at: [Accessed: 15 Jan 2013].

Dincer, I. and Kanoglu, M. 2010. *Refrigeration Systems and Applications*. Chichester, West Sussex: UK. Wiley.

Dorfner, V. et al. 1995. VISCOSITY AND SURFACE TENSION EFFECTS IN PRESSURE SWIRL ATOMIZATION. *Atomization and Sprays* 5(3), pp. 261-285.

Eggers, J. 2004. A brief history of drop formation. Bristol University of Bristol.

Fernández-Seara, J. and Pardiñas, Á. Á. 2014. Refrigerant falling film evaporation review: Description, fluid dynamics and heat transfer. *Applied Thermal Engineering* 64(1–2), pp. 155-171.

Foley, G. et al. 2000. The future of absorption technology in America. *Advanced Building Systems* [Online]. Available at: http://www1.eere.energy.gov/manufacturing/distributedenergy/pdfs/ absorption_future.pdf [Accessed: 16 June 2011].

Fong, K. F. et al. 2010. Comparative study of different solar cooling systems for buildings in subtropical city. *Solar Energy* 84(2), pp. 227-244.

Glebov, D. and Setterwall, F. 2002. Experimental study of heat transfer additive influence on the absorption chiller performance. *International Journal of Refrigeration* [Online] 25(5). Available at: http://www.sciencedirect.com/science/article/pii/S0140700701000421 [Accessed: 8 August 2011].

Guildenbecher, D. R. et al. 2009. Secondary atomization. *Experiments in Fluids* 46(3), pp. 371-402.

Haenlein, A. 1932. Uber den Zerfall eines Flus- sigkeitsstrahls (On the disruption of a liquid jet). *NACA TM Report. 659*.

Hecht, E. 2002. *Optics*. 4th ed. London: Addison Wesley.

Henning, H.-M. ed. 2004. *Solar-Assisted Air-Conditioning in Buildings, A Handbook for Planners.* New York: Springer-Verlag Wien.

Henning, H. M. et al. 2001. The potential of solar energy use in desiccant cooling cycles. *International Journal of Refrigeration* 24(3), pp. 220-229.

Herold, K. E. et al. 1996. *Absorption chillers and heat pumps*. Boca Raton: FL: CRC Press.

Hiroyasu, H. 2000. Spray Breakup Mechanism from the Hole-Type Nozzle. *Atomization and Sprays* 10(3), pp. 511-527.

Holman, J. P. 2002. *Heat Transfer*. 9th ed. London: McGraw-Hill Higher Education.

Hoyer-Klick, C. et al. 2009. Getting Solar Energy to Work: Resource Assessment by Remote Sensing as a Base for Investment Decisions. *Earthzine*.

International-Institute-of-refrigeration. 2005. *IIR-International Institute of refrigeration* [Online]. Available at: [Accessed: 5 Mar].

IPCC. 2013. *WORKING GROUP I CONTRIBUTION TO THE IPCC FIFTH ASSESSMENT REPORT CLIMATE CHANGE 2013: THE PHYSICAL SCIENCE BASIS*. Switzerland:

Jones, A. R. ed. 1982. *Design optimization of large pressure-jet atomizer for power plant*. Proceedings of the 2nd international conference on liquid atomization and sprays*.* Madison, Wis.

Kay, P. 2006. *Characterising Thermofluid Spray Dynamics For Energy-Efficient Automotive Engines.* University of Wales, Cardiff.

Kim, B. S. et al. 2001. Study on ice slurry production by water spray. *International Journal of Refrigeration* [Online] 24(2). Available at: http://www.sciencedirect.com/science/article/pii/S014070070000013X [Accessed: 20 April 2011].

Kim, J.-S. et al. 1999. Absorption of water vapour into lithium bromide-based solutions with additives using a simple stagnant pool absorber. *International Journal of Refrigeration* [Online] 22(3). Available at: http://www.sciencedirect.com/science/article/pii/S0140700798000619 [Accessed: 11 August 2011].

Konstantinov, D. 2012. *Effervescent Atomisation for Complex Fuels including Bio-Fuels.* University of Wales, Cardiff.

Lau, L. C. et al. 2012. Global warming mitigation and renewable energy policy development from the Kyoto Protocol to the Copenhagen Accord—A comment. *Renewable and Sustainable Energy Reviews* 16(7), pp. 5280-5284.

Lefebvre, A. H. 1983. *Gas turbine combustion*. Washington: Hemisphere Pub. Corp.

Lefebvre, A. H. 1989. *Atomization and sprays*. New York: Hemisphere Pub. Corp.

Lefebvre, A. H. and Wang, X. F. 1987. Mean drop sizes from pressure-swirl nozzles. *Journal of Propulsion and Power* 3(1), pp. 11-18.

Li, C. et al. 2014. Interaction between urban microclimate and electric air-conditioning energy consumption during high temperature season. *Applied Energy* 117(0), pp. 149-156.

Li, H. et al. 2012. Case study of a two-stage rotary desiccant cooling/heating system driven by evacuated glass tube solar air collectors. *Energy and Buildings* 47(0), pp. 107-112.

Li, X. 1995. Mechanism of Atomization of a Liquid Jet. Atomization and Sprays. *At. Sprays* 5, pp. 89-105.

Lin, S. P. and Reitz, R. D. 1998. DROP AND SPRAY FORMATION FROM A LIQUID JET. *Annual Review of Fluid Mechanics* 30(1), pp. 85-105.

Liu, Y. L. and Wang, R. Z. 2004. Performance prediction of a solar/gas driving double effect LiBr–H2O absorption system. *Renewable Energy* 29(10), pp. 1677-1695.

Marcos, J. D. et al. 2011. New method for COP optimization in water- and air-cooled single and double effect LiBr–water absorption machines. *International Journal of Refrigeration* 34(6), pp. 1348-1359.

Market-Research. 2013. *Global refrigerant market trends and forecasts to 2018*. Dallas:

Mateus, T. and Oliveira, A. C. 2009. Energy and economic analysis of an integrated solar absorption cooling and heating system in different building types and climates. *Applied Energy* 86(6), pp. 949-957.

Mavroudaki, P. et al. 2002. The potential for solar powered single-stage desiccant cooling in southern Europe. *Applied Thermal Engineering* 22(10), pp. 1129-1140.

Michelson, D. 1990. *Electrostatic Atomization*. Bristol: Adam Hilger.

Nasr, G. G. et al. 2002. *Industrial sprays and atomization*. London: Springer.

Ng, K. C. et al. 1994. Theoretical and experimental analysis of an absorption chiller. *International Journal of Refrigeration* 17(5), pp. 351-358.

Ni.com. 2013. *NI SignalExpress - National Instruments* [Online]. Available at: http://www.ni.com/labview/signalexpress/ [Accessed: 19 Jan].

Ohnesorge, W. V. 1936. Formation of drops by nozzles and the breakup of liquid jets. *Journal of Applied Mathematics and Mechanics* 16(6), pp. 355-358.

Pao, H.-T. and Tsai, C.-M. 2010. CO2 emissions, energy consumption and economic growth in BRIC countries. *Energy Policy* 38(12), pp. 7850-7860.

Patlitzianas, K. D. et al. 2007. An assessment of the sustainable energy investments in the framework of the EU–GCC cooperation. *Renewable Energy* 32(10), pp. 1689-1704.

Pearson, A. 2008. Refrigeration with ammonia. *International Journal of Refrigeration* 31(4), pp. 545-551.

Perez, R. A. 2007. *Heat and mass transfer effects in air-cooled vertical tube absorbers.* University of Puerto Rico - Mayaguez Campus.

Petersen, F. et al. 2001a. Effervescent Atomization of Aqueous Polymer Solutions and Dispersions. *Pharmaceutical Development & Technology* 6(2), p. 201.

Petersen, F. J. et al. 2001b. Effervescent Atomization of Aqueous Polymer Solutions and Dispersions. *Pharmaceutical Development and Technology* 6(2), pp. 201-210.

Pimbley, W. T. 1976. Drop Formation from a Liquid Jet: A Linear One-dimensional Analysis Considered as a Boundary Value Problem. *IBM Journal of Research and Development* 20(2), pp. 148-156.

Reiche, D. 2010. Energy Policies of Gulf Cooperation Council (GCC) countries—possibilities and limitations of ecological modernization in rentier states. *Energy Policy* 38(5), pp. 2395-2403.

Reitz, R. D. and Bracco, F. V. 1986. *Mechanisms of breakup of round liquid jets*. p. 233.

Rodgers, P. et al. 2012. Enhancement of LNG plant propane cycle through waste heat powered absorption cooling. *Applied Thermal Engineering* 48(0), pp. 41-53.

Rogers, G. and Mayhew, Y. 1992. *Engineering Thermodynamics, Work & Heat Transfer*. 4th ed. London: Pearson Education Limited.

Santangelo, P. J. and Sojka, P. E. 1995. A HOLOGRAPHIC INVESTIGATION OF THE NEAR-NOZZLE STRUCTURE OF AN EFFERVESCENT ATOMIZER-PRODUCED SPRAY. *Atomization and Sprays* 5(2), pp. 137-155.

Saravanan, R. and Maiya, M. P. 2003. Experimental analysis of a bubble pump operated H2O–LiBr vapour absorption cooler. *Applied Thermal Engineering* 23(18), pp. 2383-2397.

Sayigh, A. A. M. and Mcveigh, J. C. 1992. *Solar air conditioningh and refrigeration*. Oxford: Pergamon Press.

Sayigh, A. A. M. and Saada, M. K. 1982. THREE AND A HALF TON SOLAR ABSORPTION AIR CONDITIONER'S PERFORMANCE IN RIYADH - SAUDI ARABIA. In: *Proceeding of the international solar energy society congress.* pp. 537-543.

Shafiee, S. and Topal, E. 2009. When will fossil fuel reserves be diminished? *Energy Policy* 37(1), pp. 181-189.

Shin, H. T. et al. 2000. Spherical-shaped ice particle production by spraying water in a vacuum chamber. *Applied Thermal Engineering* [Online] 20(5). Available at: http://www.sciencedirect.com/science/article/pii/S1359431199000356 [Accessed: 20 April 2011].

Shinjo, J. and Umemura, A. 2011. Surface instability and primary atomization characteristics of straight liquid jet sprays. *International Journal of Multiphase Flow* 37(10), pp. 1294-1304.

Simmons, H. C. and Harding, C. F. 1981. Some Effects of Using Water as a Test Fluid in Fuel Nozzle Spray Analysis. *Journal of Engineering for Gas Turbines and Power* 103(1), pp. 118-123.

Sine.ni.com. 2013. *NI CompactDAQ - Data Sheet - National Instruments* [Online]. Available at: http://sine.ni.com/ds/app/doc/p/id/ds-178/lang/en [Accessed: 19 Jan].

Sojka, P. E. and Lefebvre, A. H. 1990. *A novel method of atomzing coal-water slurry fuels*. United States:

Solair. 2012. *Desiccant cooling systems - Solair* [Online]. Available at: http://www.solair-project.eu/146.0.html [Accessed: 21/12].

Song, S. H. and Lee, S. Y. 1996. Study of Atomization Mechanism of Gas/Liquid Mixtures flowing through Y-jet Atomizers. *Atomization and Sprays* 6(2), pp. 193-209.

Soo, S. L. 1999. *instrumentation for Fluid Particle Flow*. Park Ridge, N.J.: Noyes Publications.

Sorensen, B. 2007. *Renewable Emergy Conversion, Transmission and Storage*. London: Academic Press.

Tatlıer, M. and Erdem-Şenatalar, A. 2004. Polymeric heat exchangers to increase the COP values of adsorption heat pumps utilizing zeolite coatings. *Applied Thermal Engineering* 24(1), pp. 69-78.

Tsagarakis, K. P. et al. 2012. Implementation conditions for energy saving technologies and practices in office buildings: Part 2. Double glazing windows, heating and air-conditioning. *Renewable and Sustainable Energy Reviews* 16(6), pp. 3986-3998.

UNESCO. 2013. Energy Requirements of Desalination Processes. *Encyclopedia of Desalination and Water Resources*.

United-Nations. 1997. *A summary of the Kyoto protocol* [Online]. Available at: http://unfccc.int/kyoto_protocol/background/items/2879.php [Accessed: 5 Mar].

Uppal, A. H. and Muneer, T. 1987. Cost analysis of commerical solar absorption coolers using a detailed simulation procedure. *Applied Energy* 26(1), pp. 75-82.

Ward, D. S. and Löf, G. O. G. 1975. Design and construction of a residential solar heating and cooling system. *Solar Energy* [Online] 17(1). Available at: http://www.sciencedirect.com/science/article/pii/0038092X75900122 [Accessed: 16 June 2011].

Warnakulasuriya, F. S. K. and Worek, W. M. 2008. Drop formation of swirl-jet nozzles with high viscous solution in vacuum-new absorbent in spray absorption refrigeration. *International Journal of Heat and Mass Transfer* [Online] 51(13–14). Available at: http://www.sciencedirect.com/science/article/pii/S0017931007006795 [Accessed: 7 January 2012].

Wietelmann, U. and Bauer, R. J. 2000. Lithium and Lithium Compounds.*Ullmann's Encyclopedia of Industrial Chemistry*. Wiley-VCH Verlag GmbH & Co. KGaA.

Wimby, J. M. and Berntsson, T. S. 1994. Viscosity and Density of Aqueous Solutions of LiBr, LiCl,ZnBrz, CaC12, andLiN03, 1, SingleSaltSolutions. *Journal of Chemical and Engineering Data* 39(1), pp. 68-72.

Xie, G. et al. 2006. Improvement of the performance for absorption refrigeration system with lithium bromide-water as refrigerant by increasing absorption pressure. In: *Proceedings of the sixth international conference for enhanced building operations.* Shenzhen, China. HVAC Technologies for Energy Efficiency, p. 4.

Xu, R. 2002. *Particle Characterization: Light Scattering Methods*. New York: Kluwer Academic.

Xu, Z. et al. 2005. Atomization of a High Speed Jet. *American Physical Society*.

Yoon, J.-I. et al. 1999. The effect of surfactant in the absorptive and generative processes. *KSME International Journal* 13(3), pp. 264-272.

YORK-International. 1997. How it works - YORK Millennium YIA Absorption Chiller. Pennsylvania, USA: York International Corporation.

Yuan, Z. and Herold, K. E. 2001. Surface tension of pure water and aqueous lithium bromide with 2-ethyl-hexanol. *Applied Thermal Engineering* 21(8), pp. 881-897.

Zhai, X. Q. et al. 2008. Design and performance of a solar-powered air-conditioning system in a green building. *Applied Energy* 85(5), pp. 297-311.

Zhang, Z. 2010. *LDA Application Methods*. Berlin: Springer.

Zhao, H. et al. 2011. Breakup characteristics of liquid drops in bag regime by a continuous and uniform air jet flow. *International Journal of Multiphase Flow* 37(5), pp. 530-534.

# Appendix A – Nominal Condition

## Delevan WM054

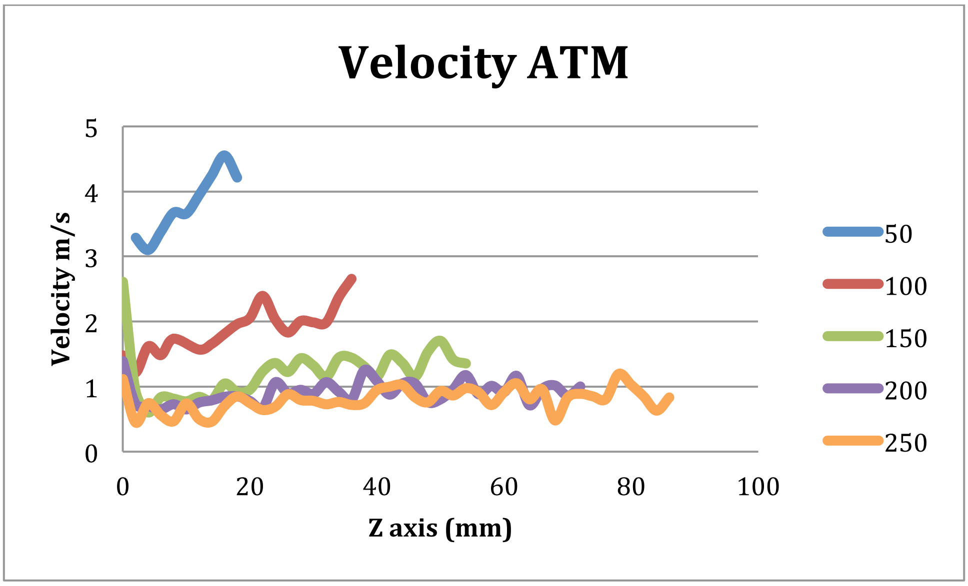

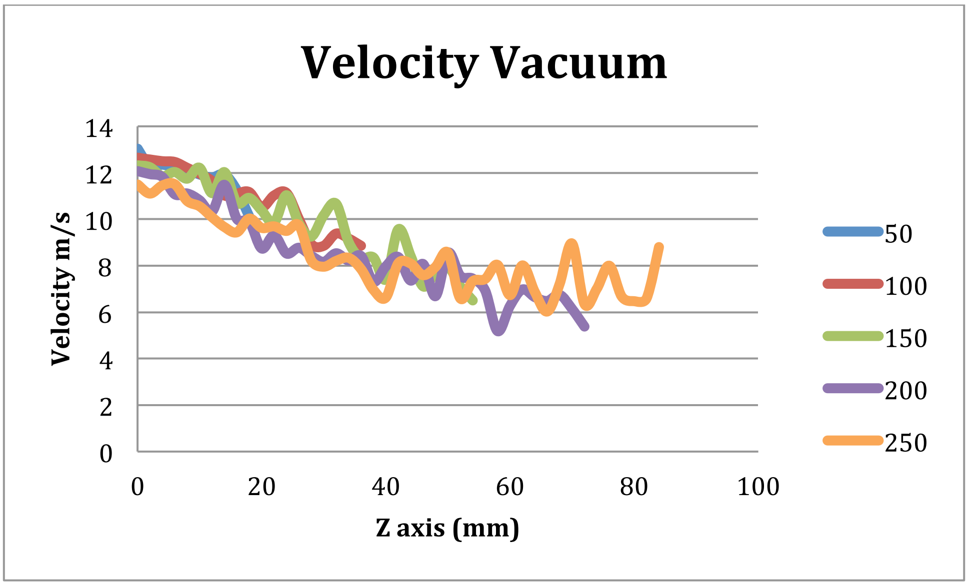

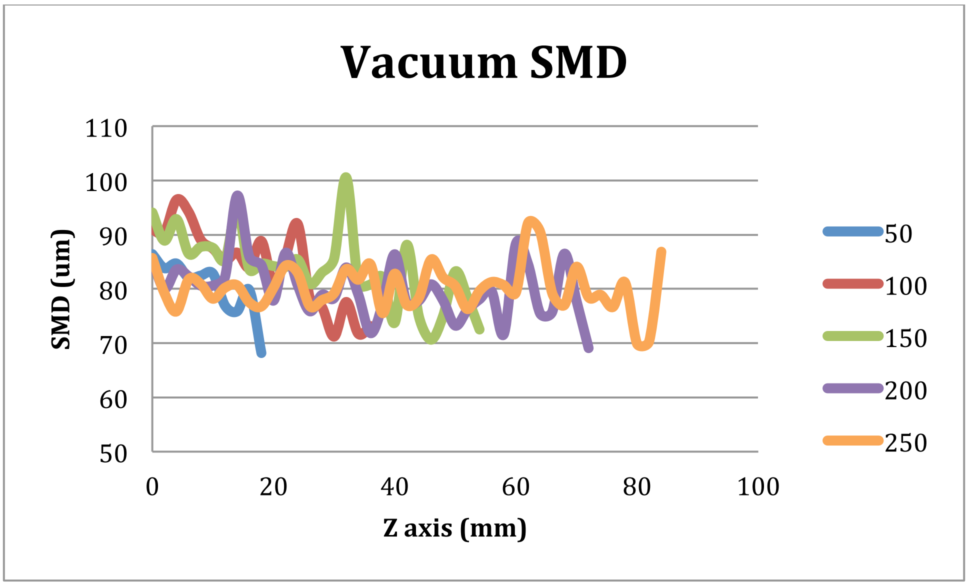
Vacuum SMD
SMD (um)
110
100
90
80
70
60
50
0
20
40
60
80
100
Z axis (mm)
50
100
150
200
250

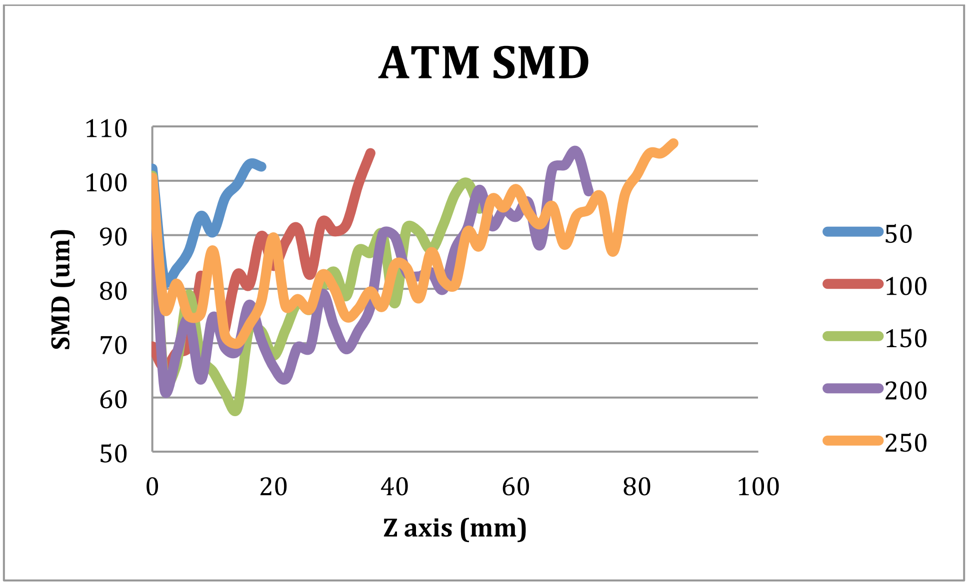
ATM SMD
SMD (um)
110
100
90
80
70
60
50
0
20
40
60
80
100
Z axis (mm)
50
100
150
200
250

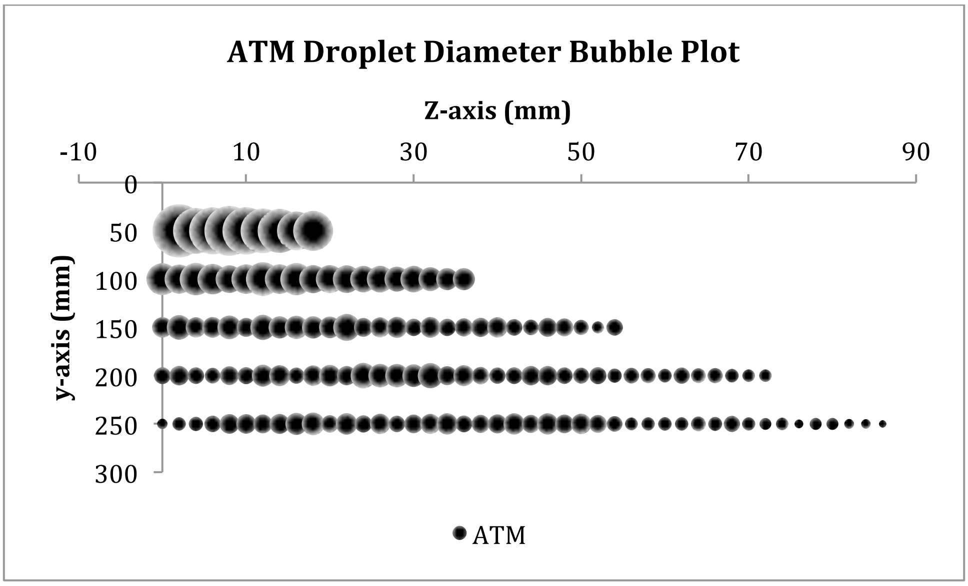
ATM Droplet Diameter Bubble Plot
Z-axis (mm)
-10
10
30
50
70
90
y-axis (mm)
0
50
100
150
200
250
300
● ATM

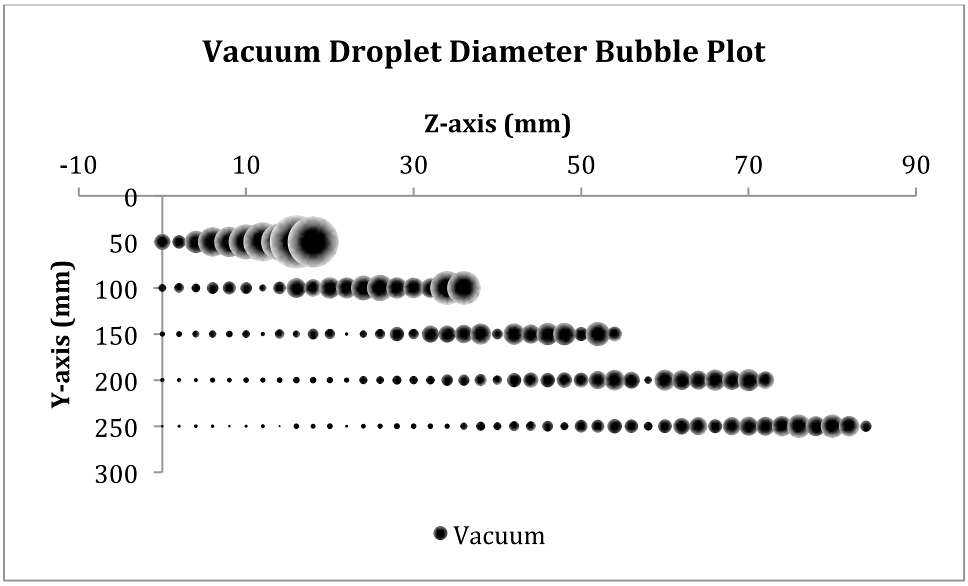
Vacuum Droplet Diameter Bubble Plot
Z-axis (mm)
-10
10
30
50
70
90
Y-axis (mm)
0
50
100
150
200
250
300
● Vacuum

**Delevan WM104**

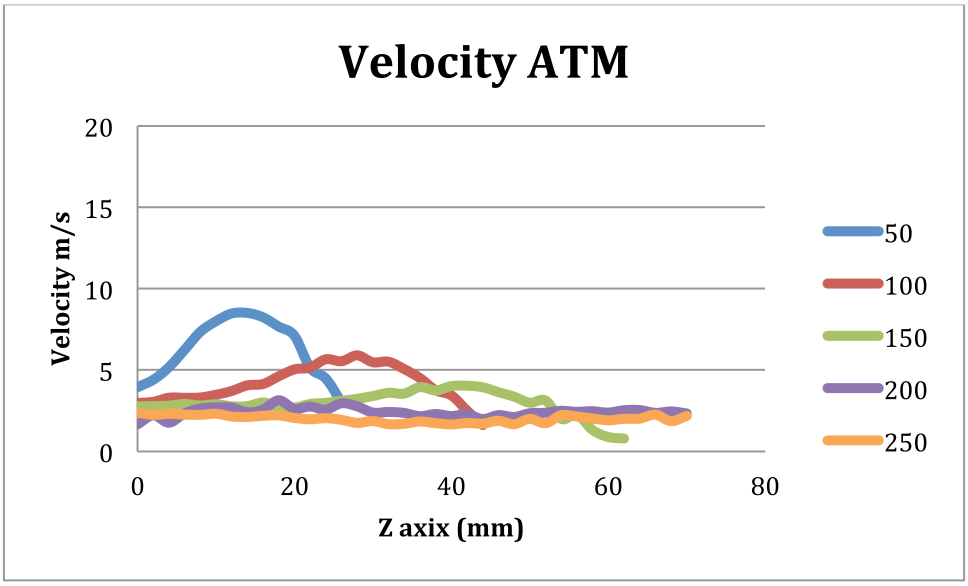

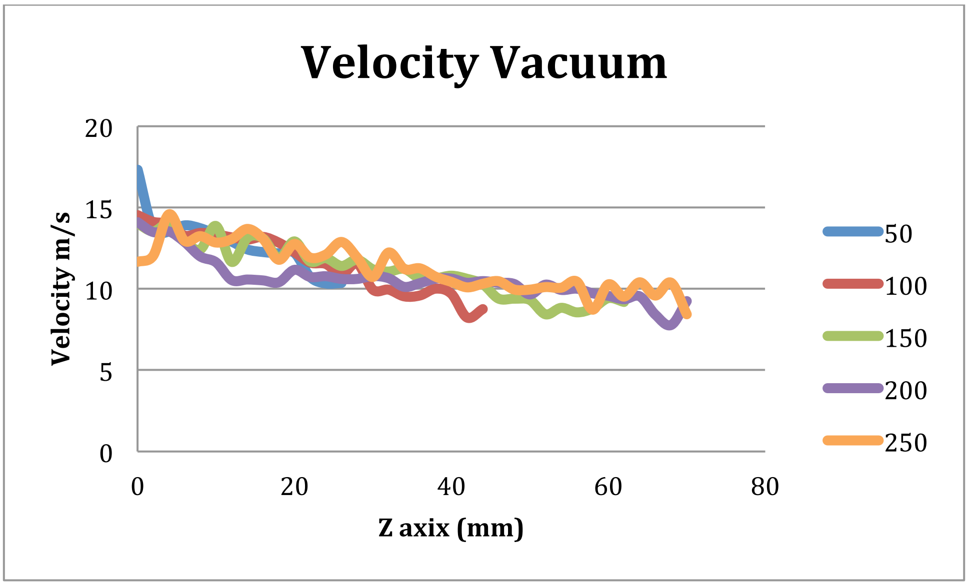

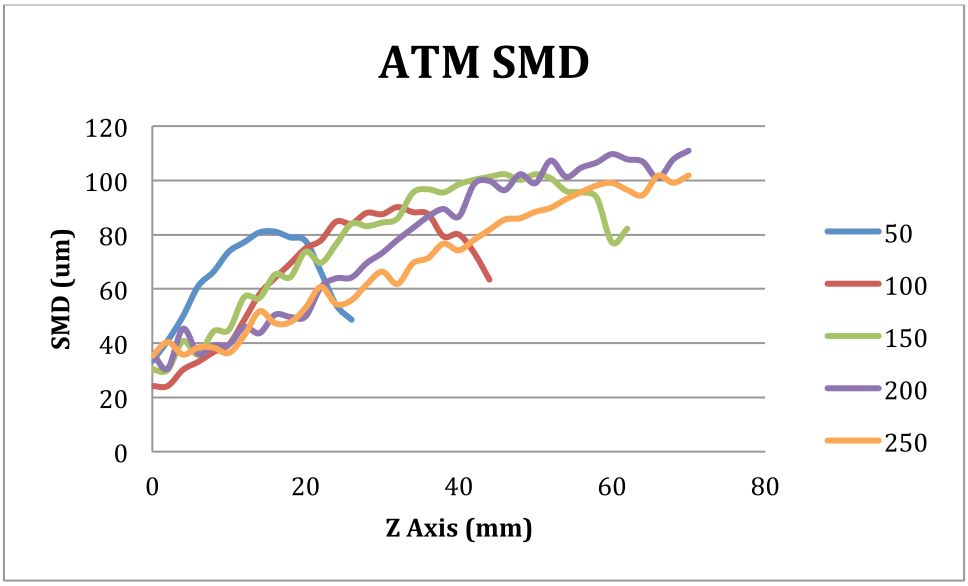
ATM SMD
SMD (um)
0
20
40
60
80
100
120
0
20
40
60
80
Z Axis (mm)
50
100
150
200
250

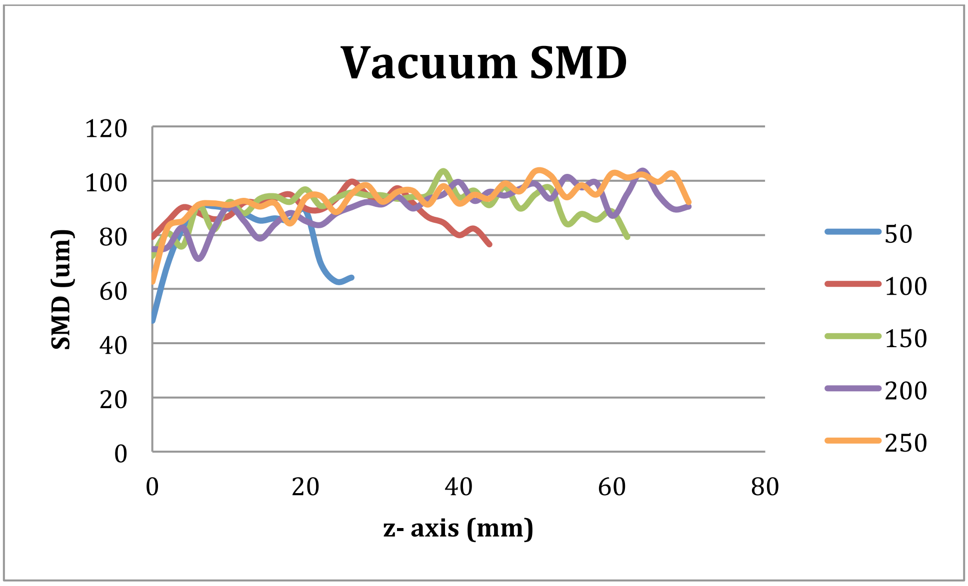
Vacuum SMD
SMD (um)
0
20
40
60
80
100
120
0
20
40
60
80
z- axis (mm)
50
100
150
200
250

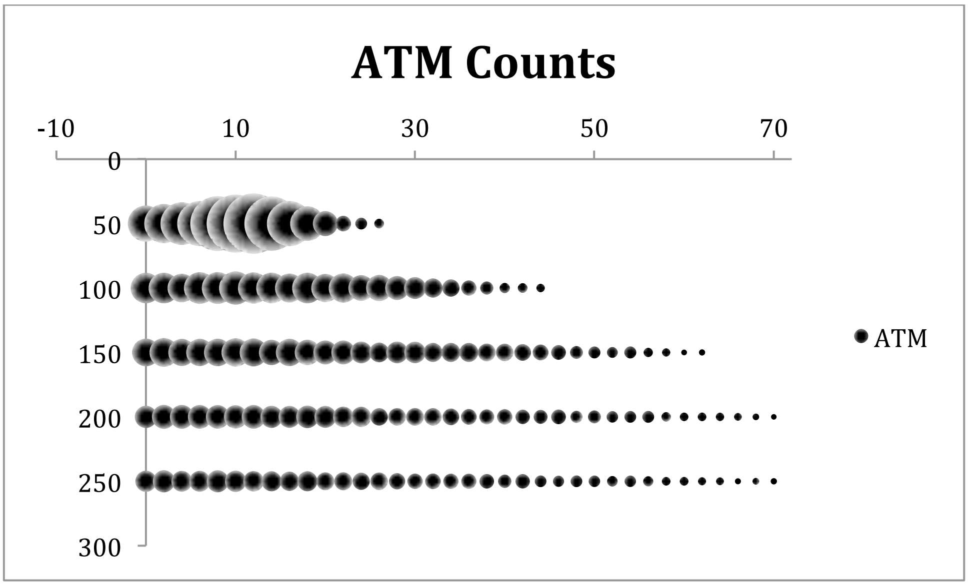
ATM Counts
-10
10
30
50
70
0
50
100
150
200
250
300
ATM

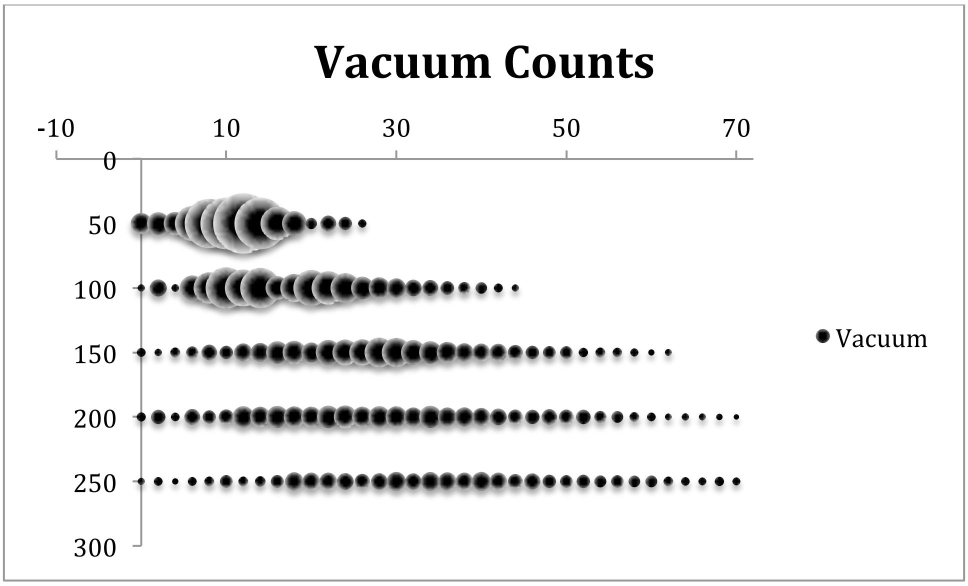
Vacuum Counts
-10
10
30
50
70
0
50
100
150
200
250
300
Vacuum

**Delevan WM1154**

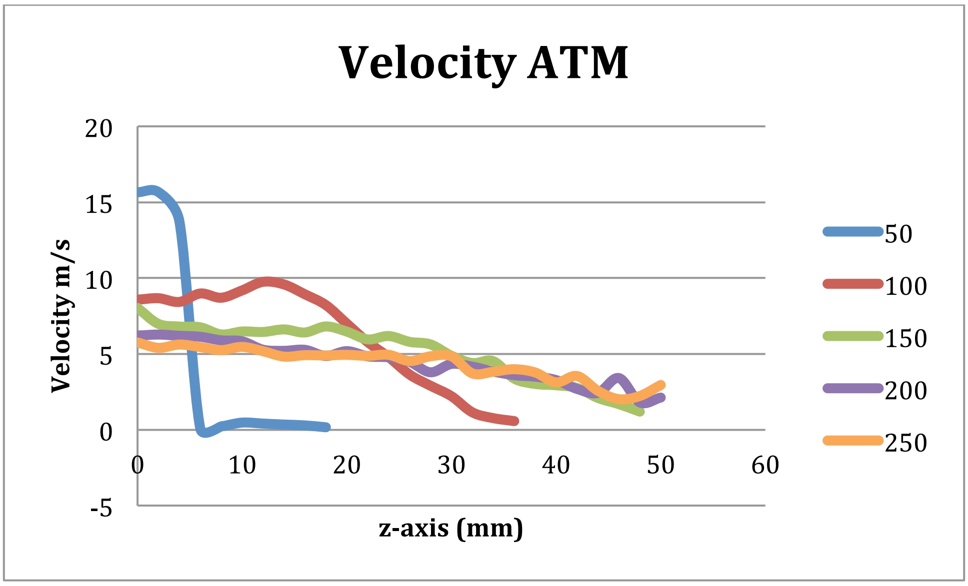

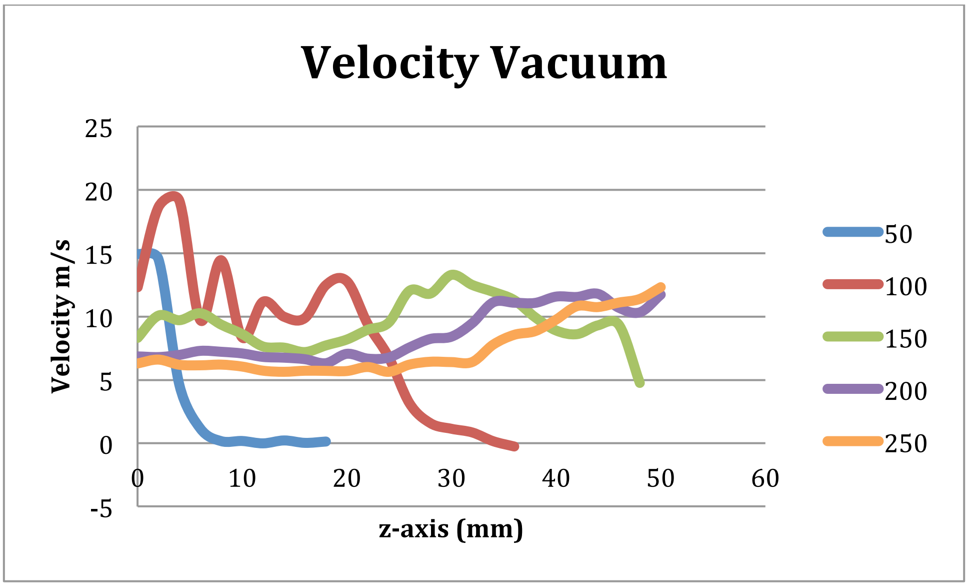

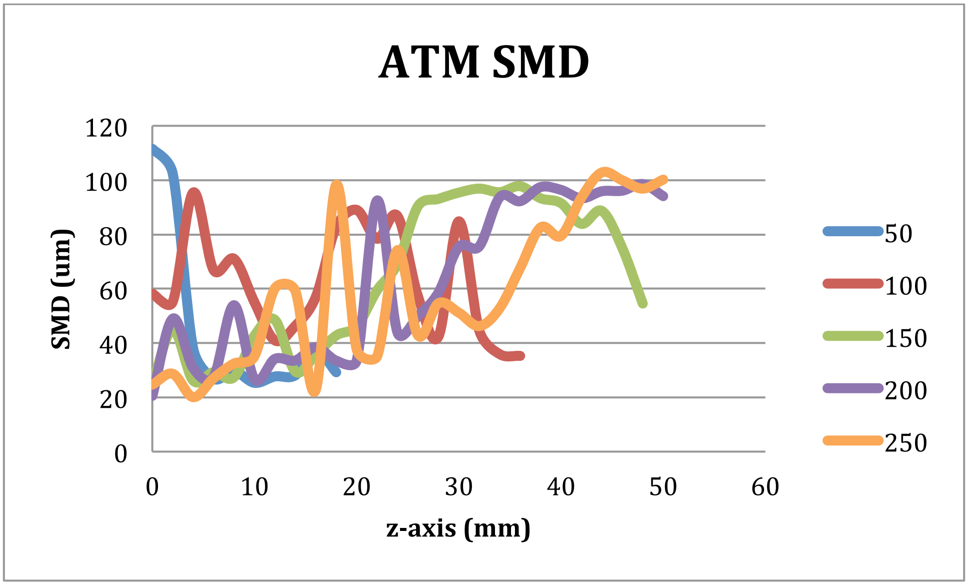

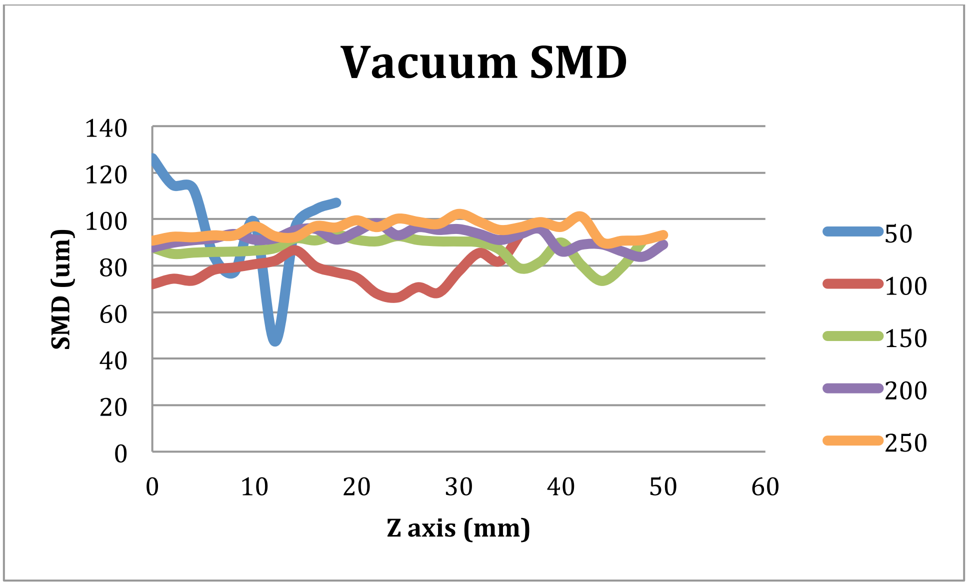
Vacuum SMD
SMD (um)
140
120
100
80
60
40
20
0
0
10
20
30
40
50
60
Z axis (mm)
50
100
150
200
250

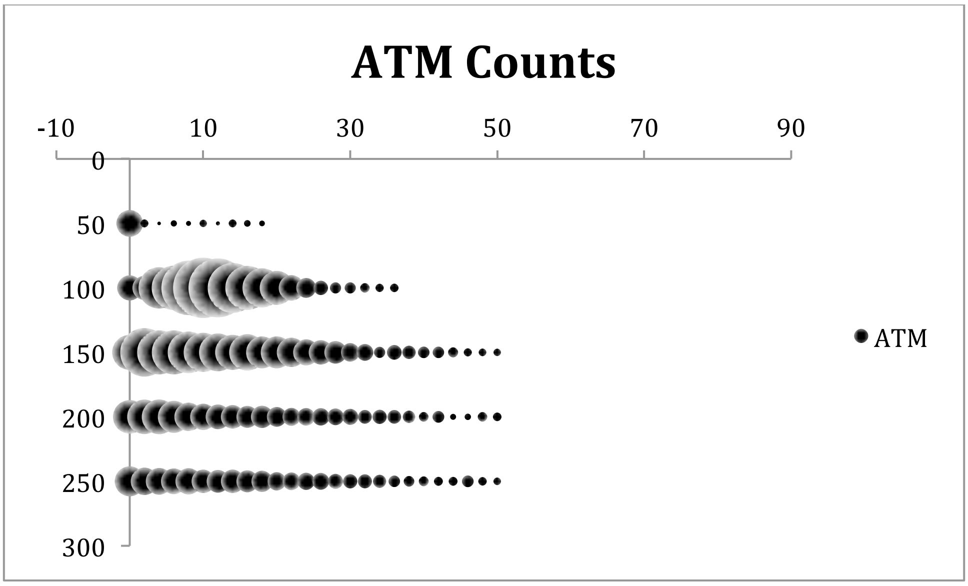
ATM Counts
-10
10
30
50
70
90
0
50
100
150
200
250
300
ATM

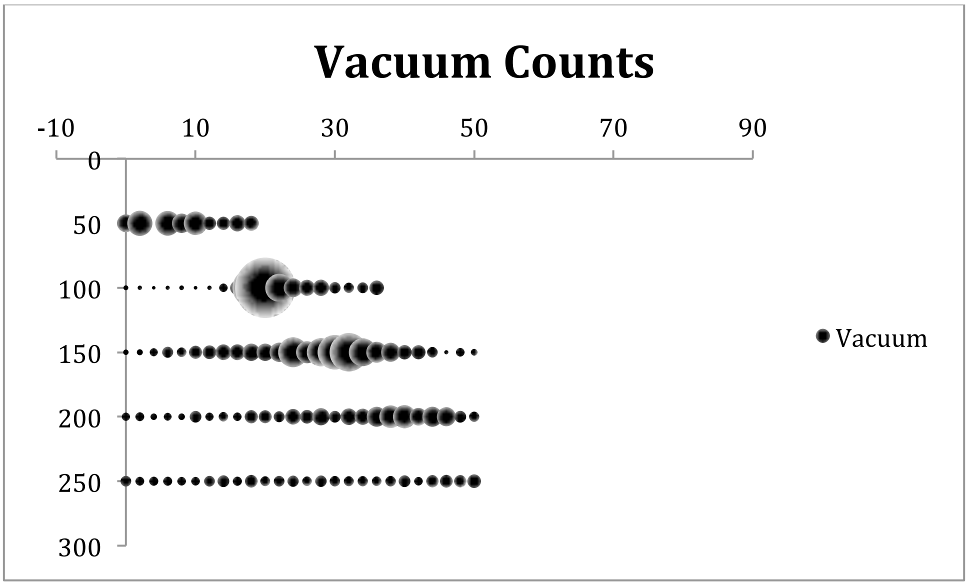
Vacuum Counts
-10
10
30
50
70
90
0
50
100
150
200
250
300
Vacuum

# Appendix B – 20% Viscosity by Volume

## Delevan WM054

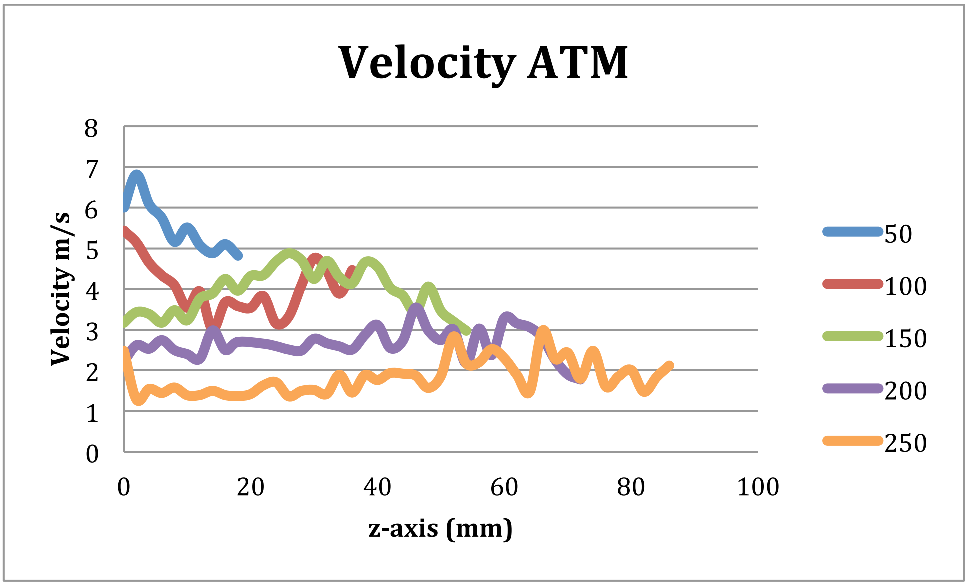

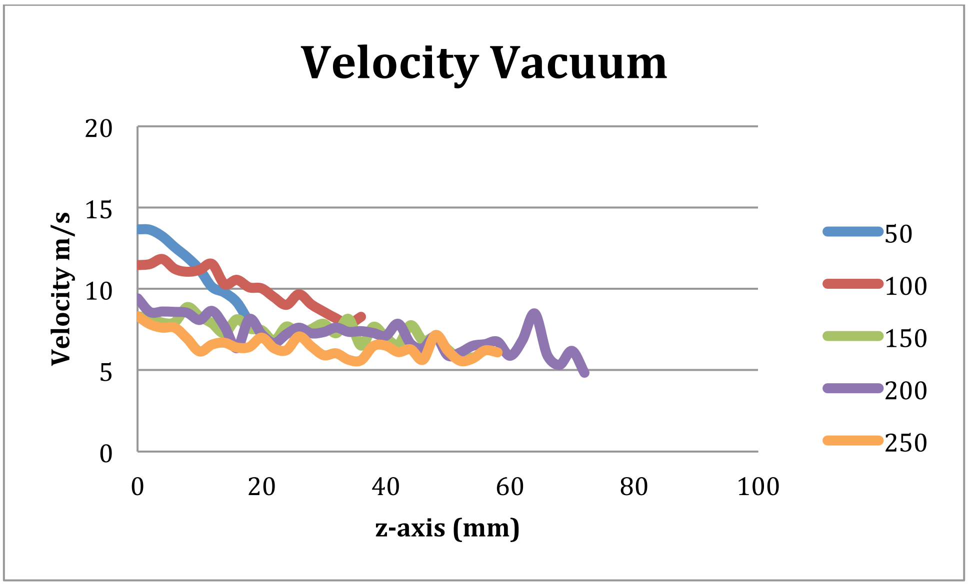

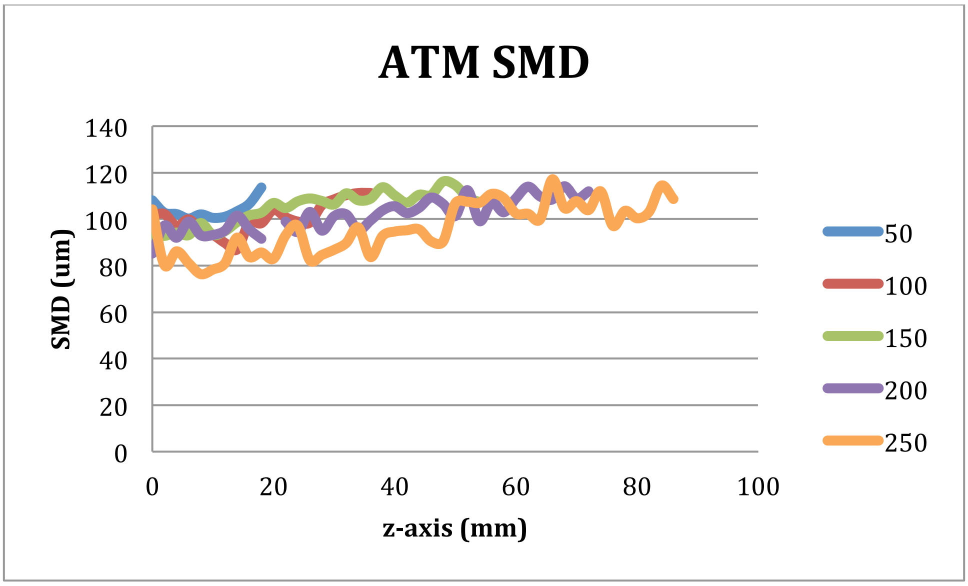
ATM SMD
140
120
100
80
60
40
20
0
SMD (um)
0
20
40
60
80
100
z-axis (mm)
50
100
150
200
250

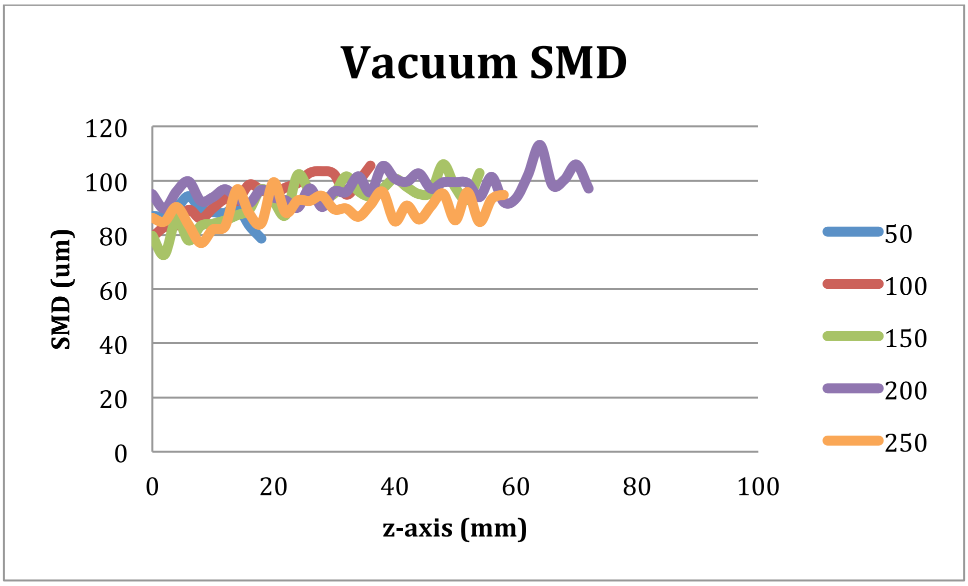
Vacuum SMD
120
100
80
60
40
20
0
SMD (um)
0
20
40
60
80
100
z-axis (mm)
50
100
150
200
250

**Delevan WM104**

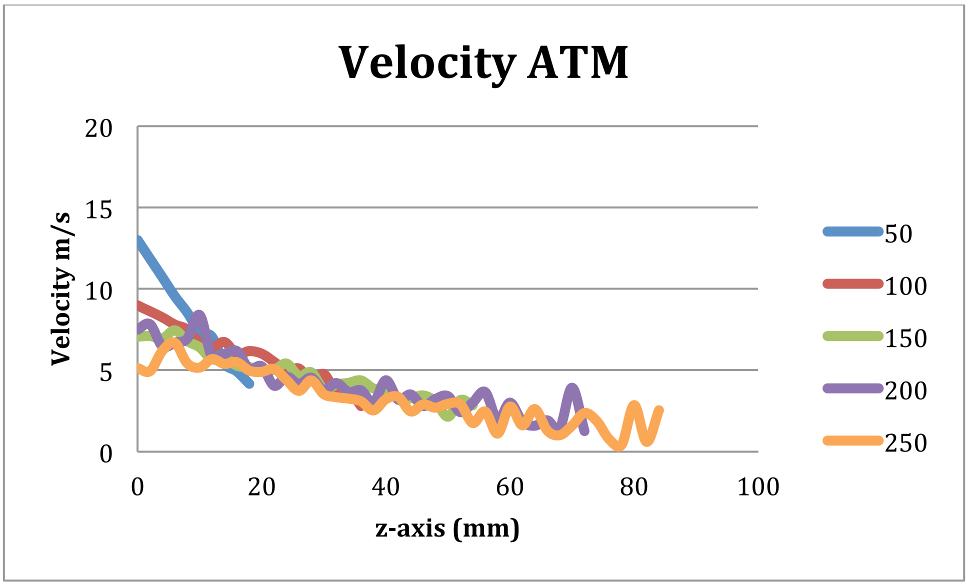

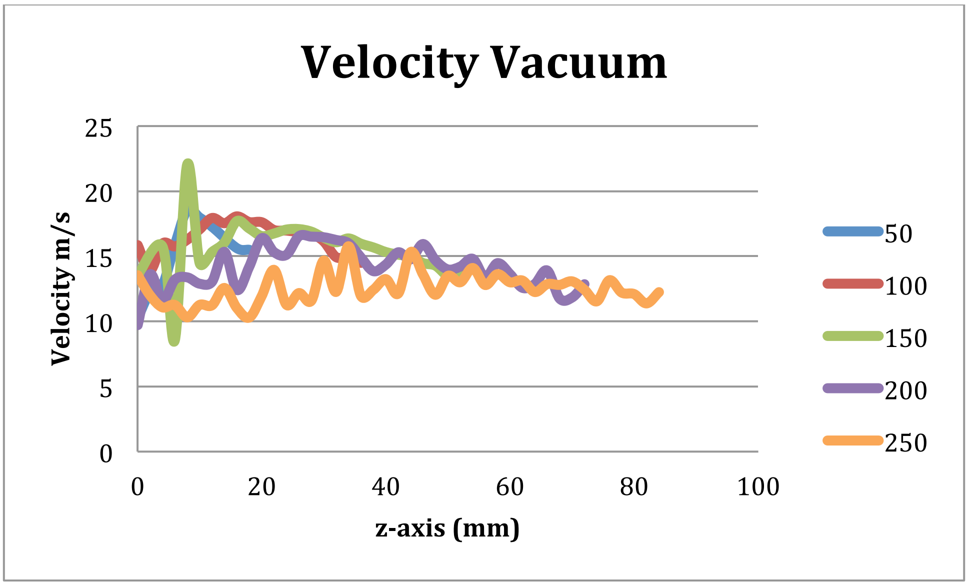

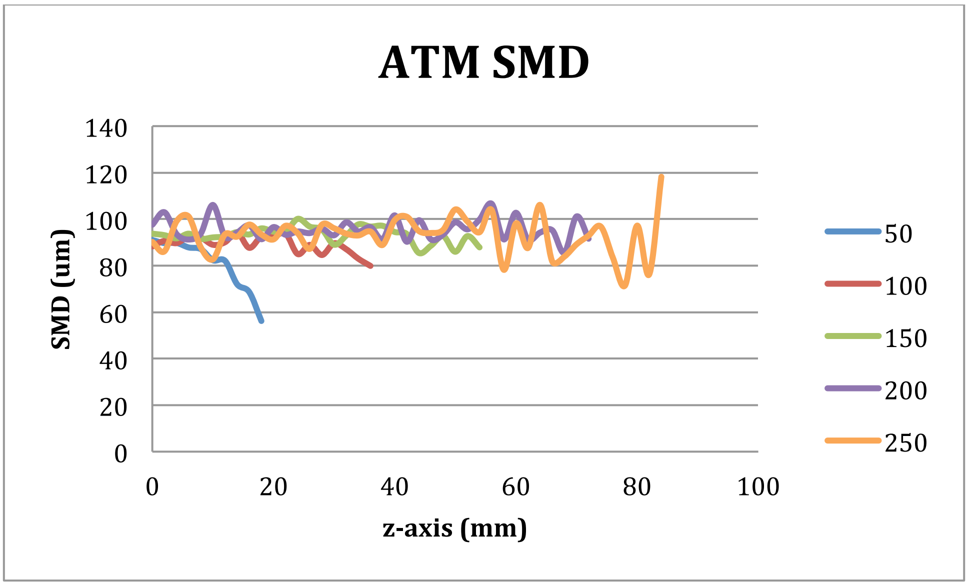
ATM SMD
SMD (um)
140
120
100
80
60
40
20
0
0
20
40
60
80
100
z-axis (mm)
50
100
150
200
250

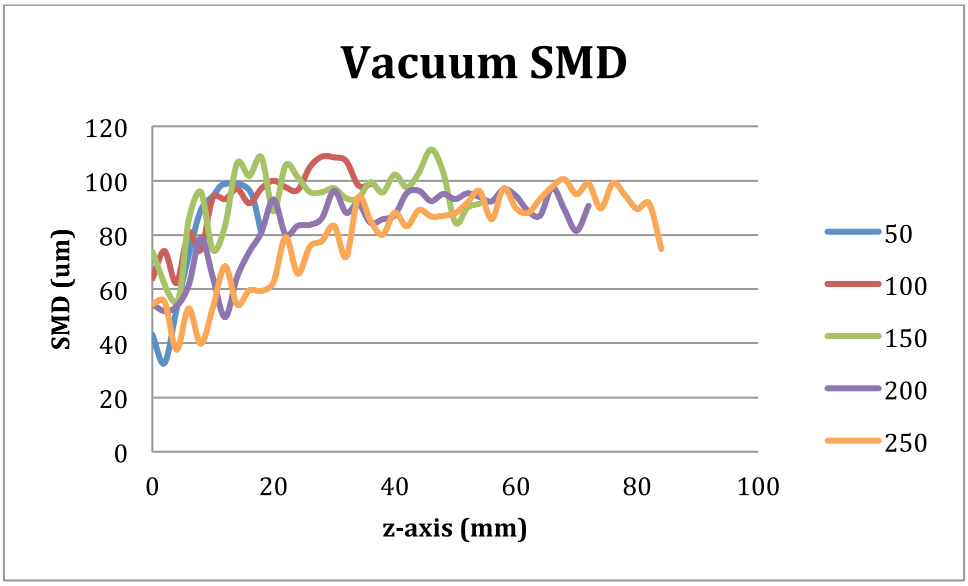
Vacuum SMD
SMD (um)
120
100
80
60
40
20
0
0
20
40
60
80
100
z-axis (mm)
50
100
150
200
250

**Delevan WM1154**

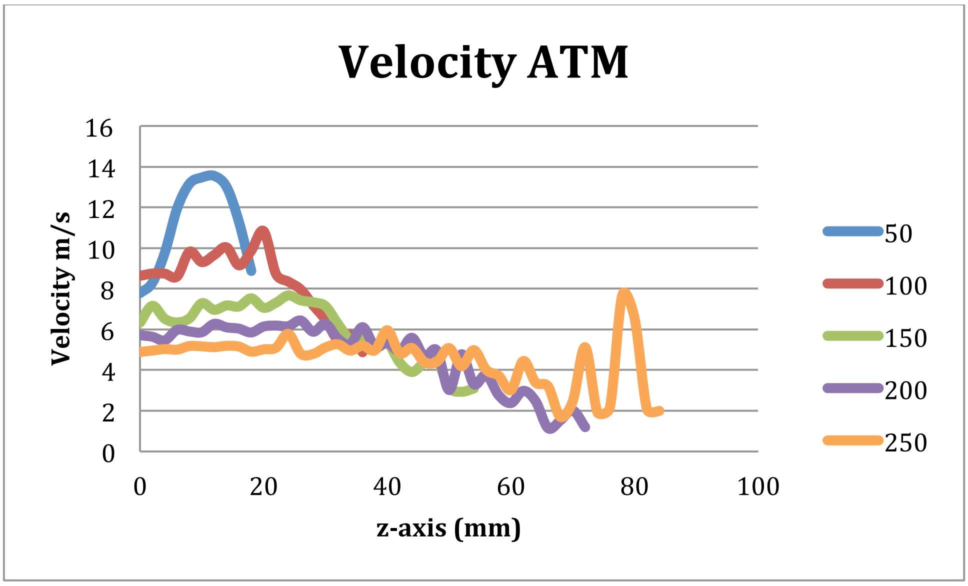

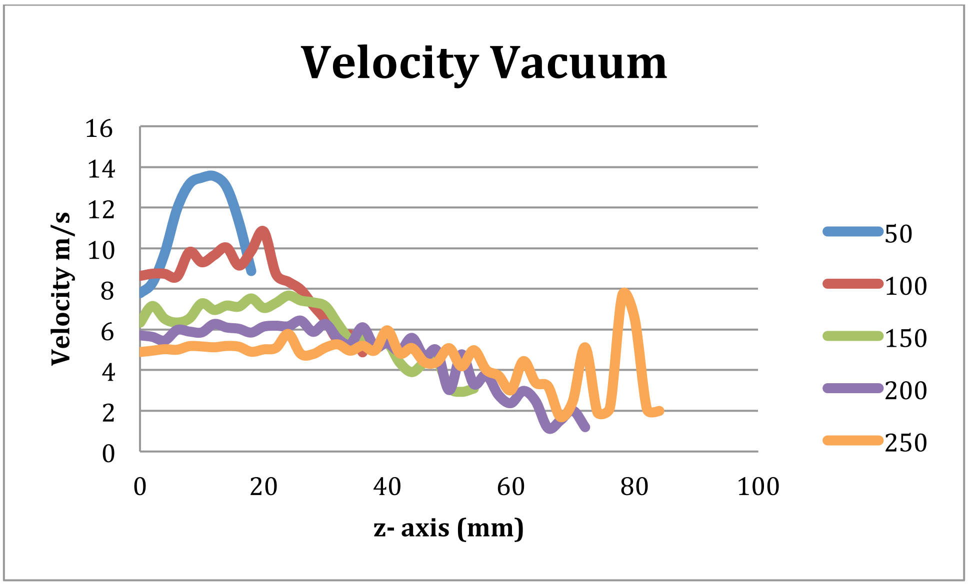

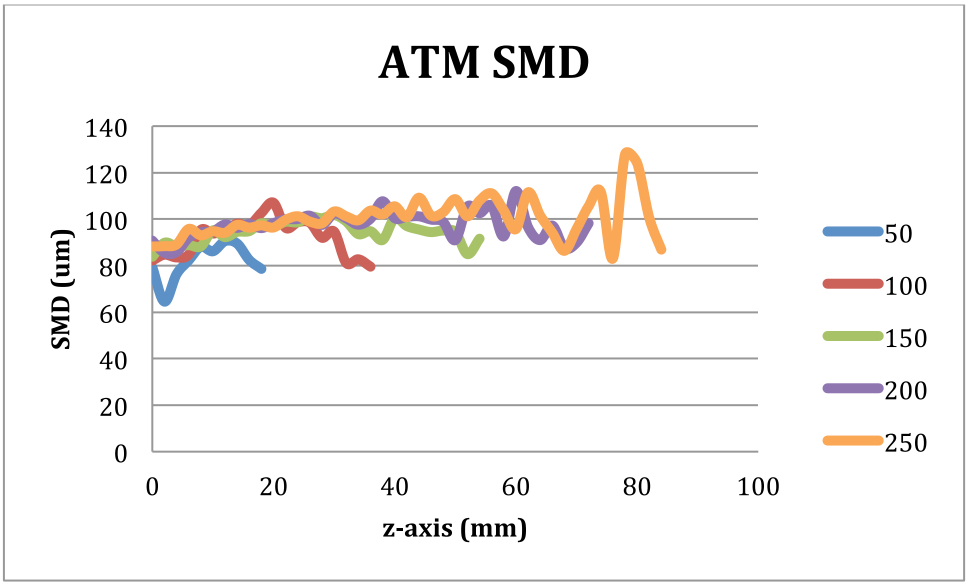
ATM SMD
SMD (um)
0
20
40
60
80
100
120
140
z-axis (mm)
0
20
40
60
80
100
50
100
150
200
250

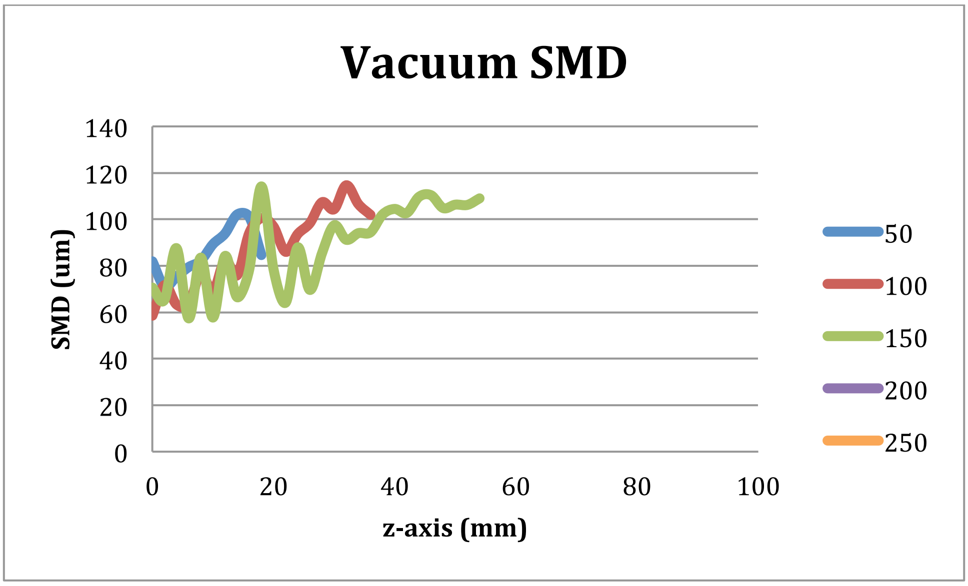
Vacuum SMD
SMD (um)
0
20
40
60
80
100
120
140
z-axis (mm)
0
20
40
60
80
100
50
100
150
200
250

# Appendix C – 20% Viscosity by Volume + 2EH

## Delevan WM054

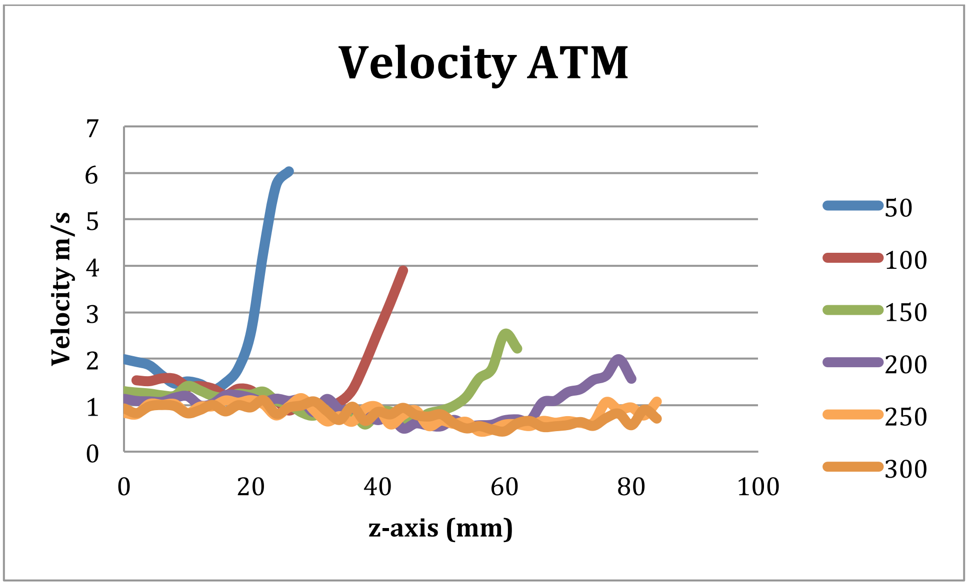

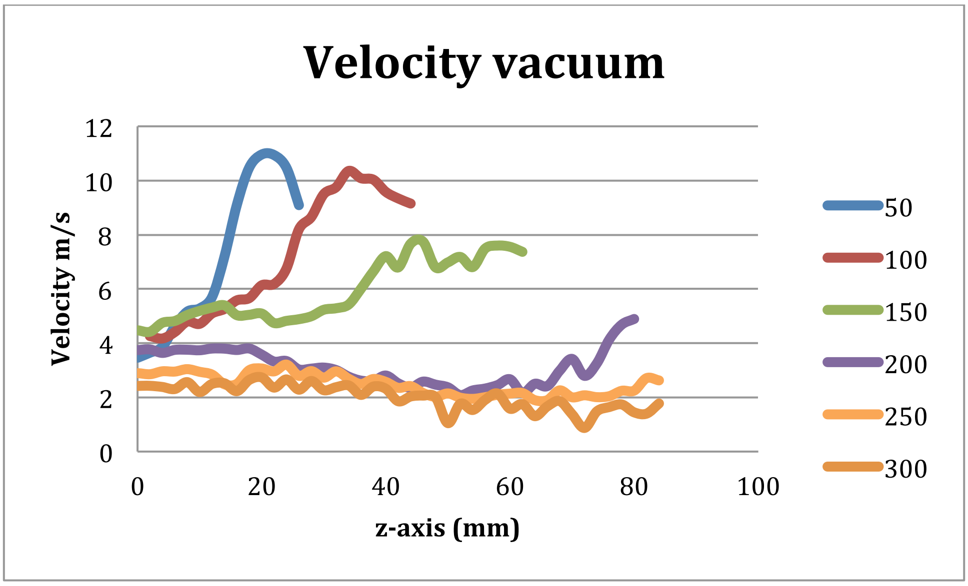

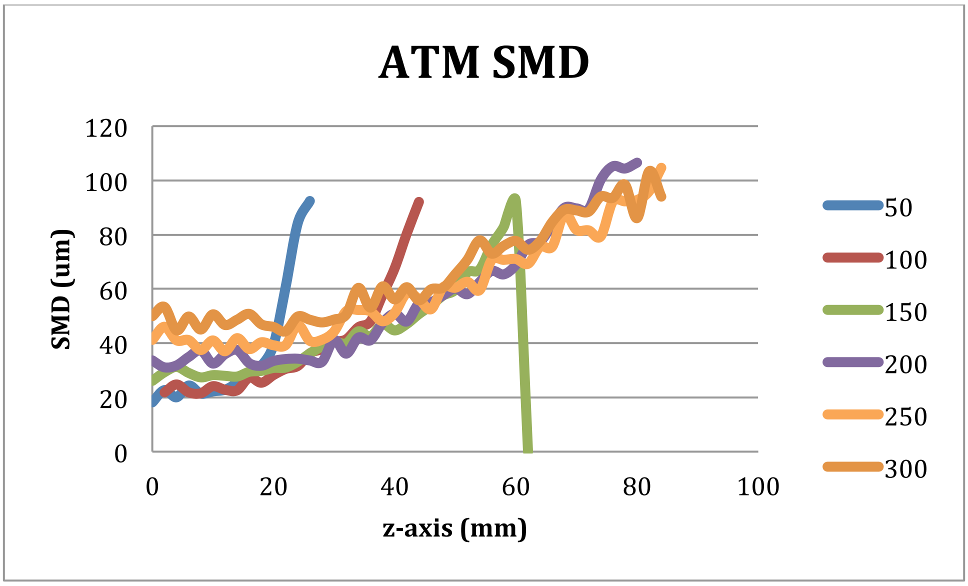
ATM SMD
SMD (um)
120
100
80
60
40
20
0
0
20
40
60
80
100
z-axis (mm)
50
100
150
200
250
300

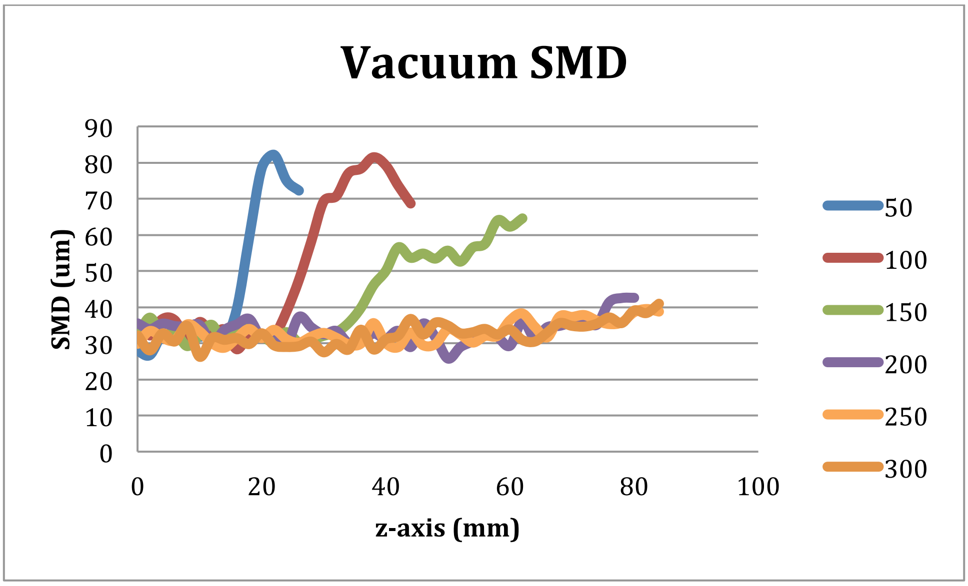
Vacuum SMD
SMD (um)
90
80
70
60
50
40
30
20
10
0
0
20
40
60
80
100
z-axis (mm)
50
100
150
200
250
300

**Delevan WM104**

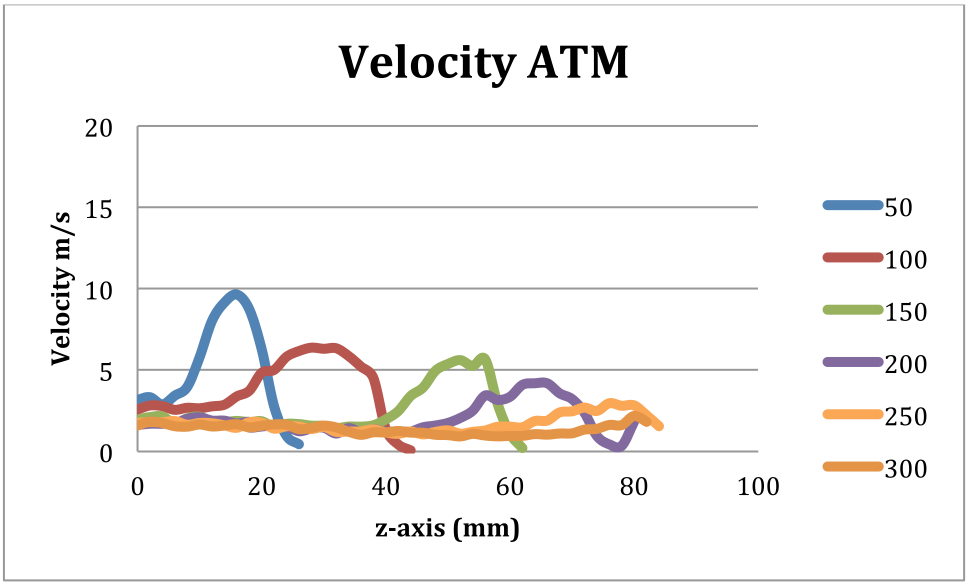

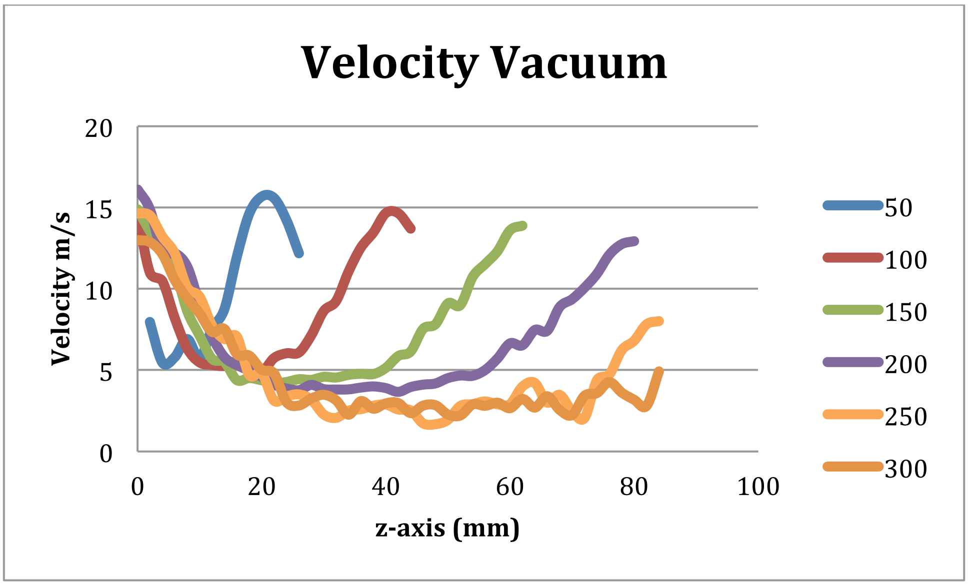

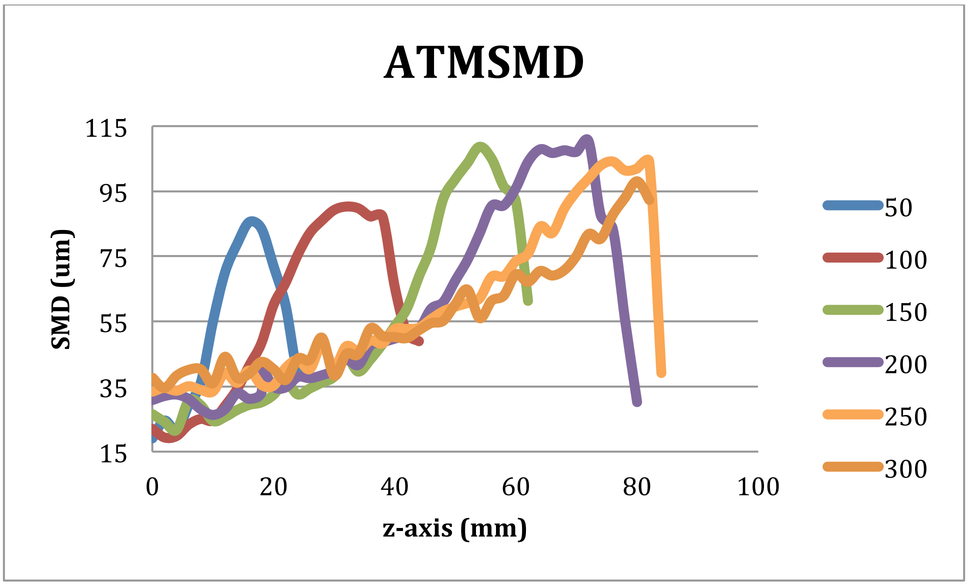
ATMSMD
SMD (um)
115
95
75
55
35
15
0
20
40
60
80
100
z-axis (mm)
50
100
150
200
250
300

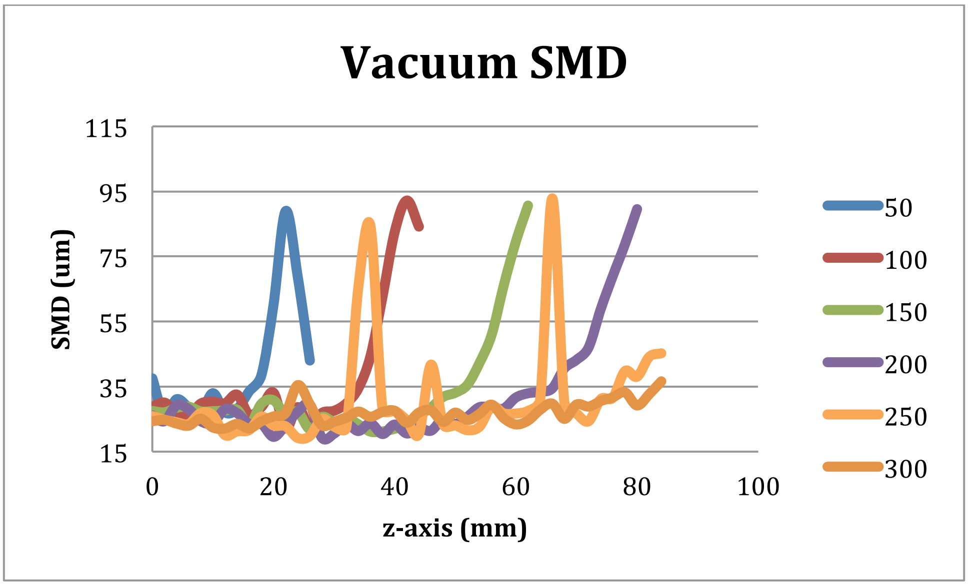
Vacuum SMD
SMD (um)
115
95
75
55
35
15
0
20
40
60
80
100
z-axis (mm)
50
100
150
200
250
300

**Delevan WM1154**

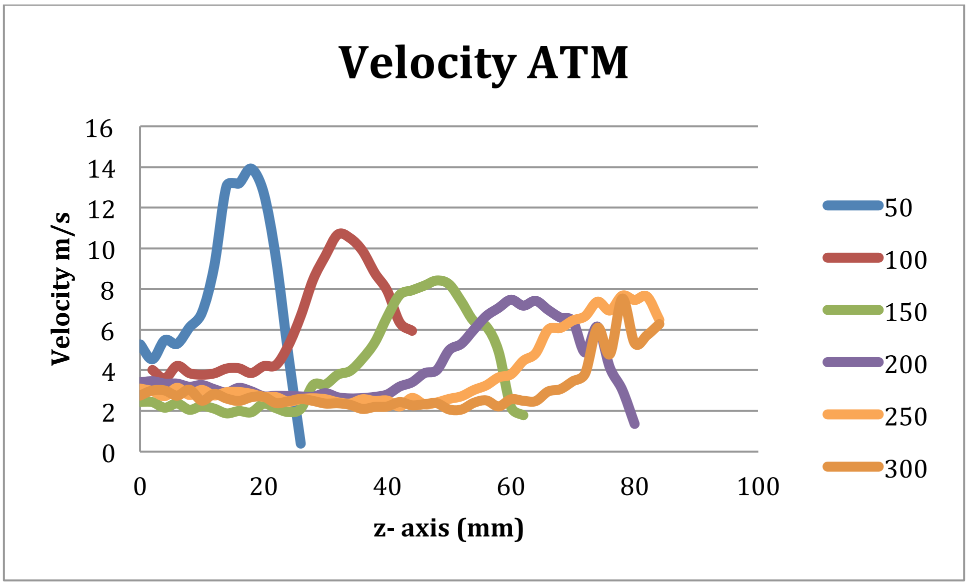

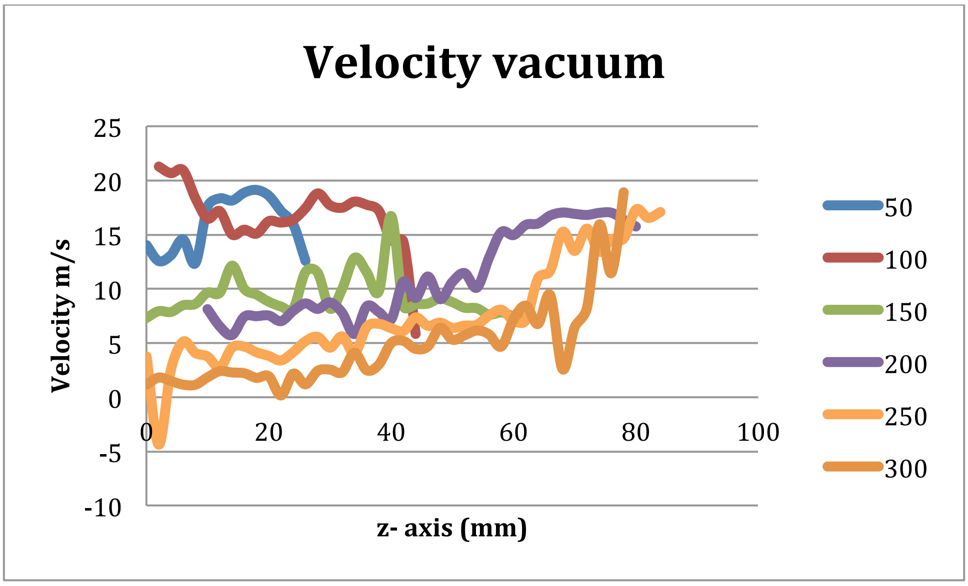

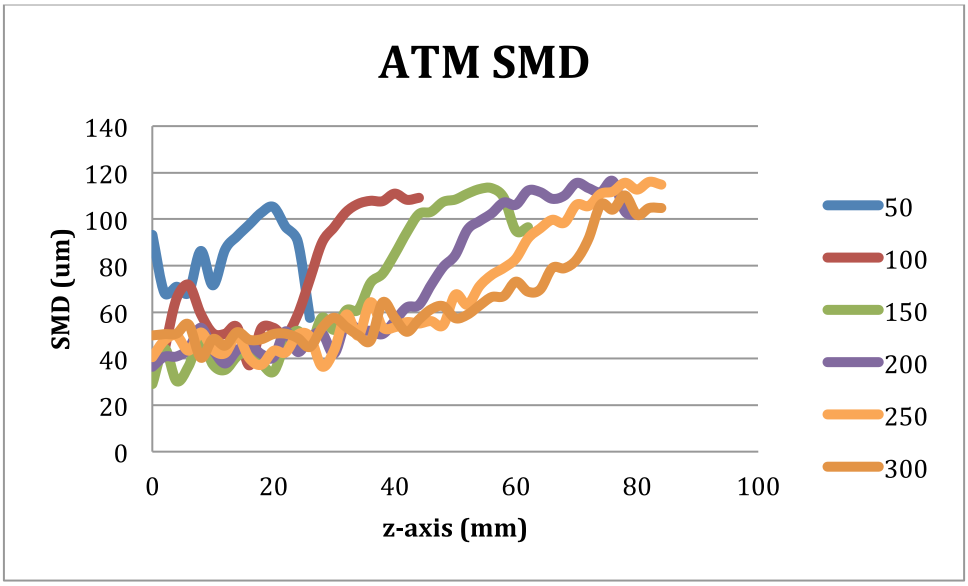
ATM SMD
140
120
100
80
60
40
20
0
SMD (um)
0
20
40
60
80
100
z-axis (mm)
50
100
150
200
250
300

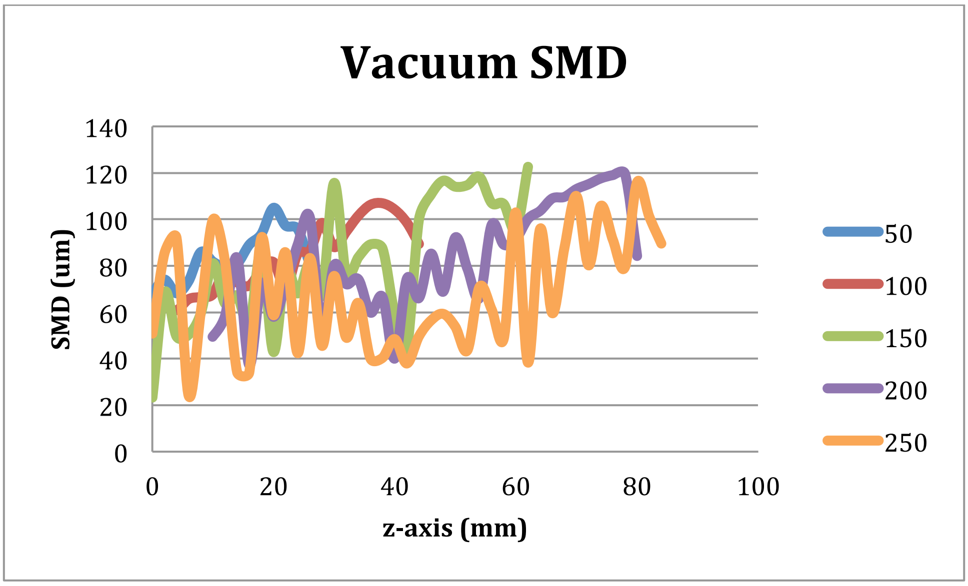
Vacuum SMD
140
120
100
80
60
40
20
0
SMD (um)
0
20
40
60
80
100
z-axis (mm)
50
100
150
200
250